



Universitat Autònoma de Barcelona

ADVERTIMENT. L'accés als continguts d'aquesta tesi queda condicionat a l'acceptació de les condicions d'ús establertes per la següent llicència Creative Commons:  http://cat.creativecommons.org/?page_id=184

ADVERTENCIA. El acceso a los contenidos de esta tesis queda condicionado a la aceptación de las condiciones de uso establecidas por la siguiente licencia Creative Commons:  <http://es.creativecommons.org/blog/licencias/>

WARNING. The access to the contents of this doctoral thesis it is limited to the acceptance of the use conditions set by the following Creative Commons license:  <https://creativecommons.org/licenses/?lang=en>



**Universitat Autònoma
de Barcelona**

Universitat Autònoma de Barcelona

Facultat de Medicina

Departament de Biologia Cel·lular, de Fisiologia i de Immunologia

Programa de Doctorat en Biologia Cel·lular

Thesis Title:

**Targeting Mek1/2-Erk1/2 signaling pathway in
pancreatic cancer**

Thesis presented by Faiz Bilal Espejo for the degree of Doctor of Philosophy
(PhD) in Cell Biology by Universitat Autònoma de Barcelona (UAB)

Barcelona, 2019

Directors

Tutor

PhD candidate

Dr. Joaquín Arribas

Dr. Ignasi Roig

Faiz Bilal Espejo

Dr. Josep Tabernero

Table of contents

ABBREVIATIONS	1
SUMMARY	6
RESUMEN	7
INTRODUCTION	8
1. Pancreatic cancer	9
1.1 Anatomy of the pancreas	11
1.2 Biology and development of pancreatic cancer	13
1.3 Genetics of PDAC	15
1.4 Pancreatic cancer stroma	17
1.5 Tumor heterogeneity	18
1.6 Pancreatic cancer treatment	20
2. MAPK signaling	23
2.1 Ras-Raf-Mek-Erk signaling pathway	24
2.1.1 Current approaches to target Ras-Mek-Erk signaling	27
2.1.2 Resistance to Raf and Mek1/2 inhibitors	28
2.2 Mek5-Erk5 signaling	30
3. Epithelial to mesenchymal transition (EMT)	30
3.1 Snail Family Transcriptional Repressor 2 (Slug)	32
4. Preclinical models of pancreatic cancer	34
4.1 Genetically engineered mouse models	34
4.2 Xenograft mouse models	36
HYPOTHESIS & RESEARCH OBJECTIVES	38
MATERIALS & METHODS	40
Commercial cell lines	41
Primary cell cultures	41
Proliferation assays	42
Cell cycle analysis	42
Generation of resistant cell cultures	42
<i>In vitro</i> adhesion, migration and invasion assays	43
Therapeutic compounds	44
PC-PDX models	44
Subcutaneous injection of MIA PaCa-2 and resistant cells	45
Hematoxylin–eosin, immunohistochemistry and fibrosis staining	46
Human phospho-kinase antibody array	47
Two-photon microscopy and second harmonics generation	47
Viral infections	48
Orthotopic mouse model of pancreatic cancer	48
Amplicon-Seq VHIO-card panel	49
Exome sequencing	49
Digital droplet PCR	50

RNA isolation and qRT-PCR	51
RNA-seq preparation and data analysis	52
RESULTS	53
SECTION 1: Pancreatic cancer heterogeneity and response to Mek1/2 inhibition.....	53
1.1 Effect of different drugs on the proliferation of pancreatic cancer cell lines.....	54
1.2 Effect of chemotherapy combinations <i>in vivo</i>	56
1.3 Addition of MEK162 increases the effectiveness of chemotherapy <i>in vivo</i>	60
1.4 Effect of the Gem/Nab-P/MEK162 combination on the growth of orthotopic xenografts.	62
1.5 Intratumor heterogeneity and resistance to MEK162.....	64
SECTION 2: The transcription factor Slug uncouples cell proliferation from the Raf-Mek-Erk signaling pathway.....	70
2.1 Generation of <i>in vitro</i> models of acquired resistance to Mek1/2 inhibition.	71
2.2 Resistance to MEK162 is recapitulated <i>in vivo</i>	74
2.3 Mek1/2 inhibition prevents Erk1/2 phosphorylation in parental and resistant cells...	75
2.4 Exome sequencing analysis.	77
2.5 RNA sequencing analysis reveals commonly altered gene signatures in resistant cells79	
2.6 Resistant cells exhibit a mesenchymal phenotype.....	82
2.6 MEK162 resistant cells display increased metastatic traits <i>in vitro</i> and <i>in vivo</i>	84
2.7 Slug is a central regulator of resistance to Mek1/2 inhibition in pancreatic cancer cells	86
2.9 Slug prevents Cyclin D1 decrease by Mek1/2 inhibition	89
2.10 Slug regulates the metastatic ability of resistant cells.	91
2.11 Slug expression correlates with resistance to Mek1/2 inhibition in a panel of pancreatic cancer cell lines and in patient-derived xenografts.....	94
2.12 Slug expression correlates with resistance to Mek1/2 inhibition in a panel of melanoma cell lines.....	97
2.13 Slug predicts poor outcome in pancreatic cancer and melanoma patients.	101
2.14 ERK5 signaling regulates Slug expression in pancreatic cancer cells with acquired resistance to MEK162.....	103
2.15 p-ERK5 correlates with high Slug expression in PC-PDXs.	106
DISCUSSION	108
Section 1: Pancreatic cancer heterogeneity and response to Mek1/2 inhibition	109
Section 2: The transcription factor Slug uncouples pancreatic cancer cell proliferation from the Raf-Mek1/2-Erk1/2 pathway.....	114
CONCLUSIONS	122
REFERENCES	123

ABBREVIATIONS

5-FU	5-fluorouracil
5-FU-FA	5-Fluorouracil-Folinic acid
Akt	Akt Murine Thymoma Viral Oncogene Homolog
ARRIVE	Animal Research: Reporting of In Vivo Experiments
ASCO	American Society of Clinical Oncology
ATCC	American Type Culture Collection
ATF-2	Activating Transcription Factor 2
Aza	Azacitidine
BBC3	BCL2 Binding Component 3
BCL2	B-Cell CLL/Lymphoma 2
Bmi1	Polycomb Complex Protein BMI-1
BMK1	Big MAPK1
BRCA2	Breast cancer gene 2
CA19-9	Carbohydrate antigen 19-9
CAFs	Cancer-associated fibroblasts
cAMP	Cyclic adenosine monophosphate
CCND1	Cyclin D1
CDH1	E-cadherin
CDK	Cyclin-dependent kinase
CDKN1A	Cyclin Dependent Kinase Inhibitor 1A
CDKN2A	Cyclin-dependent kinase Inhibitor 2A
CEEA	Ethical Committee for the Use of Experimental Animals
ChIP-seq	Chromatin immunoprecipitation sequencing
CK-19	Cytokeratin 19
CLDN1	Claudin 1
CRISPR	Clustered regularly interspaced short palindromic repeats

CTNNB1	Catenin beta 1
ddPCR	Digital droplet PCR
DMSO	Dimethyl Sulfoxide
DNA	Deoxyribonucleic Acid
ECM	Extracellular matrix
ECOG	Eastern Cooperative Oncology Group
EDTA	Ethylenediaminetetraacetic acid
Elk-1	ETS Transcription Factor ELK1
Elk-1	ETS-Like Gene 1
EMT	Epithelial to mesenchymal transition
EMT-TF	EMT-transcription factor
ERK	Extracellular-signal regulated kinase
Erk1/2	Extracellular-signal regulated kinase 1/2
Erk5	Extracellular-signal regulated kinase 5
ESPAC-4	European Study Group for Pancreatic Cancer - Trial 4
Exome-seq	Exome sequencing
FAK	Focal adhesion kinase
FOLFIRINOX	Leucovorin calcium, fluorouracil, irinotecan hydrochloride and oxaliplatin
FTI	Farnesyl transferase inhibitors
GAP	GTPase activating protein
GAPDH	Glyceraldehyde 3-phosphate dehydrogenase
GEF	Guanosine exchanging factor
Gem	Gemcitabine
Gem	Gemcitabine
GEMMs	Genetically engineered mouse models
Gli1	Glioma-Associated Oncogene Homolog 1
Gli2	Glioma-Associated Oncogene Homolog 2
GTP	Guanosine-5'-triphosphate

HDAC1	Histone deacetylase I
HRAS	Harvey Rat Sarcoma Viral Oncogene Homolog
IC50	Half maximal inhibitory concentration
IDAC	Infiltrating ductal adenocarcinoma
JNK	c-Jun N-terminal kinase
K-Ras	Kirsten Rat Sarcoma Viral Oncogene Homolog
kDa	Kilodalton
Ki67	Marker Of Proliferation Ki-67
MAPK	Mitogen-activated protein kinase
MAPKAPK2	Mitogen-Activated Protein Kinase-Activated Protein Kinase 2
MAPKK	mitogen-activated kinase kinase
MAPKKK	mitogen-activated kinase kinase kinase
MEF2C	Myocyte Enhancer Factor 2C
Mek	Mitogen-activated protein kinase kinase
Mek1/2	Mitogen-activated protein kinase kinase 1/2
Mek5	Mitogen-activated protein kinase kinase 5
MEKK2	Mitogen-Activated Protein Kinase Kinase Kinase 2
MEKK3	Mitogen-Activated Protein Kinase Kinase Kinase 3
MET	Mesenchymal to epithelial transition
MIA PaCa-2/Fluc	MIA PaCa-2 cells expressing firefly luciferase
mRNA	Messenger RNA
MUC1	Mucin 1
Myc	V-Myc Avian Myelocytomatosis Viral Oncogene Homolog
Na2PO4	Disodium phosphate
Nab	Nab-Paclitaxel
Nab-P	Nab-Paclitaxel
Nab-Paclitaxel	Nanoparticle albumin-bound paclitaxel
NaCl	Sodium chloride
nal	Nanoliposomal

NF1	Neurofibromatosis 1
NRAS	Neuroblastoma RAS Viral Oncogene Homolog
ON	Overnight
p-Akt	Phosphorylated Akt
p-Erk1/2	Phosphorylated Erk1/2
p-Erk5	Phosphorylated Erk5
PanIN	Pancreatic intraepithelial neoplasia
PBS	Phosphate-buffered saline
PC	Pancreatic cancer
PC-PDXs	Pancreatic cancer patient-derived xenografts
PDAC	Pancreatic ductal adenocarcinoma
Pdx1	Pancreatic and duodenal homeobox 1
PDXs	Patient-derived xenografts
PEI	Polyethylenimine
PI3K	Phosphoinositide 3-kinase
PKA	Protein kinase A
PLC	Phospholipase C
PSCs	Pancreatic stellate cells
PTEN	Phosphatase And Tensin Homolog
Ptf1a	pancreas transcription factor-1a
qRT-PCR	Quantitative Real-Time Polymerase Chain Reaction
R1	Resistance strategy 1
R2	Resistance strategy 2
Raf	Rapidly Accelerated Fibrosarcoma
Ral-GEF	Ras-like small GTPases
RBL1	RB Transcriptional Corepressor Like 1
RCF	Relative Centrifugal Force
RNA	Ribonucleic acid
RNA-seq	RNA sequencing

RSK	Ribosomal S6 Kinase
RTK	Tyrosine kinase receptors
Sap1a	Stress-activated protein 1a
SGK	Serum/Glucocorticoid Regulated Kinase
SHH	Sonic Hedgehog signaling
shRNA	Short hairpin RNA
SMA	Smooth muscle actin
SMAD4	SMAD family member 4
SNAI1	Snail Family Transcriptional Repressor 1
SNAI2	Snail Family Transcriptional Repressor 2
SNAI3	Snail Family Transcriptional Repressor 3
SNP	Single nucleotide polymorphism
SOS	Son Of Sevenless
Stat3	Signal Transducer And Activator Of Transcription 3
TAZ	Tafazzin
TBS	Tris-buffered saline
TBS-T	Tris-buffered saline + Tween
TBX2	T-Box Protein 2
TGF-beta	Transforming growth factor-beta
TP53	Tumor protein 53
VEGF	Vascular endothelial growth factor
YAP	Yes-associated protein 1
ZEB1	Zinc Finger E-Box Binding Homeobox 1
ZEB2	Zinc Finger E-Box Binding Homeobox 2

SUMMARY

Pancreatic cancer is one of most lethal human diseases, being the fourth leading cause of cancer-related deaths in western countries. With a 5-year overall survival of around 5%, the development of novel therapies is needed. The current standard treatment for this disease consists of chemotherapy, and many targeted therapies have failed to improve patients' survival so far. For this reason, the development of novel therapies targeting key components of this cancer as well as the study of resistance becomes necessary. 90% of pancreatic cancers are mutated in the GTPase K-Ras, required for the development of this disease. K-Ras is a GTPase that transduces signals from tyrosine kinase receptors (RTKs) and controls cell proliferation and survival. Despite the initial approaches for pharmacologically inhibiting K-Ras started more than twenty years ago, none of the inhibitors has succeed in the clinics so far. As K-Ras is still considered 'undruggable', the efforts have been focused on targeting its downstream effectors, as the Raf and Mek proteins. Despite B-Raf and Mek1/2 inhibitors have improved patients' survival in melanoma, they have failed to succeed in pancreatic cancer patients.

In this work, we assess the efficacy of Mek1/2 inhibition against pancreatic cancer. Using cell lines and pancreatic cancer-derived xenografts (PC-PDXs), we gauged the efficacy of the Mek1/2 inhibitor MEK162 in addition to the standard chemotherapy and we show that it impairs growth *in vitro* and *in vivo*. However, we also demonstrate that the effectiveness of Mek1/2 inhibition is limited by the emergence of resistant clonal populations, that result from the high degree of tumor heterogeneity and they compromise the effectiveness of this treatment.

In this thesis, we also demonstrate that, when pancreatic cancer cells acquire resistance to Mek1/2 inhibition they increase the expression of the EMT zinc finger transcription factor Slug. This transcription factor regulates resistance to Mek1/2 inhibitors in pancreatic cancer cells by uncoupling the regulation of cell division by the Mek1/2-Erk1/2 pathway, and it correlates with resistance in a panel of pancreatic cancer and melanoma cell lines. Likewise, Slug is responsible for the enhanced metastatic ability of resistant cells, and it consistently correlates with poor survival in pancreatic cancer and melanoma patients.

RESUMEN

El cáncer de páncreas es una de las enfermedades más letales, siendo la cuarta causa de muerte por cáncer en países occidentales. Con una supervivencia global a los 5 años de alrededor del 5%, el tratamiento estándar actual consiste en quimioterapia, y la amplia mayoría de terapias dirigidas que se han probado hasta ahora no han tenido éxito. Por ello, es necesario el desarrollo de nuevas terapias contra componentes clave de esta enfermedad, así como que combatan los mecanismos de resistencia.

Alrededor del 90% de los cánceres de páncreas contienen mutaciones en K-Ras, clave para el desarrollo de esta enfermedad. K-Ras es una GTPasa que transduce señales iniciadas en receptores tirosina quinasa (RTKs) y controla proliferación celular y supervivencia, entre otras funciones. A pesar del desarrollo de inhibidores específicos de K-Ras durante las últimas décadas, ninguno ha conseguido demostrar eficacia en la clínica. Como consecuencia, los esfuerzos se han dirigido a inhibir a las proteínas reguladas por K-Ras, como las Raf o las Mek. Sin embargo, a pesar de que los inhibidores de B-Raf y Mek1/2 han demostrado eficacia clínica en melanoma, en cáncer de páncreas no se ha observado tal eficacia.

En esta tesis, probamos la eficacia de la inhibición de Mek1/2 en modelos de cáncer de páncreas, en combinación con quimioterapia, utilizando líneas celulares y xenoinjertos derivados de pacientes con cáncer páncreas (PC-PDXs). Sin embargo, demostramos que este efecto se ve limitado por la aparición de clones resistentes, que resultan como consecuencia del alto grado de heterogeneidad de estos tumores.

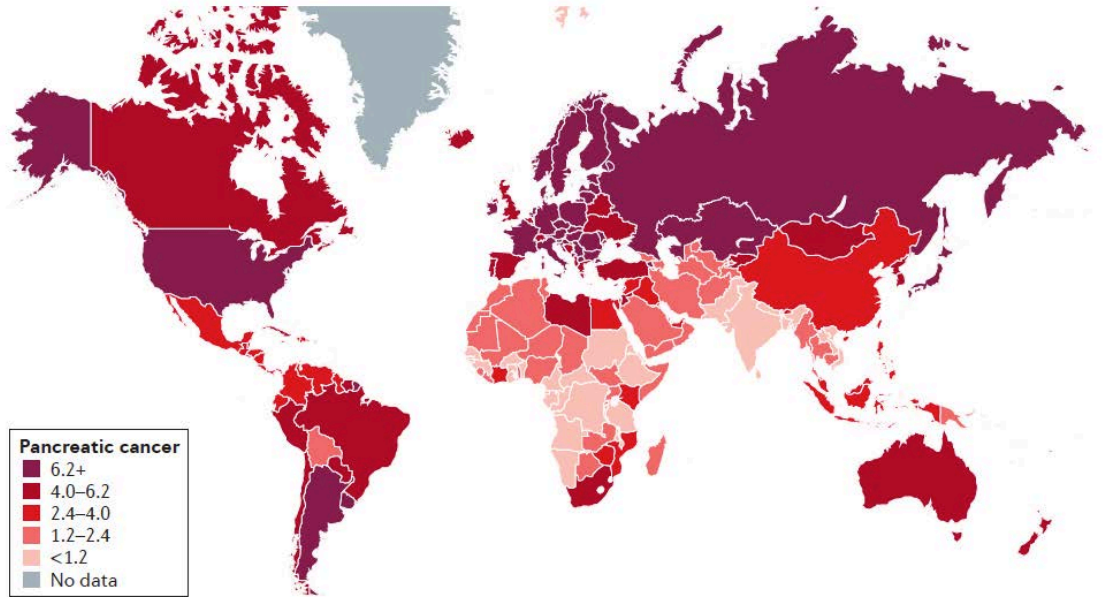
En este trabajo también se muestra que, cuando las células de cáncer de páncreas adquieren resistencia a la inhibición de Mek1/2, aumentan la expresión del factor de transcripción Slug. Este factor de transcripción induce resistencia, con un mecanismo de acción que consiste en desacoplar la división celular del control de la ruta de señalización Raf-Mek-Erk. Además, la expresión de Slug correlaciona con resistencia en células de cáncer de páncreas y melanoma. Asimismo, también mostramos que Slug controla la capacidad metastásica de las células de resistentes y es un indicador de mal pronóstico en pacientes con cáncer de páncreas y melanoma.

INTRODUCTION

1. Pancreatic cancer

Pancreatic cancer represents the fourth leading cause of cancer-associated deaths in western countries, becoming one of the most lethal cancers worldwide. Besides, it is estimated to become the second cause of cancer-associated mortality within the next decades (Rahib et al. 2014; Neoptolemos et al. 2018). Although cancer mortality rates have been generally decreasing in the last decades thanks to the advances in early detection and the development of effective therapeutic approaches, the statistics for pancreatic cancer have been far to improve. The 5-year overall survival has remained dismally low (<5%) (Ryan et al. 2014) and is paralleled by an increasing trend in mortality. Global pancreatic cancer incidence practically overlaps with mortality rates (Kleeff et al. 2016) (Figure 1). Tumor resection remains the only option for cure in pancreatic cancer, despite the fact that only between 10 and 15% of patients fulfill the criteria for surgical removal (Winter et al. 2012). However, the majority of pancreatic cancers are diagnosed when they are unresectable and/or already metastatic (Hidalgo 2010), owing to the absence of clinical screening procedures for disease detection in early stages, when tumor resection is still a curative option. Pancreatic cancer is characterized as a considerably aggressive disease in which most of the patients will die with metastasis chiefly to liver, lungs and peritoneum (Yachida & Iacobuzio-Donahue 2009). Altogether, there is an urgent need for further improvements in early detection as well as in the development of effective treatments in order to maximize pancreatic cancer patients' survival.

a Mortality ASR, both sexes



b Incidence ASR, both sexes

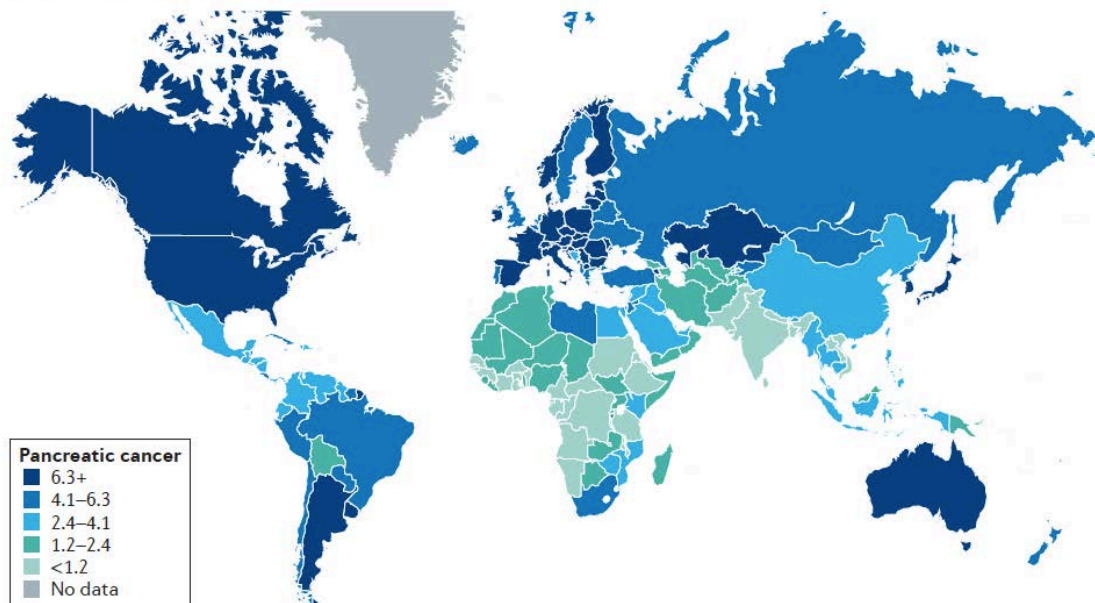


Figure 1 (Kleeff et al. 2016) **Global mortality and incidence rates of pancreatic cancer.** Estimated age-standardized rates (ASRs) of mortality (a) and incidence for both sexes (per 100,000 persons) in 2012 (b).

1.1 Anatomy of the pancreas

Pancreas (from Ancient Greek *pánkreas*, “all flesh”) is a mixed gland located behind the stomach that participates in two key physiological processes: enzymatic digestion and glucose metabolism. The gland is composed of two functional components that regulate its functions (Figure 2) (Bardeesy & DePinho 2002):

- The exocrine portion of the pancreas consists of a system of ducts and acini. The acinar cells secrete digestive enzymes and comprise the bulk of the pancreatic tissue. The ductal cells produce bicarbonate and mucus that is added to the enzymes produced in the acini, and build a network of increasing size in form of pancreatic ducts that finally drain into the duodenum. The acini are organized in grape-like structures, at the end of the ductal branching system.
- The endocrine pancreas is composed by a group of specialized cell types organized as clearly distinguishable islands distributed between the acini. The endocrine fraction of the pancreas secretes crucial hormones to the bloodstream, such as insulin, glucagon, somatostatin and pancreatic polypeptide (PP).

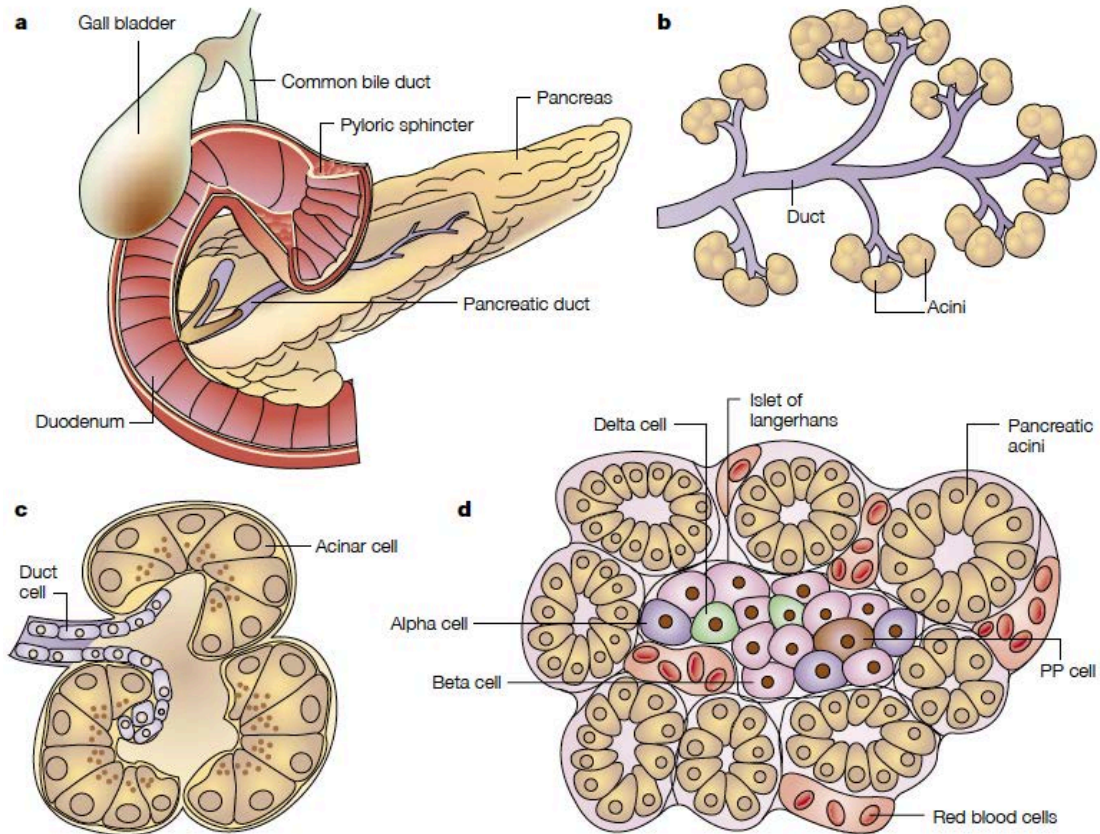


Figure 2 (Bardeesy & DePinho 2002). **Anatomy of the pancreas.** The pancreas is a mixed gland that participates in digestion and glucose metabolism and is located behind the stomach and drains into the duodenum (a). The exocrine portion of the pancreas is organized into grape-like structures of ducts and acini (b). The acinar cells (c) produce the digestive enzymes. The ductal cells add mucus and bicarbonate to the secreted enzymes and build a network of increasing size that conduct the final digestive mixture to the duodenum. The endocrine pancreas is composed by specialized cell types that form compact islands surrounded by acinar tissue (d) and produce insulin, glucagon, somatostatin and pancreatic polypeptide.

1.2 Biology and development of pancreatic cancer

Pancreatic Ductal Adenocarcinoma (PDAC) is the most common type of pancreatic cancer, representing nearly 90% of the newly diagnosed pancreatic neoplasms (Hackeng, Hruban, Offerhaus & Brosens 2016b; J. Yu et al. 2015). Neuroendocrine tumors are the next most frequent pancreatic neoplasms, accounting for 7-9% cases. Rare pancreatic neoplasms include: pseudopapillary tumors, acinar cell carcinoma, adenosquamous carcinoma, squamous cell carcinoma, colloid carcinoma, pancreatoblastoma, cystic adenocarcinomas, serous cysticadenoma or giant cell tumors (Hackeng, Hruban, Offerhaus & Brosens 2016a).

Regarding the precursor lesions that can give rise to pancreatic adenocarcinoma, the most frequent and widely studied are the pancreatic intraepithelial neoplasias (PanINs), found in more than 80% of pancreases with invasive carcinoma (Andea 2003). They consist of microscopic lesions in the primary duct that are histologically classified in three different stages of increasing cellular and nuclear atypia (PanINs 1-3) (Morris et al. 2010) (Figure 3). The advancing PanIN stages are also generally accompanied by an increase in cell proliferation (Klein et al. 2002). Because of their small size (less than 5 mm diameter), PanINs cannot be detected by noninvasive imaging and they are not related to any clinical symptomatology. This represents a major obstacle in the way of early detection of pancreatic cancer. Furthermore, despite the increasing knowledge regarding pancreatic cancer progression, the identification of the cell of origin remains elusive. Originally, it was considered that the initial lesions occurred exclusively in the ductal cells since PDAC exhibits ductal morphology and express ductal markers, such as cytokeratin 19 (CK19). However, recent reports have indicated that both acinar and ductal cells can give rise to PDAC upon K-Ras activation (Figura et al. 2014; Roy et al. 2015; La O et al. 2008).

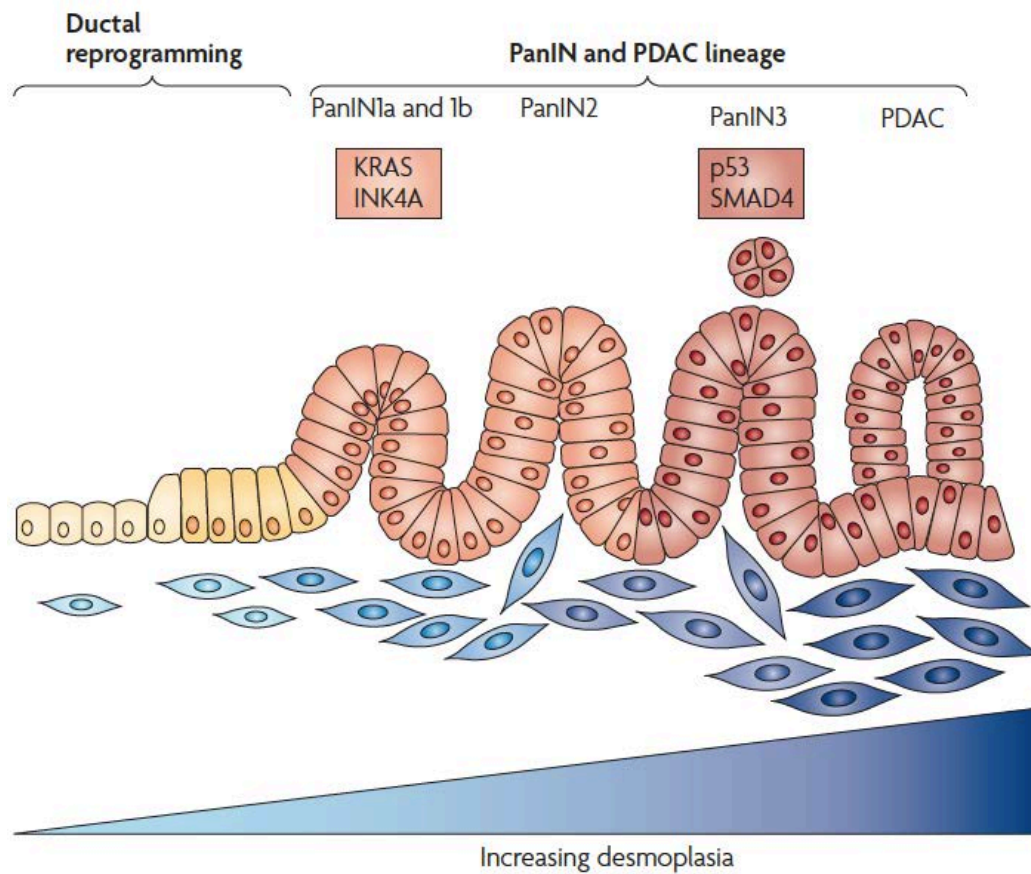


Figure 3 (Modified from Morris, Wang, et al. 2010). **PDAC initiation and progression.** Activating mutations in *KRAS* drive the formation of pancreatic intraepithelial neoplasias (PanINs), which are classified into different stages of increasing cellular atypia (PanINs 1-3). The successive PanIN stages are characterized by the acquisition of additional mutations (INK4A, TP53 and SMAD4 are well characterized). During PDAC development, the increase in cellular atypia is matched by a desmoplastic reaction of the stroma.

1.3 Genetics of PDAC

Disease progression across the different stages of pancreatic cancer, from minimally dysplastic tissue (PanINs grade 1) to more severe stages (PanINs 2-3) and finally to infiltrating adenocarcinoma, ensues in parallel with the sequential acquisition of genetic and epigenetic events (Figures 3 and 4).

Mutations in *KRAS* gene in chromosome 12p are practically universal in PDAC, accounting for approximately 95% cases (Almoguera et al. 1988; Smit et al. 1988; Hruban et al. 1993). *KRAS* belongs to the Ras family of proto-oncogenes and encodes for a small GTPase that transduces signals initiated on tyrosine kinase receptors (RTKs). Mutations in *KRAS* yield a K-Ras version with impaired hydrolase activity over GTP, thereby causing a constitutive and sustained signaling in its downstream effectors. K-Ras controls many cellular functions, and its constitutive activation culminates in many of the described phenotypic hallmarks of cancer including increase in cellular division and cell survival, metastatic dissemination, metabolic alteration, and evasion of the immune response (Bryant et al. 2014; Hanahan & Weinberg 2011; Pylayeva-Gupta et al. 2011). *KRAS* mutations have been described as the earliest genetic change detected during pancreatic cancer progression. *KRAS* activating mutation is already detected in PanIN1 lesions and the mutation frequency increases during disease progression. This, together with its almost universal presence in PDAC, has prompted some researchers to hypothesize that the appearance of activating mutations in *KRAS* are the key initiating event required for pancreatic cancer development (Kanda et al. 2012).

TP53 appears to be altered in 65-85% of pancreatic cancers (Hidalgo 2010; Yachida et al. 2012; Witkiewicz et al. 2015) leading to an oncogenic loss of function not always accompanied by a loss of protein expression. *TP53* encodes for p53, a transcription factor that can be activated by a plethora of stimuli, such as DNA damage, in different physiological contexts. When activated, p53 can trigger many cellular responses ranging from regulating cell cycle progression to apoptosis. *TP53* alterations are frequently observed in later stages, in PanIN-3.

CDKN2A is frequently (80-95%) inactivated in pancreatic cancer, either by promoter hyper-methylation, deletion or point mutations (Bardeesy & DePinho 2002; Schutte et al. 1997). *CDKN2A* is a highly complex tumor suppressor gene, located at chromosome 9q21, that encodes for two different tumor suppressor proteins: p16^{INK4A} and p14^{ARF}. Although p16^{INK4A} and p14^{ARF} transcripts differ in their first exon, they share exons 2 and

3. Of note, the exon 2 of p14^{ARF} mRNA comes from an alternative reading frame of the p16^{INK4A} (Sherr 2001). p16^{INK4A} controls cell cycle progression through the G1/S checkpoint by regulating the activity of CDKs, such as CDK4 and CDK6 and CDK-mediated phosphorylation of Rb1 protein, whereas p14^{ARF} prevents p53 degradation (Sherr 2001). *CDKN2A* loss contributes to increased genomic instability, thereby allowing for the accumulation of additional mutations. Alterations in *CDKN2A* can be broadly detected in PanIN1b and PanIN2 lesions (Kamisawa et al. 2016).

SMAD4 expression is lost in around 50% of pancreatic cancers (Hahn et al. 1996) SMAD4 is a co-transcription factor that functions as a key mediator of the canonical Transforming Growth Factor (TGF) beta signaling pathway, that is implicated in many cellular processes such as cell growth, survival, differentiation and tissue homeostasis (Shi & Massagué 2003). Loss of *SMAD4* occurs mainly in later stages, PanINs 3-4 (Wilentz et al. 2000).

Among additional genes and pathways that may be altered in pancreatic cancer we can also find *BRCA2*, *CTNNB1*, elements of the Integrin signaling and Hedgehog signaling (Jones et al. 2008).

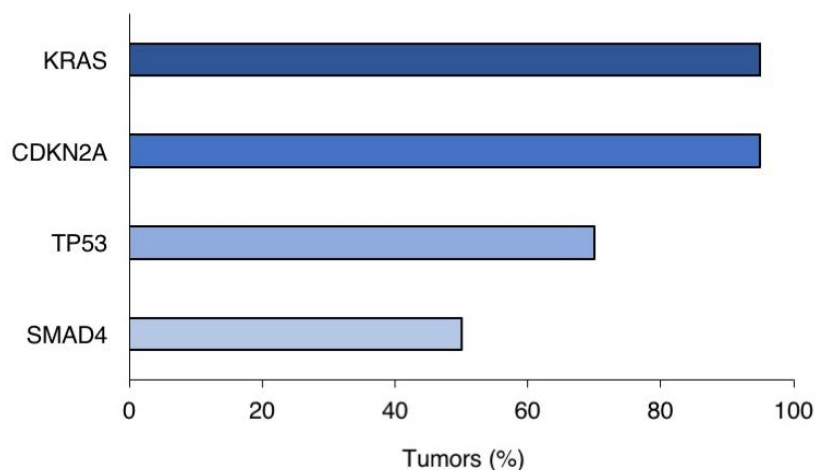


Figure 4 (Adapted from Kleeff et al. 2016). % Allele frequency of the most commonly altered genes in pancreatic cancer. The graph takes into account somatic mutations, homozygous deletions and epigenetic mechanisms of gene inactivation.

The genetic changes that promote oncogenic transformation that finally give rise to PDAC are accompanied by a profound remodeling in the tumor microenvironment.

1.4 Pancreatic cancer stroma

Pancreatic neoplasms are accompanied by a high desmoplastic reaction, that consists in the growth of connective tissue or stroma resulting in dense fibrosis surrounding the tumor. Pancreatic cancer stroma displays high degrees of inflammation, vascular collapse, poor vascularization and hypoxia. Pancreatic tumor stroma is composed of extracellular matrix (ECM) proteins such as collagen, enzymes, glycoproteins (such as fibronectin and laminin) and glycosaminoglycans. The neoplastic tissue promotes the continuous activation of pancreatic stellate cells (PSCs) into alpha smooth muscle actin positive (α -SMA)⁺ myofibroblasts (Makohon-Moore & Iacobuzio-Donahue 2016), that produce the collagenous matrix. PSCs have been suggested to facilitate, upon activation, cancer cell survival by inhibiting apoptosis (Hamada et al. 2012) and also by migrating to distant metastatic sites to help cancer cell seeding (Xu et al. 2010). In the literature, activated stellate cells are usually referred as cancer-associated fibroblasts (CAFs) (X. Chen & Song 2018). Although some findings might indicate a tumor promoting role of pancreatic tumor stroma, recent studies using genetic and pharmacological approaches to deplete pancreatic stellate cells show dissenting conclusions (Gore & Korc 2014; Rhim et al. 2014). In this thesis, we show that Mek1/2 inhibition increases collagen deposition in pancreatic tumors. Other cellular components of the pancreatic tumor microenvironment are endothelial cells and immune cells (Figure 5).

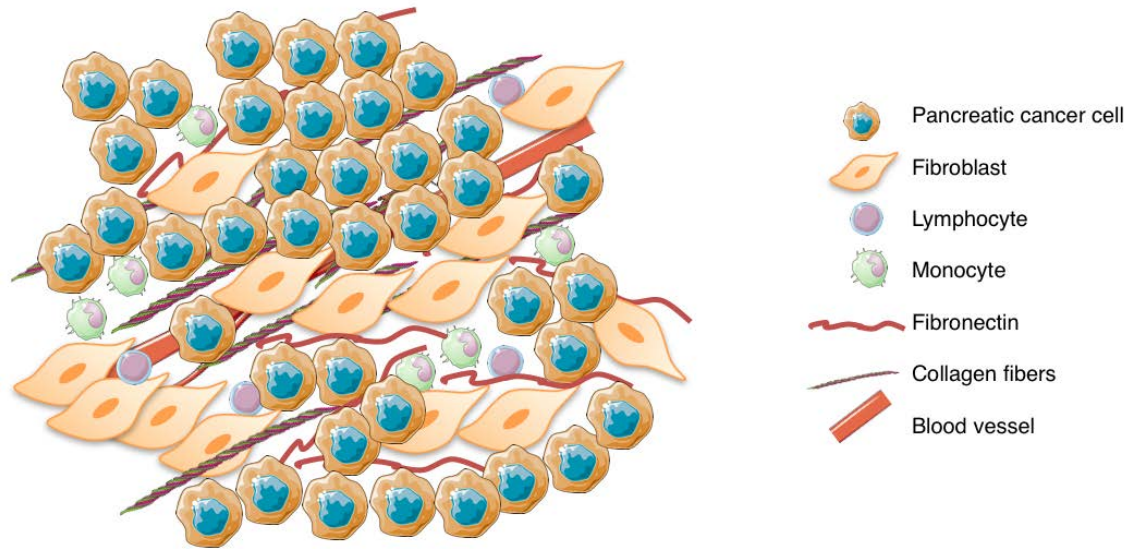


Figure 5. Pancreatic cancer microenvironment. Pancreatic cancer is composed by a highly desmoplastic stroma characterized by dense fibrosis enclosing the tumor. The pancreatic tumor stroma is composed by extracellular matrix components, such as collagen and fibronectin, among others. It also includes a variety of cell types: fibroblasts, endothelial cells and cells from the immune system.

1.5 Tumor heterogeneity

Cancer is a dynamic disease in which tumor cells can individually accumulate genetic and non-genetic alterations throughout tumor progression. Thence, tumors usually become more heterogeneous over time, harboring distinct tumor cell populations with divergent molecular alterations. The acquisition of the different clonal cell populations that constitute a heterogeneous tumor is not restricted to the early events of malignant transformation, but also occurs at later stages of tumor evolution. Heterogeneity can be due to genetic, transcriptomic, epigenetic or phenotypic changes (such as motility or metabolism). Intertumor heterogeneity applies to differences between patients with the same histological type of cancer, whereas intratumor heterogeneity is owing to differences within the same patient. In turn, intratumor heterogeneity can be classified as spatial (differences observed in the molecular profile of tumor cells across different regions of the disease) and temporal (changes in the subclonal distribution over time) (Figure 6 (Dagogo-Jack & Shaw 2018)). The development of genomic, transcriptomic and proteomic technologies has contributed to describe and better understand polyclonality in cancer. Transcriptomic profiling in patient samples and pancreatic cancer

xenografts showed differential gene expression throughout distinct regions within the same tumor (Nakamura et al. 2007; Harada et al. 2002).

Tumor heterogeneity plays a key role in tumor progression and resistance to anti-cancer therapies (Bhang et al. 2015; Jamal-Hanjani et al. 2017; Kwak et al. 2015; McGranahan & Swanton 2017). There is a considerable degree of tumor heterogeneity in pancreatic cancer (Bernard et al. 2019; Yun et al. 2018; Cros et al. 2018), which also may contribute to the clinical failure of many targeted therapies in unselected patients. Likewise, polyclonality has also been described in pancreatic cancer metastases (Campbell et al. 2010). In this work, we will address the impact of intratumor heterogeneity in pancreatic cancer in the response to Mek1/2 inhibition.

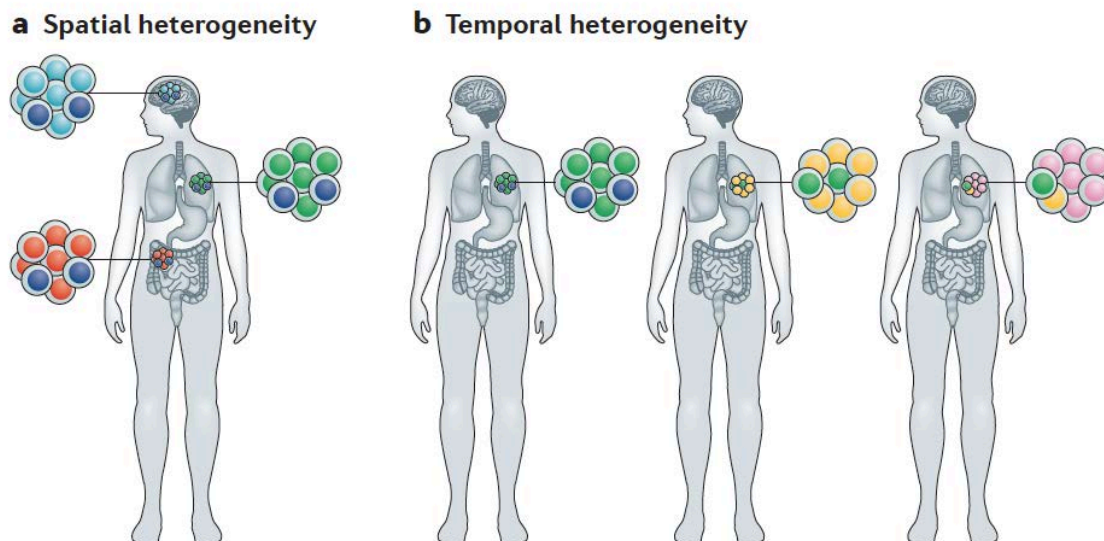


Figure 6 (Adapted from Dagogo-Jack & Shaw 2018). **Intratumor heterogeneity.** Spatial heterogeneity (a) refers to divergent clonal populations across distinct regions of the primary tumor or metastatic sites. Temporal heterogeneity (b) is acquired through the different molecular alterations that occur during disease progression and/or treatment cycles.

Overall, the degree of tumor heterogeneity observed in could contribute to explain why pancreatic cancers are so resistant to many of the therapies tested so far. However, other therapies have shed some light in the treatment of pancreatic cancer.

1.6 Pancreatic cancer treatment

The complex and heterogeneous genetics and metabolism as well as its diverse cellular components compromise the efficacy of the different therapeutic approaches tested so far. In addition, the lack of biomarkers of response does not facilitate treatment assignment and patient stratification. Although the overall 5-year survival data have remained unaltered in the last years, some improvements and advances have been reported recently.

Surgery still remains the only chance of cure; nevertheless, most patients relapse (Neoptolemos et al. 2018). The first trials showed substantial improvements in patients treated with adjuvant chemotherapy after tumor resection. Treatment with 5-fluorouracil (5-FU) after surgery for two years or until recurrence showed a significant improvement in patients' survival (Kaiser & Ellenberg 1985). Although this trial was carried out by the Gastrointestinal Tumor Study Group decades ago, it has become a solid influence for the development of further therapeutic options.

Further chemotherapeutic agents and chemoradiotherapy strategies have been tested, some of them bringing meaningful improvements. In 2017, the ESPAC-4 trial demonstrated higher potential of the combination of the chemotherapeutic agents gemcitabine and capecitabine in the adjuvant setting for resectable pancreatic cancer (Neoptolemos et al. 2017). The improved patients' survival (5-year survival near 30%) and acceptable levels of toxicity made the American Society of Clinical Oncology (ASCO) to recommend this combination of gemcitabine and capecitabine in adjuvancy for potentially curable pancreatic tumors (Khorana et al. 2017).

In borderline resectable pancreatic cancer, neoadjuvant chemotherapy with gemcitabine-capecitabine and the chemotherapy combination leucovorin calcium, fluorouracil, irinotecan hydrochloride, and oxaliplatin (combination named as FOLFIRINOX) showed a 23 month increase in patients' survival for neoadjuvant therapy and 11 months after subsequent surgery. Even in locally advanced, unresectable cases treatment with neoadjuvant FOLFIRINOX resulted in increase in resection rates, according to recent reports (Ferrone et al. 2015; Nitsche et al. 2015; Petrelli et al. 2015).

Among the palliative therapies used to treat patients with locally advanced unresectable and metastatic pancreatic cancer, monotherapy with gemcitabine remained the standard of care, based on a previous trial that compared 5-FU vs. gemcitabine in monotherapy

(Burris et al. 1997). None of the combinations tested of gemcitabine plus a second chemotherapeutic agent improved patients' survival.

However, in 2011 the PRODIGE 4/ACCORD 11 trial demonstrated that FOLFIRINOX regime had a significant superior clinical benefit, extending the median survival from 6.8 months observed with gemcitabine therapy, until 11.1 months in the FOLFIRINOX arm in metastatic pancreatic cancer (Conroy et al. 2011). Nevertheless, more adverse events were observed in the FOLFIRINOX group, for instance higher rates of febrile neutropenia. For this reason, the American Society of Clinical Oncology (ASCO) Clinical Practice Guidelines recommends both regimens in patients with good performance status, whereas only gemcitabine is recommended for metastatic pancreatic cancer patients with more delicate health status.

In 2013, a phase III trial evaluated the effect of the combination Nab-Paclitaxel plus gemcitabine compared to gemcitabine alone in metastatic pancreatic cancer. Nab-Paclitaxel is an albumin-bound, water-soluble derivative of paclitaxel. Nab-Paclitaxel can be easily administered with less adverse effects, in contrast to paclitaxel. The results of this trial revealed higher survival benefit in favor of the combination vs gemcitabine alone, with a median overall survival of 8.5 months for the combination Nab-Paclitaxel plus gemcitabine compared to the 6.7 months observed with gemcitabine alone (Hoff et al. 2013).

Despite the benefits observed in the first line treatments, most pancreatic cancer patients progress in few months. In order to meet this urgent need, research has to intensify in the finding of clinically relevant second line therapies. Although only few randomized clinical trials have been conducted, a study published in 2016 showed a clear benefit on patients treated with nanoliposomal irinotecan plus 5-FU-FA (5-Fluorouracil-Folinic acid) compared with 5-FU-FA in patients that progressed to gemcitabine treatment (Wang-Gillam et al. 2016). In this case, the median survival increased from 4.2 months to 6.1 months in the combination arm. Regarding patients that were refractory to FOLFIRINOX, gemcitabine plus nab-paclitaxel treatment resulted in a median survival of 8.8 months (Portal et al. 2015).

Figure 7 compiles the suggested therapeutic regimes successfully tested so far across the different stages of pancreatic cancer as well as second line therapies in order to circumvent patients' relapse (Neoptolemos et al. 2018). A wide number of targeted therapies have failed to improve patients' survival in the treatment of metastatic

pancreatic cancer, alone or in combination with chemotherapy. A variety of antiangiogenic compounds have been tested in metastatic pancreatic cancer. These compounds include vascular endothelial growth factor (VEGF) inhibitors and kinase inhibitors with antiangiogenic activity. However, these drugs did not provide any clinical benefit (Kindler et al. 2010; Rougier et al. 2013). Some hypotheses indicate that the dense hypovascular stroma surrounding the tumor hampers the efficacy of these compounds (Michl & Gress 2013).

In the past years, specific inhibitors targeting the multiple signaling pathways activated in pancreatic cancer have been tested in combination with the standard chemotherapies. However, the combination benefits have been sparse (Ottaiano et al. 2017). The failure of the targeted therapies tested so far can be due to a variety of factors and processes that rely on the inherent nature of pancreatic cancer, a complex disease with a high degree of tumor heterogeneity, dense desmoplastic stroma and high degrees of inflammation that can affect the delivery and half-life of the therapeutic compounds administered.

In this thesis, we will gauge the efficacy of the inhibition of the kinases Mek1/2 in pancreatic tumors as well as explore the resistance mechanisms that will compromise its effectiveness in patients.

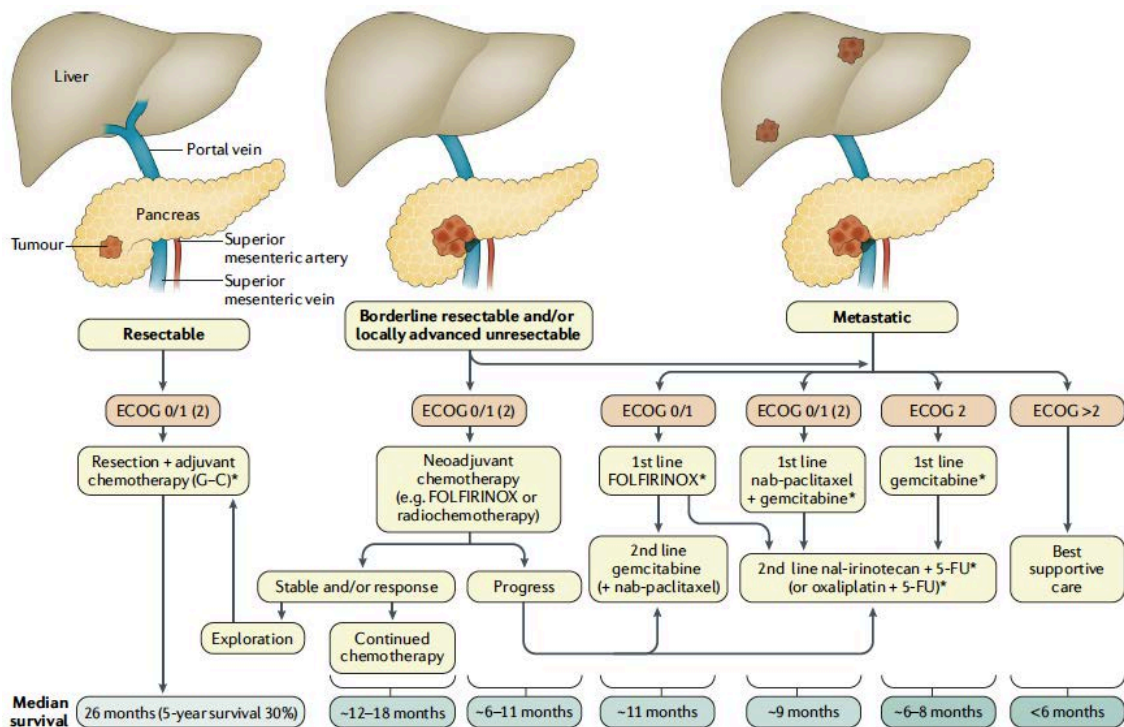


Figure 7 (Neoptolemos et al. 2018). **Suggested treatments for patients with pancreatic cancer based on the expert opinion of the authors.** The treatment regimens are given after patient stratification according to tumor stage (resectable, borderline resectable and locally advanced unresectable, and metastatic) and performance status (according to the Eastern Cooperative Oncology Group (ECOG) score). Median survival values are obtained from published trials. G-C, gemcitabine-capecitabine; nal, nanoliposomal

2. MAPK signaling

Mitogen-activated protein kinases (MAPKs) are a family of highly conserved serine/threonine/tyrosine kinases that mediate multiple intracellular processes such as growth, survival, migration, differentiation and apoptosis (Nithianandarajah-Jones et al. 2012). MAPKs transduce signals coming from growth factors, cytokines, hormones, neurotransmitters, cell-cell interactions and various environmental stressors. The MAPK signaling pathway consists of a three-tiered signaling process, that starts with the phosphorylation of the mitogen-activated kinase kinase kinase (MAPKKK) in response to distinct extracellular stimuli. The MAPKKK sequentially phosphorylates and activates its downstream target MAPKK, which phosphorylates MAPK. The final MAPK triggers the activation of its downstream effectors, that will mediate the cellular processes mentioned above. In mammals, the MAPK family is composed by four classical

subfamilies of MAPKs: extracellular-signal regulated kinases (ERK) 1/2, c-Jun N-terminal kinases (JNK) 1/2/3, p38 MAPK ($\alpha/\beta/\gamma/\delta$) and extracellular-signal regulated kinases (ERK) 5, also termed as Big MAPK1 (BMK1) (Figure 8).

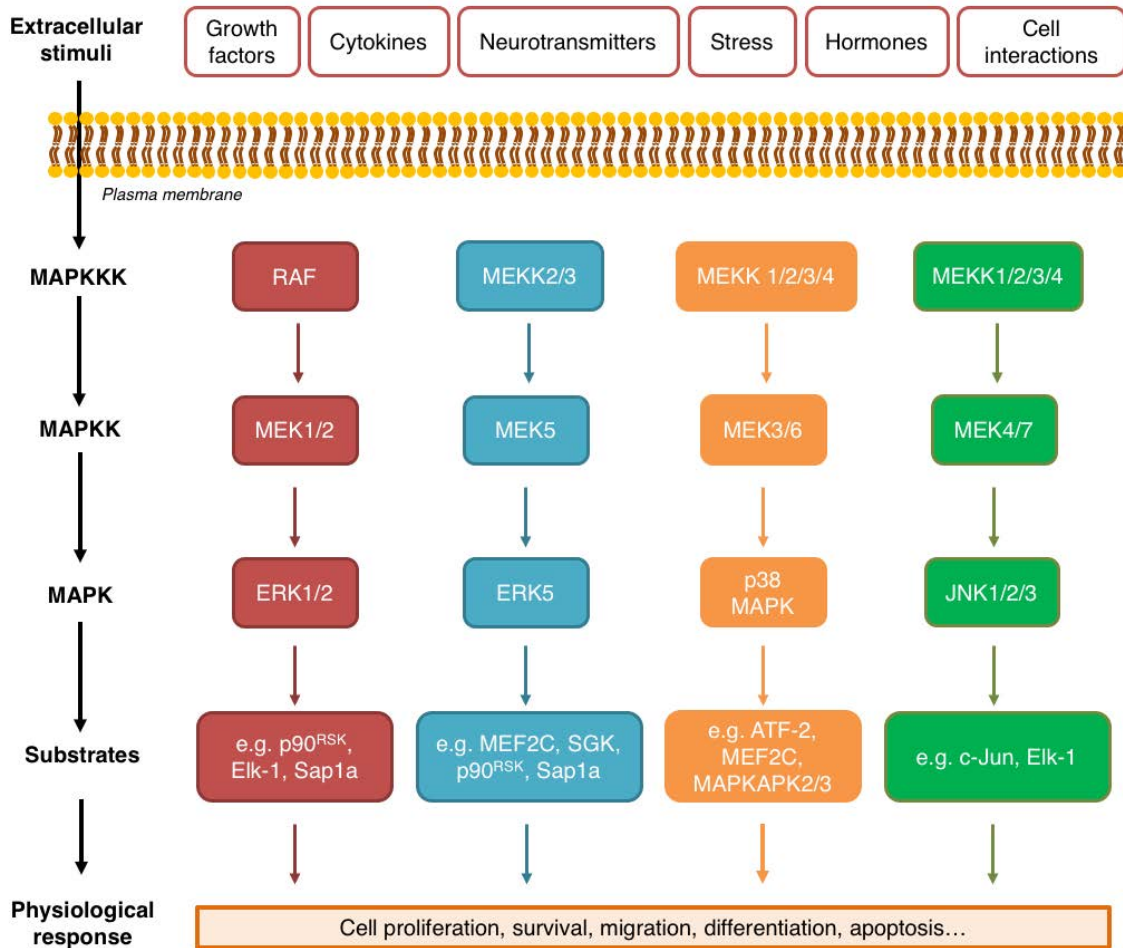


Figure 8. Overview of the distinct subfamilies of mitogen-activated protein kinases: Extracellular-regulated kinases 1/2 (red), extracellular-signal regulated kinases (ERK) 5 (blue), p38 MAPK ($\alpha/\beta/\gamma/\delta$) (purple) and c-Jun N-terminal kinases (JNK) 1/2/3 (green).

2.1 Ras-Raf-Mek-Erk signaling pathway

Ras family proteins are small GTPases that couple signals from activated tyrosine kinase receptors (RTKs). Ras GTPase activity is tightly controlled by cycling in an ON/OFF system that has been largely conserved in evolution. When Ras is active (ON state) is bound to guanosine triphosphate (GTP), whereas it turns inactive (OFF state) when

bound to guanosine diphosphate (GDP). Guanosine exchanging factors (GEFs) catalyze the exchange of GDP to GTP, whereas GTPase activating proteins (GAPs) stimulate Ras GTPase activity producing an inactive GDP-bound Ras (Bryant et al. 2014).

Ras is bound to the plasma membrane, a crucial requisite for activating downstream signaling pathways. After RTK activation, Ras is recruited by the guanosine exchanging factors (such as SOS) that catalyze its activation towards a Ras-GTP bound state. In its GTP-bound state, Ras is able to activate several effector proteins. One of the most important and frequent effectors are Raf serine/threonine protein kinases (A-Raf, B-Raf, C-Raf) that, upon homo or heterodimerization, phosphorylate and activate the kinases Mek1 and Mek2 which, in turn, activate Erk1 and Erk2 by phosphorylation at conserved threonine and tyrosine residues. The Ras-Raf-Mek 1/2-Erk 1/2 (also referred as Ras-MAPK) signaling cascade culminates in the differential activation of Erk 1/2-dependent downstream proteins, such as transcription factors that control cell proliferation and cell survival, such as Cyclin D1 (Lavoie et al. 1996) (Figure 9).

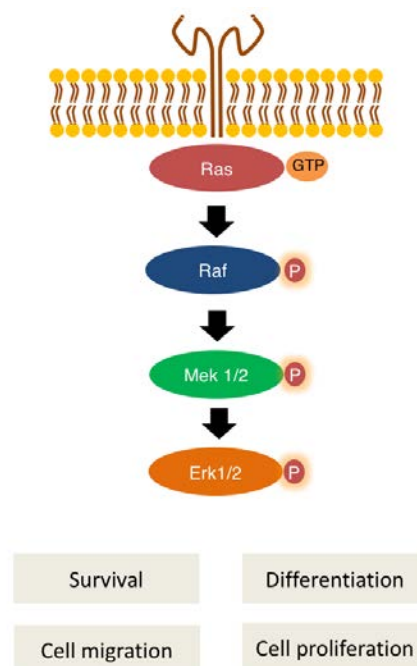


Figure 9. Ras-Raf-Mek1/2-Erk1/2 signaling pathway. Activated GTP-bound Ras phosphorylates and activates Raf, whose dimerization activates Mek1/2 which, in turn, phosphorylates Erk1/2. Phosphorylated Erk1/2 controls the expression genes involved in cell proliferation, survival, motility and differentiation, among others.

In normal conditions, after signaling activation, Ras is inactivated by GAPs, that increase the weak GTPase activity of Ras. As a result, the bound GTP is hydrolyzed to GDP, Ras is no longer active and dissociates from Raf effector proteins, turning the MAPK signaling pathway off (Figure 10). However, mutant Ras is constitutively active independently of external stimuli thereby allowing to the sustained activation of MAPK pathway. Mutant Ras cannot be longer inactivated by GAPs, which can still bind to mutant Ras but fail to trigger the GTPase activity (Bryant et al. 2014; Scheffzek et al. 1997; Scheidig et al. 1999). As a consequence, constitutive Ras-MAPK signaling leads to uncontrolled cell proliferation, an important feature of tumor cells. Genetic alterations in Ras family of proto-oncogenes are present in around 30% of cancers (Prior et al. 2012). The Ras subfamily of proteins comprises three different genes in humans: *KRAS* (present in more than 20% human cancers), *NRAS* (~8%) and *HRAS* (~3%) (Samatar & Poulikakos 2014; Baines et al. 2011). In pancreatic, colon and lung cancer, RAS family mutations almost exclusively belong to K-Ras (Simanshu et al. 2017). Although Raf kinases are the major effectors, Ras can activate additional downstream molecules, such as phosphoinositide 3-kinases (PI3Ks), phospholipase C (PLC) or Ras-like small GTPases (Ral-GEFs). As *KRAS* is almost universally mutated in pancreatic cancer, in this thesis we will target the Ras-Mek-Erk signaling pathway by inhibiting Mek1/2 in pancreatic tumor cells.

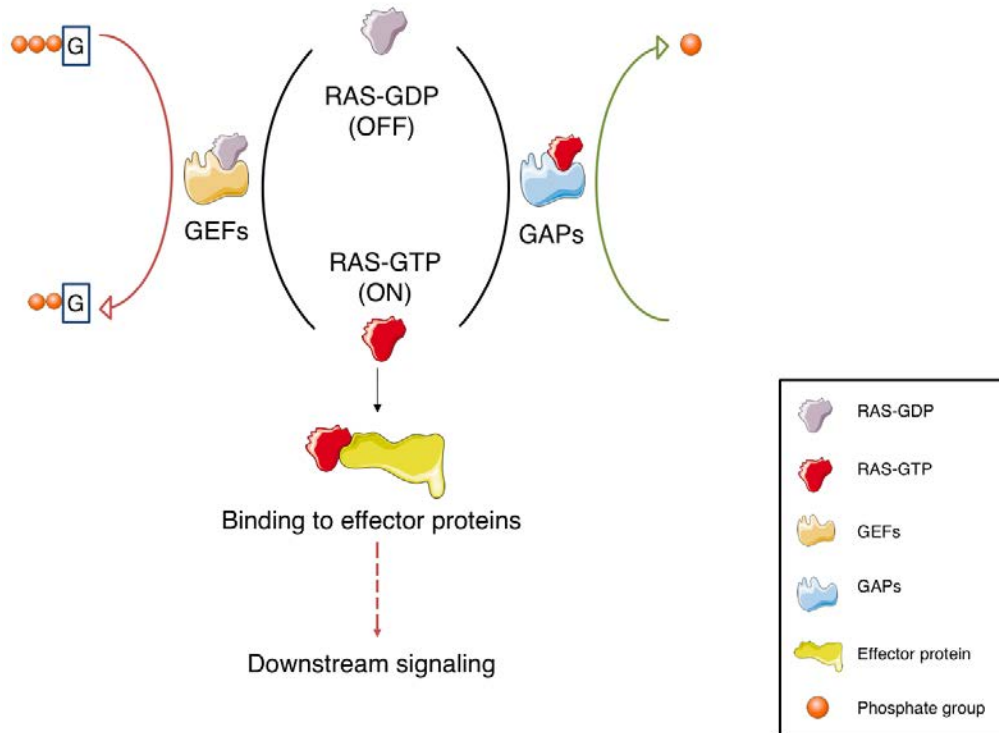


Figure 10. Ras cycles between an inactive GDP-bound and an active GTP-bound state. In normal cells, Ras is usually bound to GDP. However, after stimulation (for example, growth factors), Ras balances towards the active GTP-bound state, a process catalyzed by GEFs. Active Ras is able to bind to its several downstream effector partners (such as Raf, PI3K or PLC) thereby promoting a signaling cascade. Once Ras has exerted its function, the cycle is terminated and Ras inactivation is catalyzed by GAPs, that produce a Ras-GDP bound form.

2.1.1 Current approaches to target Ras-Mek-Erk signaling

Certainly, targeting deregulated Ras-MAPK signaling has been a major effort in cancer therapy in the last decades. The first agents intended to disrupt Ras activation were farnesyl transferase inhibitors (FTIs), that hampered Ras farnesylation, an important step for its correct association with the plasma membrane. Although FTIs showed promising results in preclinical studies in H-Ras driven tumors, these results were not achieved in K-Ras and N-Ras mutant backgrounds (James et al. 1996; Whyte et al. 1997). Despite of the plentiful efforts to efficiently target Ras driven pathway activation, this small GTPase still remains considered as “undruggable” up until now. This has changed the focus on targeting Ras downstream effectors, such as Raf, Mek 1/2 and Erk 1/2 proteins, that are crucial in the Ras-MAPK signaling cascade (Table 1).

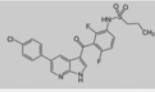
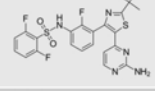
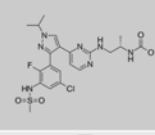
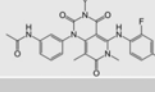
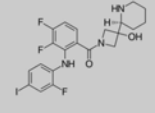
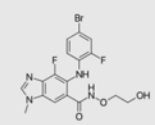
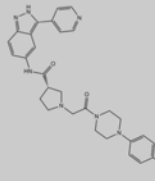
Inhibitor	Structure	Target	Clinical Phase
Vemurafenib		B-Raf (V600E)	Approved for the treatment of melanoma
Dabrafenib		B-Raf (V600E)	Approved for the treatment of melanoma
LGX818		B-Raf (V600E)	Approved for the treatment of melanoma in combination to MEK162
Trametinib		Mek1 and Mek2	Approved for the treatment of melanoma
Cobimetinib		Mek1	Approved for the treatment of melanoma in combination to vemurafenib
MEK162		Mek1 and Mek2	Approved for the treatment of melanoma in combination to LGX818
SCH772984		Erk1 and Erk2	Preclinical studies

Table 1 Summary of the most relevant available Raf, Mek1/2 and Erk1/2 inhibitors.

However, these promising strategies have also found obstacles with the emergence of resistance.

2.1.2 Resistance to Raf and Mek1/2 inhibitors

The development of efficient Raf, Mek1/2 or Erk1/2 inhibitors has supposed a major breakthrough in the preclinical and clinical setting for the personalized treatment of MAPK-dependent tumors (Yeh et al. 2007; Sebolt-Leopold et al. 1999; Samatar & Poulidakos 2014; Bollag et al. 2010; Chapman et al. 2011; Flaherty, Robert, et al. 2012b; Flaherty, Jeffery R Infante, et al. 2012a). Nonetheless, the observed initial response to these inhibitors is frequently followed by the emergence of resistance and therapy relapse. Resistance to Raf, Mek1/2 and Erk1/2 inhibitors may arise from different ways (Caunt et al. 2015):

1) Intrinsic resistance. In addition to the driver mutation causing MAPK activation, the tumor can also harbor secondary mutations that can significantly halt the anti-tumor effect of MAPK inhibition. This is the case of mutations in *PTEN*, *NF1* or *CCND1* amplifications (Smalley et al. 2008; Halilovic et al. 2010; de Bruin et al. 2014).

2) Adaptive resistance. In the presence of MAPK inhibitors, cells can rapidly adapt their signaling pathways and resume proliferation through changes in their kinome. MAPK signaling inhibits the expression of a wide range of RTKs and adaptor proteins such as B-Raf. Thence, the loss of negative feedback loops elicits the reactivation of the pathway and also the activation of alternative pathways, such as PI3K-Akt (Turke et al. 2012) or Stat3 signaling pathways (H.-J. Lee et al. 2014). Tumor associated fibroblasts can also mediate MAPK inhibitor resistance by generating drug-tolerant microenvironment with FAK-dependent survival signaling (Hirata et al. 2015).

3) Acquired resistance. Even cells that are not intrinsically or adaptively resistant almost unavoidably acquire resistance after prolonged treatments with MAPK inhibitors. Several mechanisms have been described, including gain of function mutations in Mek1/2 and amplification of the driver oncogenes B-Raf and K-Ras. These genetic alterations entail the restoration of Erk1/2 activity in the presence of B-Raf or Mek1/2 inhibitors, underscoring the dependence of these cells on active Erk1/2 signaling (Corcoran et al. 2010; Emery et al. 2009; Anon 2013). In addition, other acquired resistance mechanisms involve the activation of parallel pathways. Some of the alternative pathways heretofore reported include the activation of Hippo YAP/TAZ (Lin et al. 2015), cAMP/PKA (Johannessen et al. 2013), STAT3 (H.-J. Lee et al. 2014) or PAK signaling (Lu et al. 2017). Collectively, the activation of these signaling pathways restrain the efficacy of Raf and/or Mek1/2 inhibitors. In this thesis, we show that pancreatic cancer cells can acquire resistance to Mek1/2 inhibition after prolonged treatment and that they share similarities with intrinsically resistant cells. The mechanism of acquired resistance described in this work involves the activation of Mek5/Erk5 signaling.

2.2 Mek5-Erk5 signaling

Unlike the Mek1/2 - Erk1/2 signaling cascade, the Mek5-Erk5 signaling pathway has not been extensively studied. This signaling cascade has been implicated in the regulation of cell proliferation, anti-apoptosis, cell migration and angiogenesis (Drew et al. 2012). Mek5 is activated by MEKK2 or MEKK3 upon upstream stimuli (such as mitogens, cytokines and environmental stress). Upon activation, Mek5 phosphorylates and activates Erk5 (Figure 8). Compared to other MAP kinases, Erk5 has a particular large molecular weight (115 kDa, 44 and 42 kDa for Erk1/2), which results from its unique large C-terminus domain, that regulates activation, autophosphorylation, subcellular localization and nuclear shuttling (Drew et al. 2012). For this reason, Erk5 is also mentioned as Big Map kinase 1 (BMK1). There is an increasing knowledge about the involvement of Mek5/Erk5 signaling in the development of cancer and tumor progression (Simões et al. 2016). Mek5/Erk5 overexpression has been reported in prostate cancer (Mehta et al. 2003; McCracken et al. 2008), breast cancer (Montero et al. 2009; Miranda et al. 2015; Ortiz-Ruiz et al. 2014), colon cancer (Hu et al. 2012), osteosarcoma (Tesser-Gamba et al. 2012) and oral squamous cell carcinoma (Sticht et al. 2008). Likewise, it has been proven that Erk5 inhibition sensitizes tumor cells to various chemotherapeutic agents (Weldon et al. 2002; Montero et al. 2009; Antoon et al. 2013; Buschbeck et al. 2005). Overall, the increasingly observed influence of Mek5/Erk5 in human tumors demonstrates that this signaling is a potential target for the treatment of different types of cancer.

Additionally, Erk5 has been shown to be involved in the acquisition of mesenchymal and invasive traits of tumor cells (Pavan et al. 2018), which strengthen the increasing interest in this signaling. In this thesis, we show that pharmacological Erk5 inhibition decreases the expression of the EMT transcription factor Slug and prevents acquired resistance to Mek1/2 inhibition.

3. Epithelial to mesenchymal transition (EMT)

Epithelial to mesenchymal transition (EMT) is a highly plastic and dynamic process that has been intensively studied and characterized during the last decades. During EMT, epithelial cells lose their apical-basal polarity, detach from the epithelium and migrate to different regions. EMT has been described as a crucial event during normal

development, wound healing and the progression of diseases like organ fibrosis or malignant epithelial tumors (Nieto 2002; Cano et al. 2000). The reverse of this process is known as mesenchymal-to-epithelial transition, and it implies the cease of migration and acquisition of apico-basal polarization, as well as other epithelial hallmarks. The induction of EMT occurs in response to signaling factors that trigger the expression of tightly controlled proteins, called EMT-transcription factors (EMT-TFs), as well as microRNAs and epigenetic regulators (Nieto et al. 2016) that promote the switch towards a mesenchymal state. The EMT-TFs include the Snail superfamily of transcription factors (such as Snail and Slug), basic helix-loop-helix transcription factors (Twist1, Twist2) and zinc finger E-box binding transcription factors (Zeb1, Zeb2), among others. The acquisition of mesenchymal phenotype is classically paralleled by the loss of expression of epithelial cell markers such as E-cadherin and the gain of expression of mesenchymal markers like N-cadherin, vimentin or fibronectin (Figure 11, (Kalluri & Weinberg 2009)).

In cancer, EMT has been shown to be an initiating event for metastasis, forasmuch as it prompts the dissociation of tumor cells from the primary site towards distant organs thanks to the acquisition of mesenchymal traits (Lamouille et al. 2014). It has been reported that the expression of the EMT-TF Snail in breast tumors is sufficient to promote metastasis (Tran et al. 2014). Another Snail family transcription factor, Slug, has been shown to be essential in Twist1-induced EMT and metastasis (Casas et al. 2011). Likewise, the expression of Twist and Zeb proteins is increased in the highly aggressive, chemoresistant, claudin-low subtype of triple negative breast cancer (Prat et al. 2010). Several cancer-related processes can trigger the activation of the EMT-TFs: inflammation, physical and metabolic stress, and the aberrant activation of signaling pathways, such as TGF-beta, Wnt, Notch, Sonic Hedgehog, Ras-Erk and hypoxia. The increasing studies intended to describe the role of EMT in cancer exemplify the complexity of this process. EMT is a highly complex phenomenon, in which the functions of the different EMT-TFs are frequently non-redundant and tissue-specific. For instance, the pro-metastatic role of Snail in breast cancer could not be recapitulated in a pancreatic cancer model (Zheng et al. 2015), whereas Zeb1 silencing significantly prevented metastasis in pancreatic cancer (Krebs et al. 2017). Additionally, the EMT-TFs also exert pleiotropic roles, apart from inducing EMT. Twist proteins have been shown to inhibit the transcription of p19 and p21, thereby affecting response to p53 and preventing apoptosis (Ansieau et al. 2008; Maestro et al. 1999). Snail and Slug also alleviate the tumor suppressive activity of p53 (Wu et al. 2005; S.-H. Lee et al. 2009) and promote tumor growth (Olmeda et al. 2008). These reports indicating cell survival functions of the EMT-

TFs contribute to understand the observed role of EMT in chemoresistance (Shibue & Weinberg 2017).

In this work, we describe that the transcription factor Slug promotes resistance to Mek1/2 inhibition and metastasis in *KRAS* mutant pancreatic cancer cells.

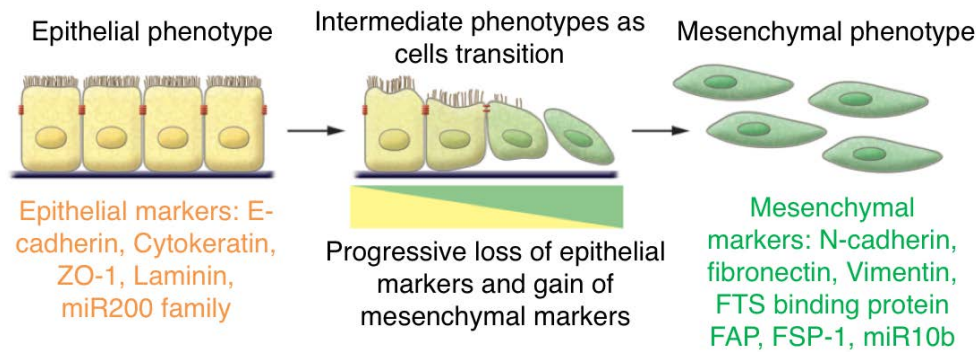


Figure 11 (Kalluri & Weinberg 2009). **Epithelial to mesenchymal transition.** Induction of EMT induces a series of changes in epithelial cells, that lose their cellular polarity and acquire mesenchymal properties. The EMT process is directed by tightly controlled EMT inducers, such as the EMT-TFs, and is paralleled by a switch from epithelial to mesenchymal cell markers.

3.1 Snail Family Transcriptional Repressor 2 (Slug)

SNAI2 (Slug) belongs to the Snail superfamily of zinc-finger transcription factors. The first identified member of this superfamily was Snail (*SNAI1*). Initially described in *Drosophila melanogaster*, it was found to be a crucial factor in mesoderm formation. In fact, its importance during embryo development is such that embryos with biallelic loss-of-function mutations in Snail were defective in gastrulation or mesoderm formation (Grau et al. 1984; Nüsslein-Volhard et al. 1984; Simpson 1983). Likewise, functional experiments conducted in chick and frog demonstrated the role of Slug in embryonic development, given that Slug silencing by siRNAs in embryos resulted in defects in early development, mainly inhibition of neural crest and mesoderm formation (Carl et al. 1999; Nieto et al. 1994). These defects were caused by a decrease in cell migration, which was the first evidence of the potential role of Snail family in EMT.

Slug-deficient mice are viable although they evidence developmental defects affecting melanocytes, hematopoietic and germ cells (Pérez-Losada et al. 2002). In human

beings, it has been found that heterozygous deletion results in piebaldism (Sánchez-Martín et al. 2003), whereas its homozygous deletion has been associated to Waardenburg syndrome type 2 (Sánchez-Martín et al. 2002). *SNAI2* is located in the chromosome 8 in the cytogenetic region 8q11.21. The encoded protein (Slug) is composed by 268 amino acids that form the final 30 kDa protein.

Regarding protein structure, Slug shares homology to other members of the Snail family of transcription factors. All family members share a highly conserved carboxyl-terminus region that consists of four to six C₂H₂-type zinc fingers that interact with specific sequences of the DNA. The consensus DNA binding site contains a core of six nucleotides (CAGGTG). The amino-terminal region is less conserved although in most of vertebrates contains an evolutionary conserved SNAG domain. In contrast to the rest of members of the family, Slug contains a SLUG domain next to the zinc fingers region. When Slug is bound to the DNA, it acts as a transcriptional repressor (Hemavathy et al. 2000). The repressor activity depends not only on the zinc fingers within the C-terminus region but also on the SNAG domain in the N-terminus (Figure 12).

Slug has been shown to regulate the expression of genes involved in self-renewal (such as *BMI1*, *NANOG*), EMT (*CDH1*, *HDAC1*, *CLDN1*, *MUC1*), cell survival (*BCL2*, *BBC3*) and cell cycle control (*CDKN1A*, *RBL1*) (Cobaleda et al. 2007). In addition, a recent report indicated that Slug auto-regulates its activity by binding to its own promoter (Kumar et al. 2015).

The role of Slug in human cancer has also been extensively studied (Cobaleda et al. 2007). Enhanced Slug expression has been found in leukemias (Inukai et al. 1999), breast cancer (Elloul et al. 2005; Hajra et al. 2002), esophageal carcinoma (Uchikado et al. 2005), colorectal carcinoma (Shioiri et al. 2006) and gastrointestinal stromal tumors (Pulkka et al. 2017), and it usually correlates with poor prognosis. Slug expression has also been associated with resistance to radiotherapy, chemotherapies and targeted therapies (Pérez-Losada et al. 2003; Lund et al. 2015; Chang et al. 2011; Mancini et al. 2010; Chung et al. 2011), which is consistent with its described role preventing apoptosis (Inukai et al. 1999; Haupt et al. 2006; Cobaleda et al. 2007; Wu et al. 2005; Inoue et al. 2002). Gene amplifications in the regions covering the *SNAI2* gene have also been reported in an array of human cancers, such as different types of leukemia, colorectal cancer, gastrointestinal stromal tumors, hepatoblastoma or breast cancer, among others (Cobaleda et al. 2007). Mice expressing a tetracycline-inducible Slug transgene

developed mesenchymal tumors, mainly leukemias and sarcomas (Pérez-Mancera et al. 2005). Thus, Slug is an attractive target for therapeutic modulation.



Figure 12. Schematic diagram of the essential domains involved in Slug function. Slug, in contrast to other Snail family transcription factors, contains a SLUG domain. The SNAG domain and the zinc finger region are crucial in the repressive activity.

4. Preclinical models of pancreatic cancer

Heretofore, there is a variety of genetically engineered mouse models and xenograft models that serve as powerful experimental and preclinical tools for the study of early detection, disease progression, therapeutic approaches for treatment, chemoresistance or chemoprevention, to finally improve patients' outcome (Herrerros-Villanueva et al. 2012).

4.1 Genetically engineered mouse models

Genetically engineered mouse models (GEMMs) can recapitulate the wide spectrum of pathological stages during pancreatic cancer progression. The use of these models has prompted some of the most significant advances in the study of the molecular mechanisms underlying the development of pancreatic cancer.

There have been many efforts to finely dissect the genetic bases of pancreatic cancer in the last decade. Indeed, the ability of mutant K-Ras to drive PDAC was clearly assessed in GEMMs. To develop a Cre-inducible conditional system (*lox-stop-lox Kras^{G12D}*), in which mutant K-Ras is expressed under an endogenous pancreatic-specific promoter, mice expressing LSL-Kras^{G12D} were crossed to mice that expressed Cre recombinase

under the control of pancreatic-specific promoters: pancreatic and duodenal homeobox 1 (*Pdx1*) and pancreas transcription factor-1 (*Ptf1a*, also mentioned as *p48*) (Hingorani et al. 2003). Intriguingly, although early-stage PanINs incidence was nearly universal and the degree of the lesions was increasing over time, the vast majority of mice failed to develop advanced PDAC and it only was observed in few mice at late stages (Morris et al. 2010), thus indicating that additional genetic events are needed for disease progression.

As the low penetrance of PDAC development in those mouse models was underscoring their potential to study advanced stages of the disease, many researchers started to generate mouse models of mutant *KRAS* combined with loss of function tumor suppressor alleles frequently altered in PDAC, such as *TP53*, *CDKN2A* or different components of the TGF beta signaling pathway (Hingorani et al. 2005; Aguirre et al. 2003; Bardeesy et al. 2006; Ijichi et al. 2006). These mice fully develop PDAC and recapitulate many aspects of the human disease such as histopathological features, genetic instability, and activation of fundamental signaling pathways required for disease progression (Table 2).

Genotype	Phenotype	Reference
Pdx1-Cre;Kras ^{G21D}	Develops PanINs, increasing severity with age. PDAC development in few cases, long latency	Hingorani et al. 2003
Ptf1a ⁺ /Cre;Kras ^{G21D}	Develops PanINs, increasing severity with age. PDAC development in few cases, long latency	Hingorani et al. 2003
Pdx1-Cre;Kras ^{G21D} ; p53 ^{R172H}	Metastatic PDAC with short latency	Hingorani et al. 2005
Pdx1-Cre;Kras ^{G21D} ; Ink4a/Arf ^{flox/flox}	PDAC with short latency and high penetrance	Aguirre et al. 2003
Pdx1-Cre;Kras ^{G21D} ; Smad4 ^{flox/flox}	IPMN to PDAC progression	Bardeesy et al. 2006
Ptf1a ⁺ /Cre;Kras ^{G21D} ; Tgfbr2 ^{flox/flox}	Accelerated PanIN formation and undifferentiated PDAC	Ijichi et al. 2006
Mist1 ^{KrasG12D/+}	Acinar-derived PanINs; mixed subtypes of pancreatic cancer	Tuveson et al. 2006
Ptf1a ⁺ /Cre;Kras ^{G21D} ; p53 ^{R172} ; Brca2 ^{Tr/D11}	Accelerated PDAC, resembling human disease	Skoulidis et al. 2010

Table 2. Summary of relevant genetically engineered mouse models for the study of pancreatic neoplasms.

However, GEMMs fail to recapitulate the complexity of the human disease and their relevance for the study of personalized cancer treatments is limited.

4.2 Xenograft mouse models

Pancreatic tumor xenograft models have emerged as a powerful tool for preclinical studies. A widely used xenograft model is the subcutaneous injection of cell lines grown in culture in immunocompromised mice. This model has the advantage that cell lines are easy to manipulate and can be rapidly expanded. The use of subcutaneous cell line-derived xenografts has favored the study of the immediate impact of specific genetic alterations *in vivo*, like tumor growth, metastatic ability or response to therapies. In order to mimic better the native microenvironment of the disease, orthotopic models, in which the tumor cells are directly implanted in the organ from which the cancer is originated, emerged as more accurate approaches. Beyond growing tumor cells in a more natural microenvironment, orthotopic models provide more insights in the study of metastasis, given that subcutaneous models rarely metastasize. However, despite their tremendous value in preclinical studies, these models fail to recapitulate the complex genetic heterogeneity observed in human samples. That particular drawback was successfully circumvented by implanting patient-derived tumor tissue in mice. Pancreatic cancer patient-derived xenografts (PC-PDXs) are an invaluable tool in the study of personalized treatments since they retain the individual characteristics of the tumor of origin, such as histological architecture as well as tumor heterogeneity (DeRose et al. 2011; Hidalgo et al. 2014). PC-PDXs can be maintained and propagated from mouse to mouse once the tumor burden reaches a determinate size (Figure 13).

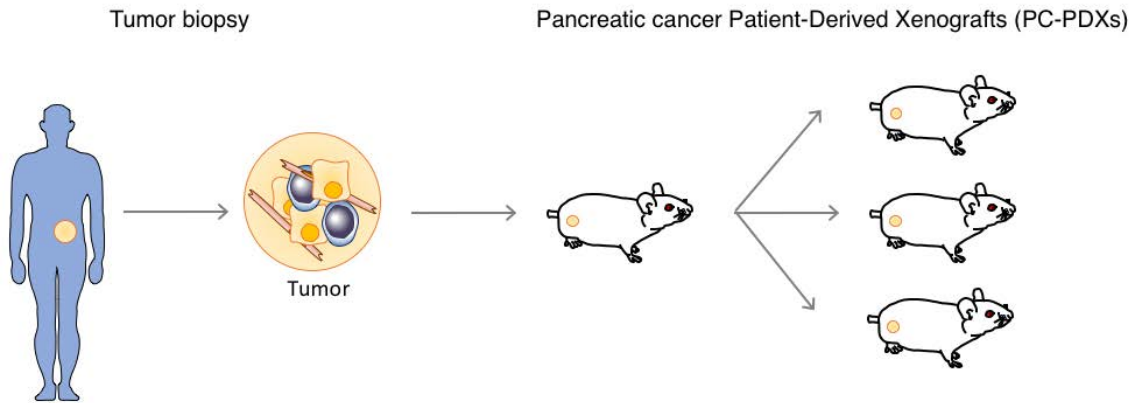


Figure 13. Pancreatic cancer patient derived-xenografts (PC-PDXs) constitute a powerful approach in the field of personalized medicine. PC-PDXs are established directly from implanting patient tumor tissue into immunocompromised mice, and can be propagated to additional mice once the tumor reaches a considerable size.

In this thesis, we will use both cell line models and PC-PDX models to evaluate the effectiveness and resistance of the selective Mek1/2 inhibitor MEK162 either alone or in combination with the standard chemotherapy.

HYPOTHESIS & RESEARCH

OBJECTIVES

I. HYPOTHESIS 1

Mek1/2 inhibition in combination with standard chemotherapy is a useful therapeutic strategy against PDAC.

To test this hypothesis, the following objectives were established:

- Compare the effect of different chemotherapeutic regimes in the growth of pancreatic cell lines and PC-PDXs.
- Test the effectiveness of the Mek1/2 inhibitor MEK162 alone and in combination with chemotherapy *in vitro*.
- Assess the efficacy of MEK162 alone and in combination with chemotherapy in pancreatic cancer patient-derived xenografts and cell lines implanted subcutaneously and orthotopically in mice.
- Explore potential mechanisms of resistance.

II. HYPOTHESIS 2

Pancreatic cancer cells acquire resistance after prolonged treatment of Mek1/2 inhibition.

To test this hypothesis, the following objectives were established:

- Generate resistance to MEK162 in MIA PaCa-2 cells.
- Characterize the mechanisms of resistance by genomic and transcriptomic analyses.
- Validate candidate genes and pathways that could be responsible for resistance.
- Study the relevance of the resistance mechanisms in additional models and cohorts of patients.

MATERIALS & METHODS

Commercial cell lines.

The pancreatic cancer cell lines MIA PaCa-2, Panc 10.05, HPAF-II, CFPAC-1 and BxPC-3 were purchased from ATCC (Manassas, VA, USA). The cells were grown at 37 °C in presence of 5% CO₂ and in pancreatic medium: Dulbecco's modified Eagle's medium/F-12 (Invitrogen, Thermo Fisher Scientific, Waltham, MA, USA) supplemented with 10% fetal bovine serum, 2.5% horse serum, 2 mM L-glutamine and 1x antibiotic–antimycotic (Gibco, Thermo Fisher Scientific).

The melanoma cell lines A375, SK-MEL-37, SK-MEL-131 and MeWo were a gift from Dr. Laura Soucek lab. The cells were grown in DMEM (Invitrogen, Thermo Fisher Scientific, Waltham, MA, USA) supplemented with 10% fetal bovine serum, 2 mM L-glutamine and 1x antibiotic–antimycotic (Gibco, Thermo Fisher Scientific).

Primary cell cultures.

To obtain primary cell cultures from pancreatic cancer PDXs, tumor pieces of approximately 750-1000 mm³ were minced with scalpels and digested in digestion solution: 300 U/ml collagenase IA (Sigma-Aldrich, St Louis, MO, USA) in 10 ml pancreatic medium for 1 hour at 37°C in a 15 ml conical tube (Corning Life Sciences, New York, NY, USA). The digested tissue was centrifuged at 300 RCF for 5 minutes. The pellet of digested tissue was resuspended in 13 ml pancreatic medium. 15-20'' were allowed for the undigested tissue to precipitate at the bottom of the conical tube. The supernatant containing the digested tissue was seeded in a 10 cm cell culture dish (Corning Life Sciences, New York, NY, USA). Once several colonies of epithelial cells were attached, the medium was replaced twice a week until confluence and then cell cultures were expanded.

For colony isolations, 2-4 weeks after seeding, individual colonies of epithelial cells were collected using 150 µl cloning cylinders (Sigma-Aldrich). 50 µl 0.05% Trypsin-EDTA (Gibco) were loaded into each cylinder. The colonies were subsequently grown and expanded until they were ready for experiments.

Proliferation assays.

To determine proliferation, MIA PaCa-2, Panc 10.05, HPAF-II, CFPAC-1, HPAF-II, BxPC-3, A375, SK-MEL-37, SK-MEL-131 and MeWo cells were seeded in two 96-well plates (time 0 and time 72h) with 1100 cells in 85 μ l per well, except for one column to which 85 μ l of medium without cells was added to provide a background reference value. After 24 h, the cells were fixed in the first plate (time 0) by adding 80 μ l 10% glutaraldehyde to each well followed by 30-min incubation. After washing wells with water, this plate was kept at 4 °C and later stained together with the other plates. In the rest of the plates, 85 μ l of medium with or without different concentrations of drug was added to all wells and then returned to the cell incubator for another 72 h. After 3 days, cells were fixed. The wells were washed in water, dried for 5 min upside down on paper and then stained with 70 μ l of 0.1% crystal violet solution. Finally, the wells were washed, dried overnight and assayed with 10% acetic acid and 560 nm absorbance measurements. For the pancreatic cancer-derived primary cultures, 2400 cells were seeded in 85 μ l per well and cells were grown for 6 days.

Cell cycle analysis.

Cells were analyzed for cell cycle progression after 24 h in the presence or absence of the different drugs. First, cells were trypsinized, washed with 1X phosphate-buffered saline (PBS) and fixed with 70% ethanol for 30 min. After two washes in PBS, cells were incubated with DNA extraction solution (0.2 M Na₂PO₄, 0.1 M citric acid, pH = 7.8) for 10 min at 37 °C. Finally, cells were incubated with propidium iodide/RNase solution (40 μ g/ml PI and 10 μ g/ml RNase in 1X PBS) for half an hour followed by flow cytometry analysis.

Generation of resistant cell cultures.

In the first approach (R1), cells were treated after attachment with 1.2 μ M MEK162, that corresponded to 10-12 times the IC₅₀, previously determined by dose-response assays. After 2 days, cell culture was replenished with drug-free medium until cells were confluent. In the second strategy (R2), MIA PaCa-2 cells were treated with increasing concentrations of MEK162, starting from 2x IC₅₀ and increasing over time,

until reaching around 1.2 μM in the last round of treatment. During this strategy, MEK162 was maintained in the medium until confluence.

In vitro adhesion, migration and invasion assays.

For assessing cell adhesion, cells were labeled with 5 μM of Cell Tracker Green reagent (Invitrogen), following the manufacturer's protocol, and kept overnight in serum-free medium. 24 hours later, 5×10^4 cells were seeded in triplicates in 24-well plates previously coated with 300 $\mu\text{g}/\text{ml}$ Corning Matrigel matrix (Corning) in 1X DMEM F-12. Two hours after seeding, cells were washed carefully with 1X PBS and fixed with 4% formalin. Fixed cells were visualized and counted using the Fiji software (Schindelin et al. 2012). A total of 5 pictures per well were taken. Normalized number of cells are shown, and two-sided t-test was used to analyze statistical differences between groups.

Migration assay. Cells were labeled with 5 μM of Cell Tracker Green reagent (ThermoFisher), following the manufacturer's protocol, and kept overnight in serum-free medium. 24 hours later, 5×10^4 cells were seeded in triplicates in 10 $\mu\text{g}/\text{ml}$ fibronectin (Sigma-Aldrich) coated Fluoroblok BD Biocoat Cell Culture Inserts (Corning) in serum-free medium, while the wells were loaded with complete growth medium.

Eight hours after seeding, cells were washed with 1X PBS and fixed with 4% formalin. Migration to the basolateral side was visualized and counted using the Fiji software. A total of 5 pictures per well were taken. Normalized number of cells are shown, and two-sided t-test was used to analyze statistical differences between groups.

Invasion assay. Cells were labeled with 5 μM of Cell Tracker Green reagent, following the manufacturer's protocol, and kept overnight in serum-free medium. Next day, 5×10^4 cells were seeded in triplicates on 300 $\mu\text{g}/\text{ml}$ matrigel-coated Fluoroblok BD Biocoat Cell Culture Inserts in serum-free medium, while the wells were loaded with complete medium. Eight hours after seeding, cells were washed with PBS and fixed with 4% formalin. Migration to the basolateral side was visualized and counted using the Fiji software. A total of 5 pictures per well were taken. Normalized number of cells are shown, and two-sided t-test was used to analyze statistical differences between groups.

Therapeutic compounds.

Gem was purchased from Vall d'Hebron's University Hospital pharmacy as a 38 mg/ml perfusion solution. Nab-P and Aza were provided by Celgene (Summit, NJ, USA) as Abraxane (5 mg/ml) and Vidaza (25 mg/ml), respectively.

For *in vitro* uses, Gem, Nab and Aza were re-suspended in medium. For *in vivo* experiments, Gem, Nab and Aza were diluted in 0.9% NaCl to 4 mg/ml, 2 mg/ml and 0.4 mg/ml before administration by intraperitoneal injection of 20, 10 and 2 mg/kg, respectively.

The Mek1/2 inhibitor MEK162 was provided as powder by Novartis (Basel, Switzerland). For *in vitro* experiments, MEK162 was diluted in DMSO (ATCC, Manassas, VA, USA) to a final concentration of 10 mM. For *in vivo* administration, a suspension of MEK162 in 10% Tween-80 was incubated ON at 4 °C before diluting 20-fold with 1% Na-carboxymethylcellulose and 0.5% methylcellulose, respectively. The final concentration of active MEK162 was 1.5 mg/ml, which was administered orally by gavage to 15 mg/kg morning and evening.

The Erk1/2 inhibitor SCH772984 and the Erk5 inhibitor XMD8-92 were purchased from Selleckchem (Houston, TX, USA) and diluted in DMSO for *in vitro* use. The Mek5 inhibitor BIX02189 was purchased by MedChem Express (Monmouth Junction, NJ, USA).

PC-PDX models

All animal studies were performed in accordance with ARRIVE guidelines and the three Rs rule of replacement, reduction and refinement principles. Mice were housed and treated according to protocols approved by the CEEA (Ethical Committee for the Use of Experimental Animals) at the Vall d'Hebron Institute of Oncology (VHIO), Barcelona, Spain. NOD-SCID and BALB-c Nude mice were purchased from Charles River Laboratory (Wilmington, MA, USA). Mouse weights were determined twice a week and recorded for every experiment. The anonymized human samples used were part of the tissue biological material of the Vall d'Hebron University Hospital. The samples had been collected with a signed patient consent form and were used with the approval of the Ethics Committee of the Hospital. Heterotopic xenografts were generated from tumors of patients that underwent pancreatectomy at the hospital: when routine pathological

gross examination of a resected pancreas led to the detection of a suspected neoplasia, a slice with a thickness of 1–3 mm was transferred to RPMI-1640 medium containing 1x antibiotic–antimycotic (Gibco, Thermo Fisher Scientific) and kept on ice; within approximately 30 min the tissue sample was cut into pieces of about 10 mm³ under sterile conditions, suspended in Matrigel (BD Biosciences, Franklin Lakes, NJ, USA) and transported to the specific pathogen free area of the animal facility. One tumor piece was implanted subcutaneously into the flank of two or three female 6-week-old NOD-SCID mice. When successfully grafted, tumors reached a size of around 750 mm³ they were transplanted to new mice. From the third round of transplantation, 6-week-old BALB-c Nude mice were used for further expansion of the xenografts.

The samples used for the generation of PC-PDX6, 10, 21 and 27 were classified as classic ductal adenocarcinomas during their pathological evaluation. The sample that produced PC-PDX30 originated from a needle biopsy of a liver metastasis in a patient with advanced PC. The passages of the PDX used in each experiment are labeled using the following nomenclature: PC-PDX6.p7 (PC-PDX6.Passage 7).

Animals from the same round of transplantation were randomized into the different experimental groups 2 days before the first treatment. Tumor size was evaluated every third day by caliper and tumor volume calculated using the formula: volume = 0.5 × length × (width²). After the treatment ended the animals were killed, tumors collected and fixed overnight in neutral pH-buffered 4% formalin. A pathologist confirmed the histopathological characteristics of xenografts from the expansion phase and after the treatments. PDXs intended for two-photon microscopy analysis, were resected after perfusion with 0.9% NaCl followed by 4% formalin. The tissue samples were preserved by incubation in 30% sucrose in 1x PBS at 4 °C ON and subsequently embedded in OCT.

Subcutaneous injection of MIA PaCa-2 and resistant cells

0.8×10^6 MIA PaCa-2 and resistant cells were resuspended in 50% Matrigel:PBS and injected subcutaneously in BALB-c Nude mice. When tumors were palpable (2-3 weeks after injection) and reached a 100-200 mm³ of tumor volume, mice started to be treated with MEK162 5 times a week during 4 weeks.

Hematoxylin–eosin, immunohistochemistry and fibrosis staining

For immunohistochemistry, fixed tissue samples embedded in paraffin were sectioned at 4 μm thickness. Sections were heated at 60°C, deparaffinized with xylene and hydrated with two steps of incubation with different dilutions of ethanol. Antigen retrieval was performed by boiling the samples for 20 minutes in citrate buffer pH 6. Endogenous peroxidase was blocked by incubating the slides in the presence of 3% peroxide hydrogen (Merck Millipore) diluted in absolute methanol. Slides were also blocked with 3% BSA (Sigma-Aldrich) in 1x PBS for 10 minutes. Then, samples were incubated with primary antibodies diluted in EnVision FLEX Antibody Diluent (Agilent technologies, Santa Clara, CA, USA) overnight. Primary antibodies used were as follows: Ki67 (30-9; Ventana Medical System, Roche, Basel, Switzerland), CK19 (A53B/A2.26; Cell Marque, Sigma-Aldrich), P53 (DO-7; Ventana Medical System, Roche), MUC1 (H23; Ventana Medical System, Roche), Ca19.9 (121SLE; Ventana Medical System, Roche), p-ERK1/2 (Thr202/Tyr204; Cell Signaling, Danvers, MA, USA), Slug (1:500, ab27568, Abcam), p-ERK5 (1:100, #3371, CST). Next, the slides were incubated in EnVision System- HRP Labelled Polymer Anti-Rabbit Secondary antibody. The samples were finally stained with DAB substrate chromogen (Agilent technologies) for 1-4 minutes and counterstained with Harris Hematoxylin for 2 minutes, followed by dehydration with ethanol and xylene, and finally mounted in DPX.

Picrosirius Red stain kit (Polysciences, Inc., Warrington, PA, USA) was used to stain for collagen types I and III according to the manufacturer instructions. Images were obtained with an Olympus (Shinjuku, Tokyo, Japan) BX41 microscope and DP71 camera.

For western blot, protein extracts were isolated by lysing the cells in Radioimmunoprecipitation Assay Buffer (RIPA) buffer (150 mM NaCl, 1% NP-40, 0.5% Sodium Deoxycholate, 0.1% SDS and 50 mM Tris pH 7.4) supplemented with 5 μM β -glycerophosphate, 5 μM sodium fluoride, 1 μM sodium orthovanadate and cOmplete™, EDTA-free Protease Inhibitor Cocktail (Sigma-Aldrich, 1 tablet per 50 ml lysis buffer). Protein lysates were resolved by SDS PAGE and then transferred to a 0.45 μm nitrocellulose membrane (GE Healthcare Biociences, Chicago, IL, USA). 20-30 μg protein lysate were loaded per experiment. Membranes were incubated with 5% BSA (Sigma-Aldrich) or 5% milk in 1X Tris-buffered saline (TBS) with 1% tween (TBS-T, Sigma-Aldrich). After blocking, membranes were incubated overnight with primary antibodies.

After washing three times with TBS-T, membranes were incubated with horseradish peroxidase-conjugated antibodies (GE Healthcare) for 1 hour. Membranes were developed with Immobilon Western Chemiluminescent HRP Substrate (Millipore) and protein bands were visualized in Amersham™ Imager 600 (GE Life Sciences).

Antibodies used were: ERK1/2 (1:1000 from stock; #9102, Cell Signaling Technology (CST)), p-ERK1/2 (1:1000; #9101, CST), AKT (1:1000 from stock; #9272, Cell Signaling Technology (CST)), p-AKT (1:1000; #9271, CST), Tubulin (1:1000; sc-9104, Santa Cruz Biotechnology (SCBT)), GAPDH (1:5000; 2275-PC-100, Trevigen), Slug (1:1000, #9585, CST), Fibronectin (1:1000, Ab299, Abcam), Vimentin (1:1000, #5741, CST), ERK5 (1:1000, #3372, CST), p-ERK5 (1:1000, #3371, CST).

Human phospho-kinase antibody array

The relative levels of phosphorylation of 43 kinase phosphorylation sites and two related total proteins were assessed by using a commercial human phospho-kinase antibody array (R&D systems, Minneapolis, MN, USA).

Whole cell lysates were prepared according to manufacturer's protocol. 300 µg protein were diluted in array buffer and loaded into the corresponding membranes containing the spotted capture antibodies overnight. Protein expression was detected by biotinylated phospho-specific detection antibodies and then visualized by chemiluminescence according to the manufacturer's protocol.

Two-photon microscopy and second harmonics generation

Unstained Xenograft tumors were cut 300 µm thick and visualized using a two-photon microscope (2PM:Zeiss LSM 510 META NLO; equipped with a broadband Mai Tai-HP-femtosecond single box tunable Ti-sapphire oscillator, with automated broadband wavelength tuning 700–1,020 nm from Spectraphysics, Newport (Irvine, CA, USA), for two-photon excitation) with Plan Apochromat 20/0.8 (Carl Zeiss, Oberkochen, Germany).

For collagen second harmonic imaging, a wavelength of 880 nm was used.

Viral infections

For lentivirus production, HEK293T cells were transfected with the pMD2.G (#12259, Addgene, Watertown, MA, USA) envelope expressing plasmid and the psPAX2 (#12260, Addgene) lentiviral packaging vector, using polyethylenimine (PEI, Polysciences, Warrington, PA, USA) as transfection agent. 24 hours after transfection, the growth medium was replaced with medium containing 5mM sodium butyrate. 48 hours later, viral particles-containing supernatant was harvested and filtered with 0.45 µm con PVDF filters. For infections, approximately 35% confluent target cells were incubated with the viral supernatants (diluted 1:5 in growth medium) and 1:1000 polybrene (Sigma) overnight. Infected cells were selected with 1 µg/ml puromycin, starting 2 days after infection, and subsequently maintained with 0.5 µg/ml puromycin in the growth media.

For retrovirus production, HEK293T cells were transfected with pCMV-VSV-G (#8454, Addgene) envelope plasmid and pUMVC packaging vector (#8449, Addgene), using PEI as transfection agent. The rest of the steps proceeded as described above.

For expressing luciferase, the Lentiviral Dual Reporter CMV-GFP-T2A-Luciferase plasmid (system biosciences, Palo Alto, CA, USA) was used. pPGS-hSLUG.fl.flag was used for overexpressing Slug (#25696, Addgene). For Slug silencing, the plasmids were obtained from the MISSION® shRNA Library (Clones TRCN0000271239, TRCN0000271298, TRCN0000271300, TRCN0000271362 and TRCN0000271389, Sigma).

Orthotopic mouse model of pancreatic cancer

To study the effect of MEK162 in the metastatic ability of MIA PaCa-2, cells expressing firefly luciferase were suspended in 1 × PBS and 50% Matrigel to 80000 cells/µl. Using a 27-gauge needle, 10 µl cell suspension was injected into the tail of the pancreas of 7-week-old female BALB-c Nude mice. The rate of tumor growth was monitored weekly by in vivo bioluminescence imaging with the IVIS-200 imaging system from Xenogen (PerkinElmer, Waltham, MA, USA). The day after the last treatment, the mice were sacrificed and all major organs resected in order to determine the existence of distant metastasis by IVIS imaging. Orthotopic tumors of PC-PDX10 were prepared by injection of 10 µl cell suspension in NOD-SCID mice. The cell suspension was prepared from a subcutaneously grown PDX of ~ 500 mg that was minced with a scalpel, digested in 10 ml Dulbecco's modified Eagle's medium/F-12 containing 500 U/ml Collagenase type IV

(Worthington, Lakewood, NJ, USA) at 37 °C for 30 min, washed in pancreatic medium and then 1x PBS, and finally suspended in 0.5 ml 1 × PBS and 0.5 ml Matrigel.

For comparing the metastatic ability of MIA PaCa-2 and resistant cells expressing firefly luciferase, cells were suspended in 1 × PBS and 50% Matrigel to 80000 cells/μl. Using a 27-gauge needle, 10 μl cell suspension was injected into the tail of the pancreas of 7-week-old female BALB-c Nude mice. The rate of tumor growth was monitored weekly by in vivo bioluminescence imaging with the IVIS-200 imaging system from Xenogen. To study the metastatic ability of the injected cells, mice were sacrificed and all major organs resected in order to determine the existence of distant metastasis by IVIS imaging

[Amplicon-Seq VHIO-card panel](#)

An initial multiplex-PCR with a proof-reading polymerase was performed on the samples, using a panel of over 600 primer pairs targeting frequent mutations in oncogenes plus several tumor suppressors, covering 57 different genes (Supplementary Table S2). SBS-Illumina compatible libraries were generated by adapter ligation after end repair and A-tailing of amplicon products. Indexed libraries were pooled and loaded onto a MiSeq instrument and sequencing performed (2X100). Initial alignment was performed with BWA after primer sequence clipping and variant calling was done with the GATK Unified Genotyper (Cambridge, MA, USA) and VarScan2 (St Louis, MO, USA) followed by ANNOtate VARIation annotation. Mouse genome reads were filtered, as well as single-nucleotide polymorphisms (using dbSNP and 1000 genome data sets). All detected variants were manually checked.

[Exome sequencing](#)

DNA was isolated from fresh cell pellets washed in 1x PBS, using the QIAmp DNA Mini kit (Qiagen, Hilden, Germany) according to the manufacturer's protocol. DNA libraries were prepared using the Agilent (Santa Clara, CA, USA) SureSelect XT Library Prep Kit according to the manufacturer's protocol. Target enrichment was performed using the Agilent SureSelect XT Human All Exon v5 capture set. Sequencing with 100 base paired end reads of targeted enrichment libraries was performed on the HiSeq 2500 sequencer. A quality check of the raw data was performed using the FastQC tool (<http://www.bioinformatics.babraham.ac.uk/projects/fastqc/>). Reads were filtered first by

quality using FASTX-Toolkit (v. 0.0.14, http://hannonlab.cshl.edu/fastx_toolkit/index.html) and then by length using HOMER (La Jolla, San Diego, CA, USA) (v. 4.7). The remaining reads were mapped to the Sanger human reference (hg19) by bwa (v. 0.6.2) with default settings. The resulting binary alignment map files were processed using SAMtools (San Francisco, CA, USA) (v. 0.1.19) and the Genome Analysis ToolKit (GATK) release 3.2.0. (Cambridge, MA, USA). In brief, binary alignment map files were binary compressed, sorted, and indexed by SAMtools (samtools view, sort, and index tools), duplicated reads were then removed by the SAMtools function rmdup, and base quality score recalibration and local realignment around indels followed the recommended workflow of the GATK toolkit (RealignerTargetCreator, IndelRealigner, BaseRecalibrator and PrintReads). Variants were called by VarScan (v2.3.7) with the following parameters: minimum variant allele frequency of 5%, a minimum coverage of 10 reads, at least 7 reads that confirm the mutation and a P-value below 0.05. Annotation of the vcf files was performed with ANNOtate VARIation. Variants were filtered: variant positions must not be listed as a single-nucleotide polymorphism in the 1000 genome project; variant position must be annotated as exonic by RefSeq (Release 45); and synonymous/nonsynonymous calls were made and the synonymous excluded from further analysis. All filtering was performed using in house parsers.

Digital droplet PCR

To determine the frequency of the mutation E193Q in LRRC69, L11V in CCDC151 and P934L in FLT3, DNA samples were analyzed by the ddPCR system QX100 from Bio-Rad (Hercules, CA, USA) according to and with reagents from the manufacturer. The DNA oligos used were designed and supplied by Applied Biosystem (Foster City, CA, USA) (custom TaqMan single-nucleotide polymorphism genotyping assays). Amplification oligos for LRRC69 E193Q were 5'-GAAGCTTTTGCTAGCCAGAAACAA-3' and 5'-AGCAAACACTACTGTGGTTCCATGTT-3', whereas wild type and mutant-specific probes were 5'-TTTTGCCGGAGGTAAG-3' (-VIC) and 5'-TTGCCGCAGGTAAG-3' (-FAM), respectively.

For CCDC151 L11V, amplification oligos were 5'-TCCACACCCACACATGCA-3' and 5'-GGCCTCGTGTAGGTGTGAAC-3', whereas wild type and mutant-specific probes were 5'-CACCTCAGTTTCTTAC-3' (-VIC) and 5'-CACCTCACTTTCTTAC-3' (-FAM),

respectively. For FLT3 P934L, amplification oligos were 5'-GCTGGGCTTTTGAAGCAAGGA-3' and 5'-CATCTGCCAGCTGACATCCTAAAA-3', whereas wild-type and mutant-specific probes were 5'-TAGGGAAGGATGGCCGTT-3' (-VIC) and 5'-TAGGGAAGGATAGCCGTT-3' (-FAM), respectively. A gradient analysis revealed that the optimal annealing temperature for these oligo-set was 59 °C for LRRC69 E193Q and FLT3 P934L, and 60 °C for CCDC151 L11V. Genomic DNA samples were prepared with the QIAamp DNA Mini kit from Qiagen and digested with EcoNI (New England Biolabs, Ipswich, MA, USA) for LRRC69 mutations and EcoRI (Sigma-Aldrich) for CCDC151 and FLT3 mutations. Duplicate reactions for analysis of samples prepared from *in vitro* grown clones contained 250 ng of DNA each. The analysis of PCPDX21 and PC-PDX27 DNA were performed on pooled data from 15 reactions for each condition with 500 ng DNA in each well.

The DNA probes for detecting the different KRAS mutations were supplied by Bio-Rad Laboratories (ddPCR probes for mutation detection in human). Droplets were thermal cycled according to the manufacturer's protocol. The references for the different probes were: WT: dHsaCP2500597; G12D: dHsaCP2500596; G12V: dHsaCP2500592; G12R: dHsaCP2500590.

RNA isolation and qRT-PCR

Total RNA was isolated from adherent cells by using the RNeasy Mini Kit (Qiagen, Hilden, Germany) according to the manufacturer's protocol. RNA was eluted from silica-membrane RNeasy spin columns in RNase-free water and quantified using NanoDrop™ 2000 spectrophotometer (Thermo Fisher Scientific).

cDNA was prepared from 2 µg template RNA using the High Capacity cDNA Reverse Transcription Kit (Thermo Fisher Scientific) according to manufacturer's protocol.

Real-time quantification of transcript abundance was determined by qRT-PCR using the Taqman Gene Expression probes and TaqMan Universal Master Mix II, with UNG (Thermo Fisher Scientific) following the manufacturer's protocol, in 384-well plates in 7900HT Fast Real-Time PCR System (Thermo Fisher Scientific).

RNA-seq preparation and data analysis

RNA was extracted using the RNeasy Mini Kit (Qiagen) according to the manufacturer's recommendations. RNA quantity and purity were measured with the NanoDrop spectrophotometer (Thermo Scientific). TruSeq Stranded Total RNA kit protocol (Illumina Inc. San Diego, CA, USA) was used to prepare the RNA-Seq libraries: Briefly, Ribosomal RNA (rRNA) was depleted from 1.0 ug of total RNA using the RiboZero Magnetic Gold Kit (Illumina Inc.). rRNA-depleted samples were fragmented, cDNA was synthesized and converted into sequentiable libraries. The size and quality of the libraries were assessed with a High Sensitivity DNA Bioanalyzer assay (Agilent Technologies).

Libraries were sequenced in a HiSeq2000 instrument, with a read length of 2x100bp. On average, 84 million paired-end reads were generated per sample. Images analysis, base calling and quality scoring of the run were processed using the manufacturer's software Real Time Analysis (RTA 1.18.64) and followed by generation of FASTQ sequence files by CASAVA. The quality of the reads was checked using the FastQC tool (<https://www.bioinformatics.babraham.ac.uk/projects/fastqc/>) and RNA-SeQC (DeLuca et al. 2012). Low-quality reads were discarded by fastx toolkit (v. 0.0.14) (http://hannonlab.cshl.edu/fastx_toolkit/). TopHat was used to map the RNA-Seq reads to the GRCh37/hg19 genome allowing a maximum of three mismatches. The resulting bam files were sorted, indexed using the picard tool (v. 1.79) (<http://broadinstitute.github.io/picard/index.html>) and were used to calculate the numbers of the reads which were mapped to the exons of a gene based on Cufflinks (Trapnell et al. 2012). Data were normalized to reads per kilo-base of the exon model per million mapped reads (RPKM), which is the representation of the expression values of the genes. Finally, through Cuffdiff in Cufflinks, Differentially Expressed Genes (DEGs) were obtained with the cutoff of $|\log_2(\text{Ratio})|$ more than 1 and an FDR-adjusted-pvalue less than 0.05.

RESULTS

SECTION 1: Pancreatic cancer heterogeneity and response to Mek1/2 inhibition

1.1 Effect of different drugs on the proliferation of pancreatic cancer cell lines.

To identify effective and clinically relevant therapeutic combinations for the treatment of pancreatic cancer, we chose the therapeutic agents Gemcitabine (Gem), Azacitidine (Aza), Nab-Paclitaxel (Nab-P) and MEK162 (also known as binimetinib) and we assessed their efficacy in four K-Ras mutant pancreatic cancer cell lines.

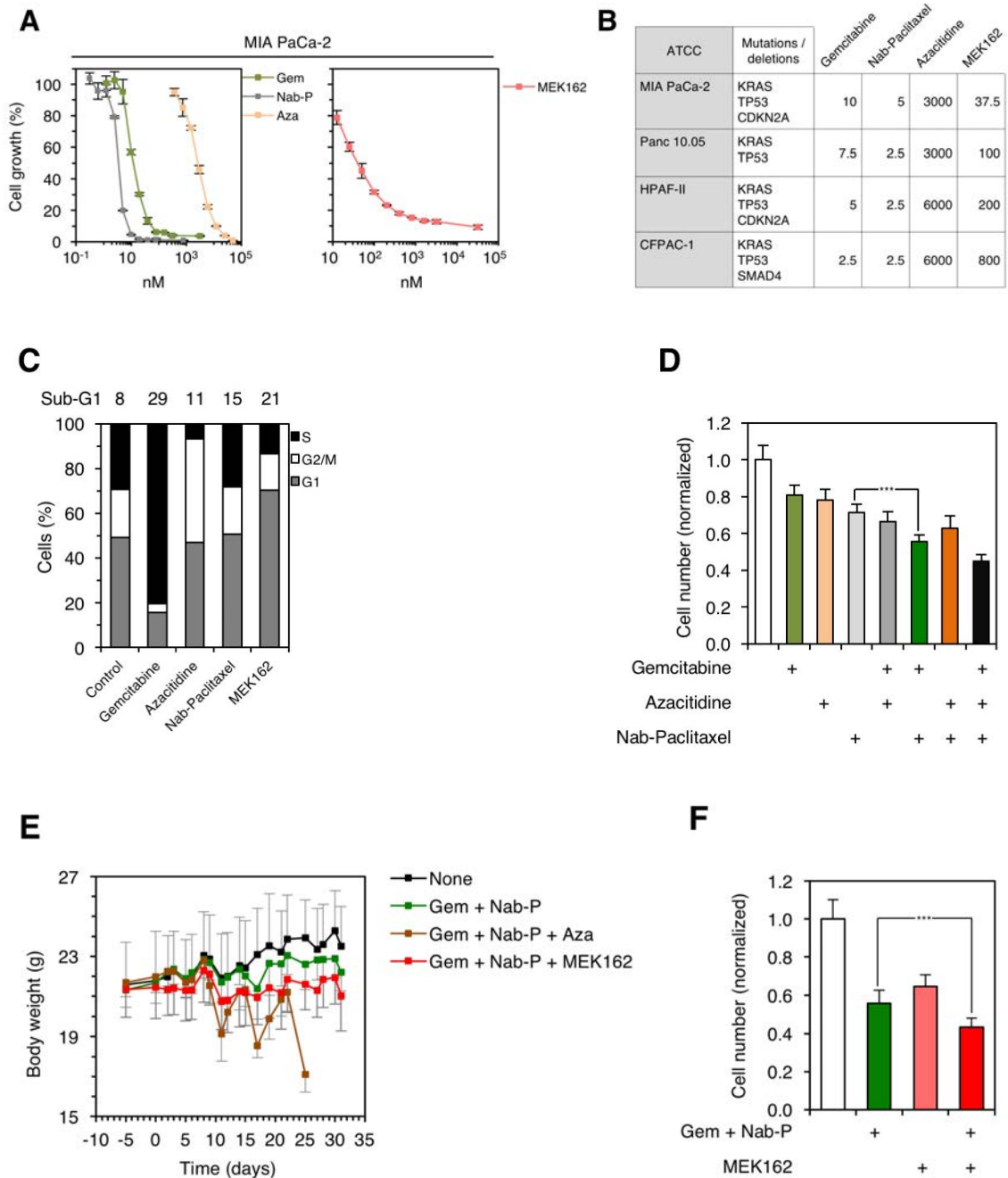
Gem is a nucleoside analog that induces DNA damage and apoptosis due to inappropriate DNA replication. Aza is an inhibitor of DNA methyltransferases that has been proposed to impair tumor cell proliferation by inducing the expression of epigenetically silenced tumor suppressor genes, such as p16. Nab-P is a taxane that stabilizes microtubules, impairs chromosome segregation and prevents cell division. In addition to these chemotherapeutics, we also tested the effect of MEK162, a small molecule inhibitor that targets Mek1 and Mek2, key regulators of Erk1/2 signaling, theoretically required by PDACs to progress.

Dose-response experiments *in vitro* showed that the three chemotherapeutic drugs had similar effectiveness, that is, comparable IC50s, in the four pancreatic cancer cell lines (MIA PaCa-2, Panc 10.05, HPAF-II and CFPAC-1) (Figure 12A, left and B). In contrast, the sensitivities to Mek1/2 inhibitor varied among the different cell lines, as the IC50s ranged from ~ 50 nM in MIA PaCa-2 cells to ~ 800 nM in CFPAC-1 cells (Figure 12A, right and 12B).

To better understand the anti-proliferative effects of these drugs, we studied their influence in the cell cycle in MIA PaCa-2 cells. According to cell cycle distribution, Gem and Aza exerted a marked cell cycle arrest in the S and G2/M phase, respectively, whereas MEK162 induced arrest in G1 phase. Gem, Nab-P and MEK162 increased apoptosis, as determined by the percentage of cells in the sub-G1 phase (Figure 12C).

To test the effect of chemotherapeutic combinations, we used Gem, Nab-P and Aza at sub-optimal concentrations, corresponding to approximately IC25. The combination Gem/Nab-P inhibited cell proliferation more efficiently than the combination Aza/Nab-P and Gem/Aza (Figure 12D). The triple combination Gem/Nab-P/Aza was the most effective *in vitro*; nonetheless, it was excessively toxic *in vivo*, as assessed by a dramatic decrease in body weight in mice. (Figure 12E). Therefore, we focused on the Gem/Nab-P combination as a chemotherapeutic backbone to test the efficacy of further drugs.

In this context, the Mek1/2 inhibitor, MEK162, increased the efficacy of Gem/Nab-P in MIA PaCa-2 cells (Figure 12F). Certainly, MEK162 efficiently prevented Erk1/2 phosphorylation at the concentration tested for the study (Figure 12G). Importantly, this combination did not show toxicity *in vivo*, according to the body weight of treated animals (Figure 12E). Based on these results, we determined the efficacy of the selected drug combinations *in vivo*.



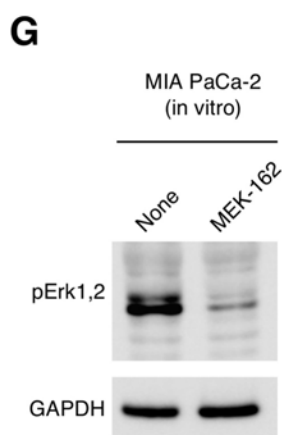
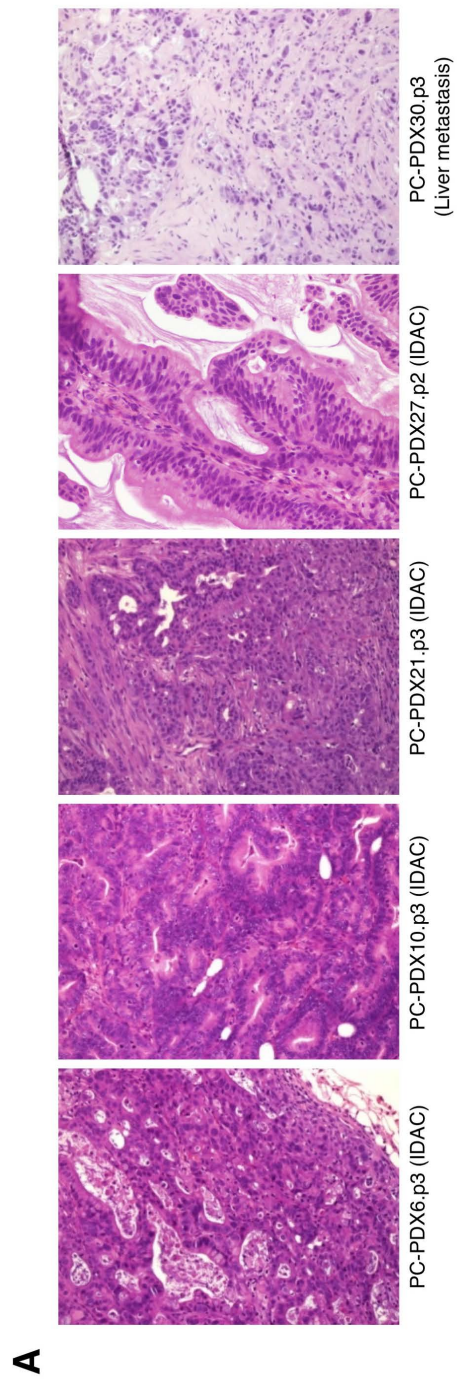


Figure 12. Effects of different drugs and drug combinations on the proliferation of pancreatic cancer cell lines. (A) MIA PaCa-2 cells were treated with different concentrations of the indicated drugs during 3 days. Then, cell proliferation was measured with the crystal violet staining assay. The results are expressed as averages and the error bars correspond to 95% confidence intervals of three independent experiments. P values were calculated using the two-sided Student's t test. (B) Genetic mutations/deletions of the cell lines and response to the different drugs tested. (C) MIA PaCa-2 cells were treated with drug concentrations corresponding to IC50s for 24 hours. Then, the percentages of cells in each phase of the cell cycle were analyzed by propidium iodide staining and flow cytometry. The percentages of cells in the sub-G1 area and excluded from the cell cycle analysis are positioned at the top. (D) MIA PaCa-2 cells were treated with sub-optimal concentrations (corresponding to IC25) of the indicated drugs for 72 hours. Cell proliferation was measured by crystal violet assay. (E) Effect of different drug combinations on the body weight of BALB-c Nude mice. Three groups of mice (n=7 per group) were treated with vehicle or the indicated combinations of Gem (20 mg/kg), Nab-P (10 mg/kg), Aza (2 mg/kg) and/or MEK162 (15 mg/kg). At the indicated time points mice were weighted. (F) MIA PaCa-2 cells were treated with sub-optimal concentrations (corresponding to IC25) of the indicated drugs for 72 hours. Cell proliferation was measured by crystal violet assay. (G) MIA PaCa-2 cells were treated with 30nM of MEK162 for 24 hours and the cell lysates were analyzed by Western blot with antibodies against phospho-Erk1,2; GAPDH was used as endogenous control.

1.2 Effect of chemotherapy combinations *in vivo*.

Compared with xenografts from established cell lines, PDXs better recapitulate the architecture as well as the molecular and cellular heterogeneity of the tumors from which they are derived (Kopetz et al. 2012). We established a collection of PC-PDXs, coming from four primary tumors and one from a liver metastasis (Figure 13A). All of them retained the histopathological and genetic characteristics of the original tumors as confirmed by Ki67, cytokeratin 19 (CK19), p53, Mucin 1 and carbohydrate antigen 19-9

(CA19-9) expression (Figure 13B), and these features were preserved during the successive passages (Figure 13C).



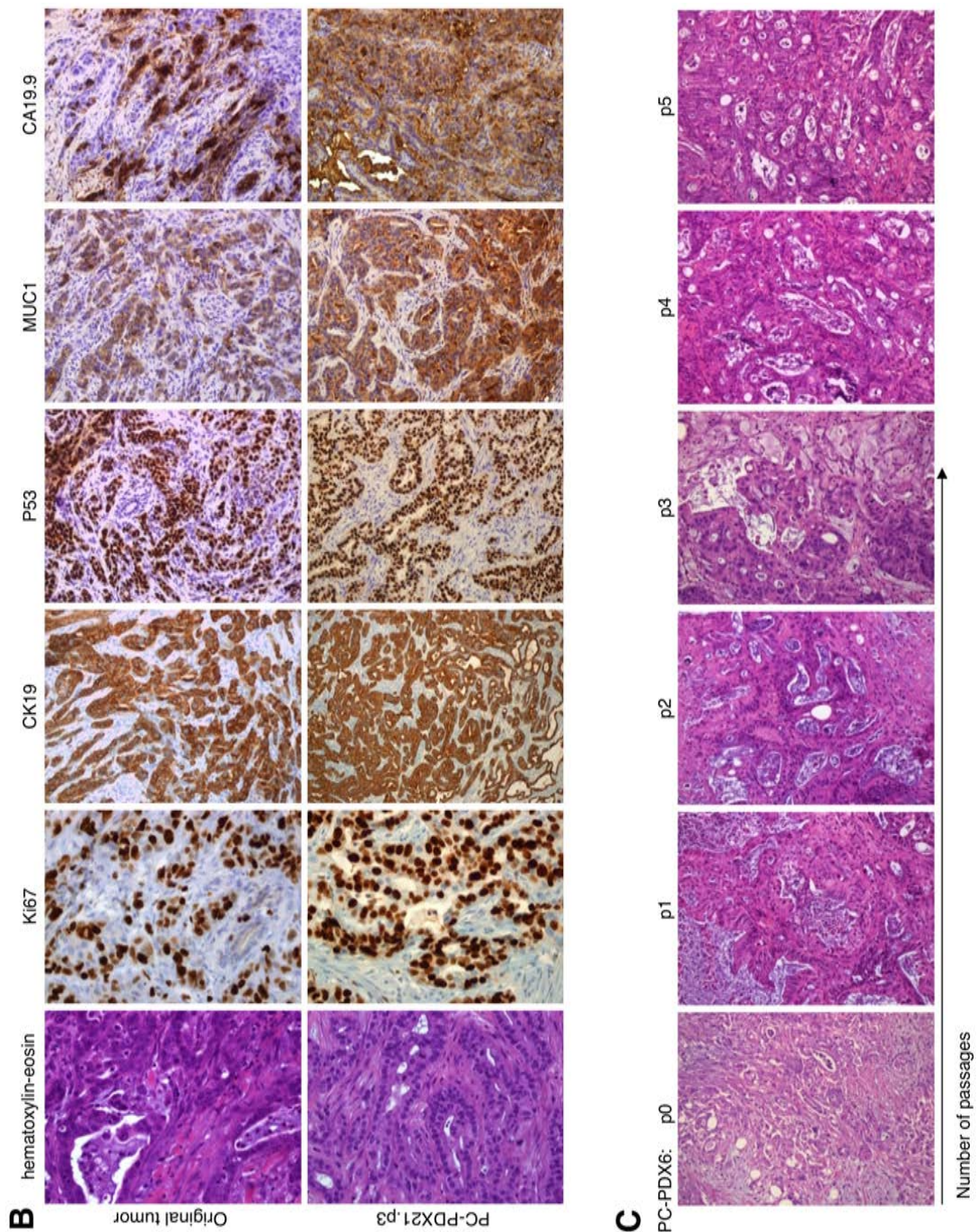


Figure 13. Characterization of the PC-PDXs. (A) Representative digital micrographs of hematoxylin-eosin-stained sections from the indicated PC-PDXs. The passage (p) used is indicated by the corresponding number. (B) Representative digital micrographs of immunostained sections from the original tumor and its corresponding PC-PDX21 (after third passage, indicated by p3). Sections were stained with antibodies against the proliferation marker Ki-67, the cytoskeletal protein cytokeratin-19 (CK-19), the tumor suppressor P53, the cell surface transmembrane protein mucin-1 (Muc-1), and the pancreatic cancer marker CA19.9. (C). Representative digital micrographs of hematoxylin-eosin-stained sections from the indicated passages of PC-PDX6. p0 designates originally implanted sample and p1-p5, represent successive passages.

Next, we compared the effectiveness of the two chemotherapy regimens. The combinations Gem/Nab-P and Aza/Nab-P impaired the growth of the PC-PDXs, albeit, overall, the combination Gem/Nab-P was slightly more effective (Figure 14A), in agreement with the *in vitro* data (Figure 12). Likewise, tumor weight at the end of the treatment confirmed the tumor volume data (Figure 14B). Therefore, we selected Gem/Nab-P combination to add further drugs for treating pancreatic cancer.

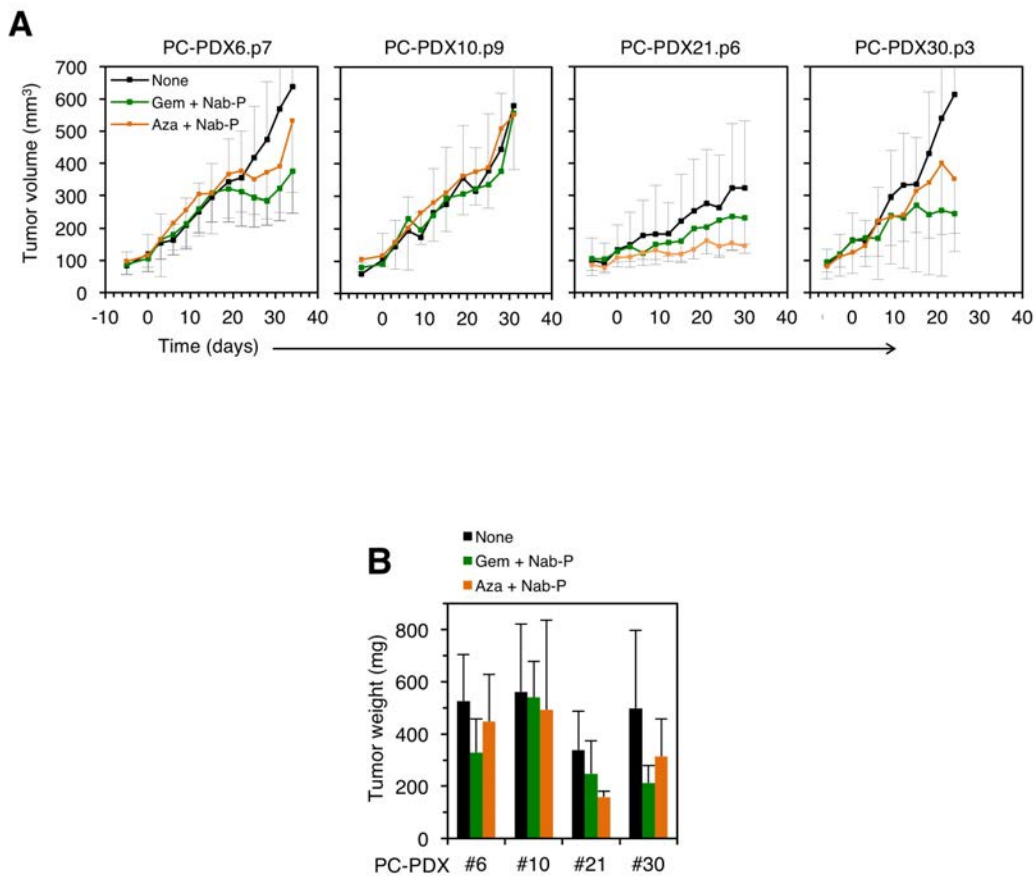
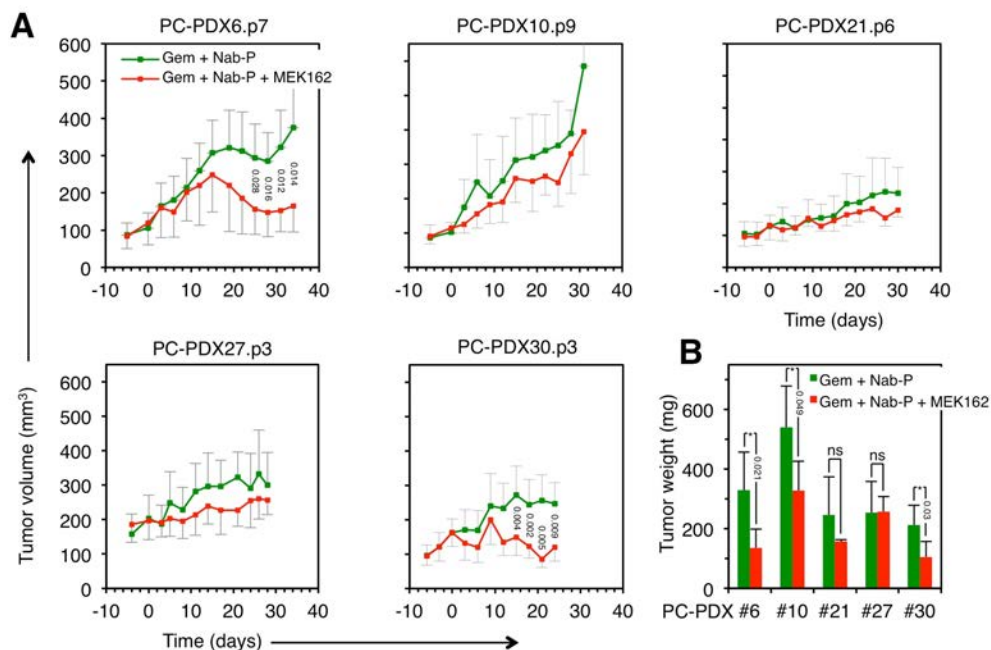


Figure 14. Response of PC-PDXs to chemotherapy. (A) Tumor volume was determined at different time points (n = 6 in each group). The passage (p) used is indicated by the corresponding number. Error bars correspond to 95% confidence intervals. (B) Tumor weight at the end of the experiment. The results are expressed as averages and the error bars correspond to 95% confidence intervals.

1.3 Addition of MEK162 increases the effectiveness of chemotherapy *in vivo*.

Next, we tested whether MEK162 added efficacy to the Gem/Nab-P backbone. MEK162 improved the effect of chemotherapy in three out of five PDXs in a statistically significant manner (Figure 15A and B). In one of the PDXs (PC-PDX10), the reduction in tumor volume was not significant, but we observed a statistically significant reduction in tumor weight of 39.2% (Figure 15B).

To monitor the effect of MEK162 at the molecular level, we determined the phosphorylation levels of Erk1/2 in tumors at different time points in an independent experiment. Foreseeably, the activity of Mek1/2 was inhibited after administration of MEK162 at days 12 and 17 (Figure 15C and D) but quickly recovered after two days (Figure 15 D, day 14). To quantify the necrotic and fibrotic areas, tumor sections were stained with Picrosirius red. Interestingly, the percentages of necrotic and fibrotic areas were higher in all the tumors treated with MEK162 (Figure 15, day 31 and Table 3), indicating that the effect of the Mek1/2 inhibitor on tumor growth was probably underestimated in the analysis of tumor volume or weight. Overall, MEK162 adds antitumor efficacy to the Gem/Nab-P based chemotherapy backbone used as the standard of care in three out of five PC-PDX models tested.



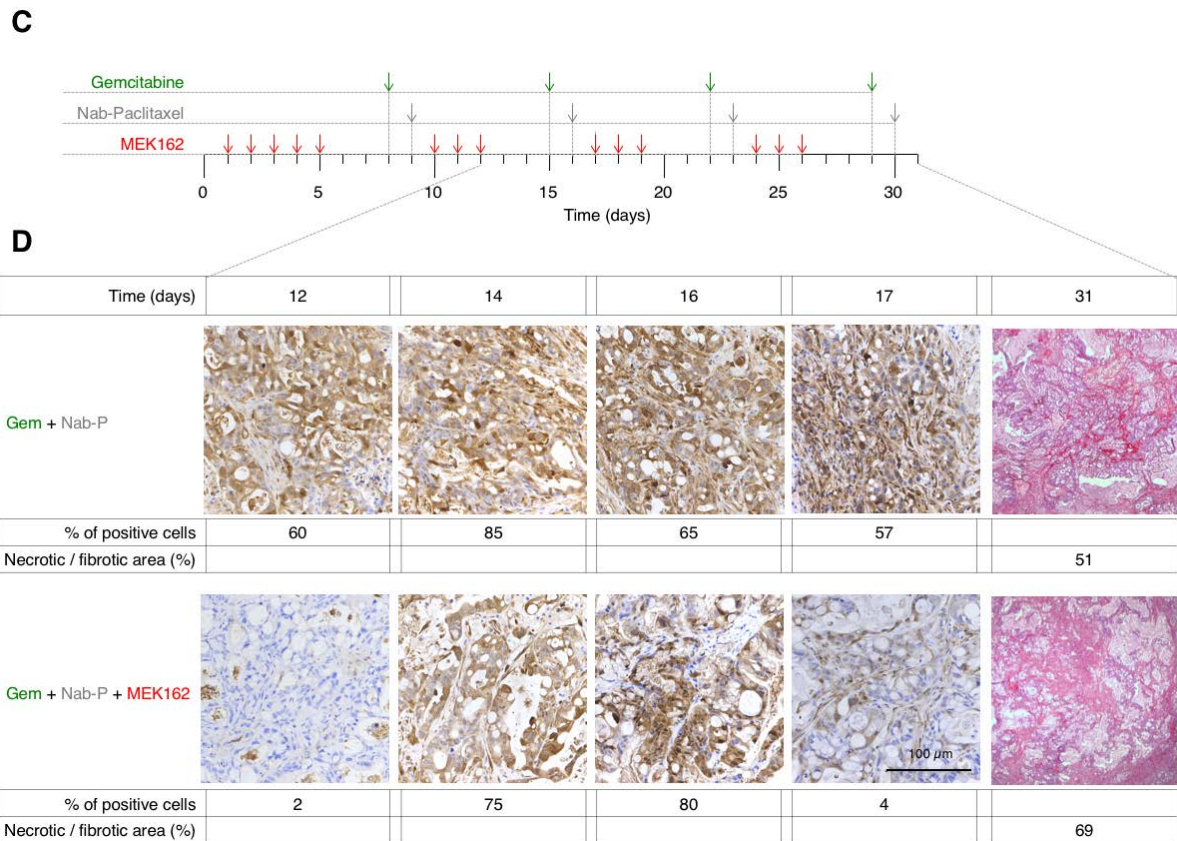


Figure 15. Effect of Mek1/2 inhibition on the growth of PC-PDXs treated with backbone chemotherapy. (A) the volumes of PC-PDXs, treated as indicated in (C) were determined at different time points (n = 6 in each group). Error bars correspond to 95% confidence intervals. P values were calculated using the two-sided Student's t test. (B) Tumor weight was determined at the end of the experiments. The results are expressed as averages and the error bars correspond to 95% confidence intervals. P values were calculated using the two-sided Student's t test. (C) Schematic drawing depicting treatment regimen. (D) At the indicated time points mice bearing PC-PDX6.p8 treated as in (A) were sacrificed and samples from the tumors were stained with anti-phospho-Erk1,2 or, to visualize the necrotic/fibrotic areas, with picrosirius red.

Time of tumor resection (days)	Tumor	Gem + Nab-P		Gem + Nab-P + MEK162		Average necrotic and fibrotic areas (%)	
		% Necrosis	% Fibrosis	% Necrosis	% Fibrosis	Gem + Nab-P	Gem + Nab-P + MEK162
12	A	77,5	7,5	70	10	68.8	84.3
	B	50	2,5	77,5	11		
14	A	47,5	17,5	75	10	62,5	90
	B	37,5	22,5	75	20		
16	A	52,5	5	17,5	50	67,5	76,3
	B	35	42,5	70	15		
19	A	20	10	32,5	35	40	73,8
	B	40	10	25	55		
31	A	40	20	60	15	50	68,3
	B	20	20	55	15		
	C	30	20	20	40		

Table 3. Quantification of the necrotic and fibrotic areas in representative samples from the tumors analyzed in Figure 14D

1.4 Effect of the Gem/Nab-P/MEK162 combination on the growth of orthotopic xenografts.

Although the desmoplastic component of the original tumor was preserved in the PC-PDXs implanted subcutaneously (Figure 13A and B), orthotopic models better recapitulate the desmoplastic reaction observed in PDACs (M. P. Kim et al. 2009). Hence, we orthotopically implanted mice with PC-PDX #10. Two weeks after implantation, mice were treated with Gem/Nab-P or with Gem/Nab/MEK162 as detailed in Figure 15C. Tumors were found in four out of four mice treated with backbone chemotherapy and in two out of four mice treated with chemotherapy and MEK162 (Figure 16A). In agreement with the higher percentage of fibrotic area observed in subcutaneous tumors (Figure 15, day 31 and Table 3), orthotopic tumors treated with MEK162 displayed an increased content in extracellular collagen deposition and a higher level of alpha-smooth muscle actin positive cells (Figure 16B), indicating an increased desmoplastic reaction following Mek1/2 inhibition.

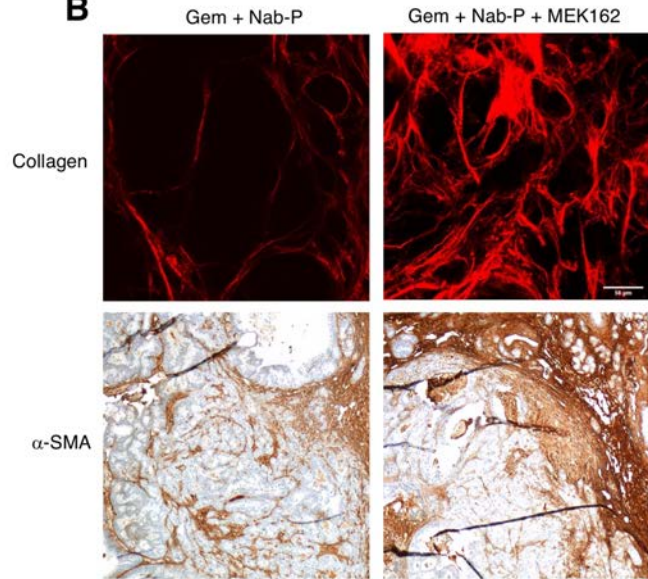
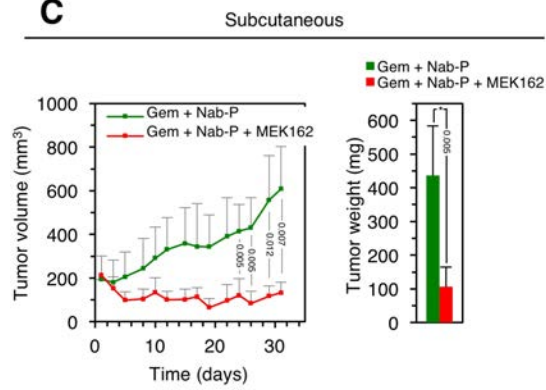
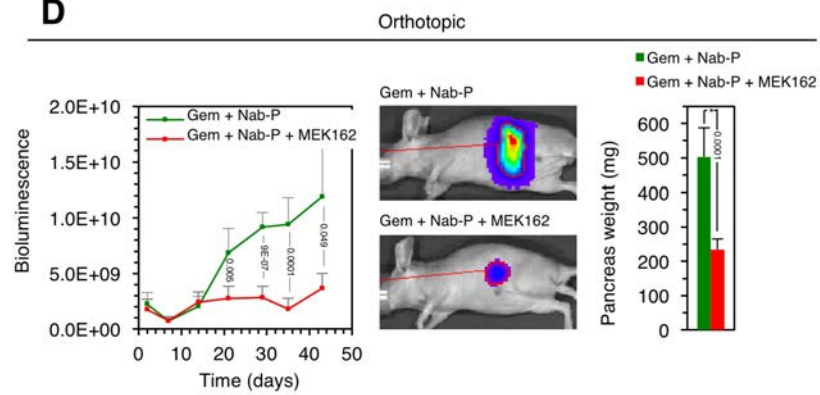
To precisely quantify the effect of MEK162 in an orthotopic model, we injected MIA PaCa-2 cells expressing firefly luciferase (MIA PaCa-2/Fluc) in the pancreases of BALB/c Nude mice. As a control, MIA PaCa-2 cells were also injected subcutaneously in another group of mice. In both models, the Mek1/2 inhibitor added efficacy to Gem/Nab-P approximately to the same extent (Figure 16B and C).

Next, we assessed the effect of these drug combinations on the metastatic ability of MIA PaCa-2/Fluc cells. Analysis of *ex vivo* luminescence showed metastases in 8 out of 10 mice treated with the Gem/Nab-P backbone in lung, spleen, liver and diaphragm (Figure 16D). Remarkably, addition of MEK162 reduced the metastatic growth, as we detected only one spleen metastasis in 10 mice treated with the triple combination (Figure 16D).

These results strengthen the effectiveness of the Gem/Nab-P/MEK162 combination to prevent the growth of pancreatic carcinomas and their metastatic progression.

A

Treatment	Implanted	Grown
Gem + Nab-P	4	4
Gem + Nab-P + MEK162	4	2

B**C****D**

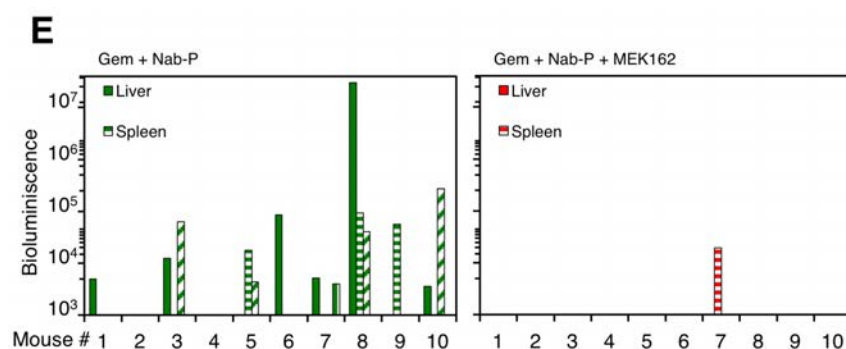


Figure 16. Effect of Mek1/2 inhibition on the growth of orthotopic xenografts. (A) Number of resected tumors in mice after one month of treatment with backbone chemotherapy or chemotherapy plus MEK162. (B) Analysis of collagen deposition and positivity for alpha-SMA in tumors of approximately equal size, corresponding to the two treatments. (C) and (D) MIA PaCa-2 cells expressing luciferase were injected subcutaneously (C) or orthotopically (D). Tumor growths were monitored by assessing volumes in the subcutaneous model (C, left) or luminescence in the orthotopically implanted mice (D, left). Representative luminescence images are shown (D, middle). At the end of the experiments, mice were euthanized and the subcutaneous tumors or pancreases were removed and weighed (C and D, right bar graphs). The results are expressed as averages and the error bars correspond to 95% confidence intervals. P values were calculated using the two-sided Student's t test. (E) At the end of the experiment, metastatic growths were assessed by ex vivo quantification of luminescence in liver, spleen, lung and diaphragm.

1.5 Intratumor heterogeneity and resistance to MEK162.

Intratumor heterogeneity has been intensively studied as an underlying mechanism of tumor evolution and adaptation to anticancer therapies (Fisher et al. 2013). To characterize the potential impact of tumor heterogeneity on the resistance to Mek1/2 inhibition, we analyzed the mutational profile of the different PC-PDXs by sequencing a panel of 57 cancer-related genes.

Regarding frequently mutated genes in pancreatic cancer, we found mutations in *KRAS* and *TP53* in all tumors (Figure 17A). Intriguingly, we found additional *KRAS* mutations within the same tumor in two of the PC-PDXs, 10 and 21, indicating that these PC-PDXs may be composed of different clones. Specifically, in the PC-PDX21, along with the predominant mutation (c.G35T:p.G12V), we found two additional *KRAS* mutations (c.G35A:p.G12D and c.G34C:p.G12R), albeit with low allele frequencies (2% and 1%, respectively). In PC-PDX 10, we identified the c.G35T:p.G12V mutation (1% allele frequency) along with the predominant one, c.G35A:p.G12D (Figure 17A). To accurately

confirm the existence of these mutations, we also analyzed their allele frequencies by digital droplet PCR (ddPCR), a more sensitive technique that allows for the reliable detection of allele frequencies lower than 0.1%. All the detected mutations were also found in the original patient samples and, importantly, despite their low frequency, all but one were also present in the PC-PDXs, further reinforcing the reliability of this experimental model (Figure 17B).

To further analyze intratumor heterogeneity in the two PDXs resistant to Mek1/2 inhibition, we established *in vitro* cultures from PC-PDXs 21 and 27 and isolated individual cell colonies. Targeted sequencing of the 57 cancer-related genes was also performed in the different colonies isolated. Mutations in the *SMAD4*, *STK11*, *CDKN2A* and *VHL* genes showed that at least three of the four colonies from PC-PDX21 harbored genetically distinguishable cells (Figure 17C), indicating that PC-PDX21 was highly polyclonal. Moreover, the low allele frequencies of some of the mutations identified indicated that even the isolated colonies contained more than one cell clone.

We also observed unequal response to MEK162 across the different colonies. The sensitivities of the cells obtained from the different colonies to the Mek1/2 inhibitor were different; their IC50s ranged from ~ 30 nM to ~ 800 nM (Figure 17D, PC-PDX 21), indicating that the original tumors were composed of cells with a wide range of tolerances to Mek1/2 inhibition.

Although cells from the B2 and B6 colonies, obtained from the PC-PDX21, showed different sensitivities to MEK162 (Figure 17D, PC-PDX 21), we did not find any difference in the sequences of the genes included in the gene panel (Figure 17C). The same was observed in the C1 and C2 colonies, isolated from the PC-PDX27 and displaying different sensitivity to MEK162 (Figure 17D, PC-PDX 21). Thence, to fully determine if they were genetically different, we sequenced exome libraries prepared from these colonies. Exome sequencing analysis revealed that all the colonies analyzed contained genetically distinguishable cells (Figure 17E).

A

	PC-PDX6.p4	PC-PDX10.p6	PC-PDX21.p2	PC-PDX27.p3	PC-PDX30.p1
KRAS G12V	89	1	25		
KRAS G12D		51	2	32	
KRAS G12R			1		63
TP53 A161T	94				
TP53 V272M			98		
TP53 Y163N					73
TP53 R337C		99			
TP53Y103*				90	

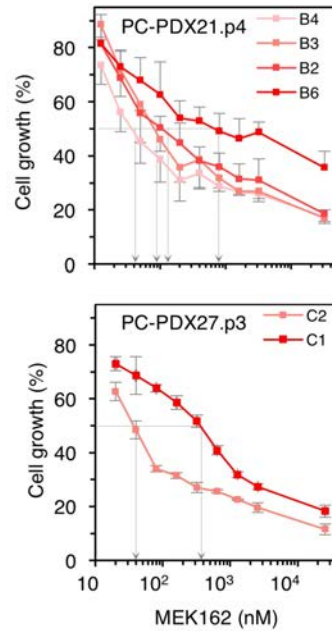
B

		PC-PDX6			PC-PDX10			PC-PDX21				PC-PDX27			PC-PDX30		
		OT	p4		OT	p6		OT	p2	p6	B4	OT	p3		p3		
KRAS	Seq	KRAS G12V	12	89	KRAS G12V	1	1	KRAS G12V	6	24	25	28	KRAS G12D	14	32	KRAS G12R	63
	ddPCR				KRAS G12D	15	51	KRAS G12D	0	2	0	0					
TP53	Seq	TP53 A161T	16	94	TP53 R337C	11	99	TP53 V272M	9	98	98	99	TP53 Y103*	26	90	TP53 Y163N	73
	ddPCR				KRAS G12V	0.52	0.145	KRAS G12V	7.65	45.65	47.1						
		KRAS G12D	12.95	47	KRAS G12D	0.26	0.49	0.35	KRAS G12R	0.44	0	0					

C

	PC-PDX21.p4				PC-PDX27.p3	
	B4	B3	B2	B6	C1	C2
KRAS G12V	41	49	42	39		
KRAS G12D					52	55
TP53 V272M	99	99	99	99		
TP53 Y103*					90	90
SMAD4 P246Q	15					
SMAD4 G247R		26				
STK11 A273T	4					
STK11 P324L	19					
CDKN2A G114C	10					
VHL W88C	6					

D



E

	PC-PDX21.p4		PC-PDX27.p3	
	B2	B6	C1	C2
LRRC69 E193Q		47	FLT3 P934L	37
VCX V206M		43	SMARCA2 Q222delinsQQ	25
CCDC151 L11V		43	FIP1L1 R483fs	17
TSPAN12 L14F		32	H3F3A A115G	16
CRYBA2 A80S		32	METTL2B E169K	12
DVL3 A565T		32	PRDM10 Q1035del	10
PADI3 G331S		30	USP6 R133K	14
GLDN K195M		27	RNF225 Q38_E39delinsQ	13
POTEI K913T	100		MARS Y68fs	11
IRF2BPL 114_115del	63		HCAR2 M317I	10
RASA4B E141G	58			
PRODH T466M	55			
ZNF814 A337V	39			
SEZ6L F17L	38			
CTTNBP2 R1286X	36			
KIF2B A175T	31			
NAT9 C115Y	30			
HSF4 K404R	29			
SPAG5 I480L	28			

Figure 17. Intratumor heterogeneity and response to Mek1/2 inhibition. (A) Results from targeted sequencing of 57 cancer-related genes in the indicated PC-PDXs. The allele frequencies of the found mutations are shown. (B) Sequences of a panel of 57 cancer-related genes were determined by amplicon sequencing (indicated by Seq) from the original tumors (OT) or the indicated PDXs (the passages are specified). The allele frequencies of the mutations found are shown. The KRAS mutations found in PC-PDX10 and 21 were confirmed by digital droplet PCR (ddPCR) and the allele frequencies are indicated. (C) PC-PDX-21 and 27 were disaggregated and cultured *in vitro*. Several cell colonies (named B2, B3, B4, B6 coming from PC-PDX 21 and C1, C2 for PC-PDX 27) were isolated and sequences of the panels of 57 cancer-related genes were determined. The allele frequencies of the mutations identified are shown. (D) Response to MEK162 was assessed in cells from the different colonies isolated. (E) Exome sequencing results from colonies B2, B6, C1 and C2. Mutations with allele frequencies higher than 10% in one of the colonies and non-detectable in the other are shown.

The detected polyclonality suggests that the moderate responses of the PC-PDXs 21 and 27 to MEK162 could be caused by the selection of pre-existing cells resistant to Mek1/2 inhibition. To test this hypothesis, we mixed (1:1) cells from colonies B2 and B6 and cells from colonies C1 and C2, cultured them in the presence or absence of MEK162 and followed the evolution of gene copies bearing the mutation *LRRC69* E193Q or *FLT3* P934L by ddPCR. We used these mutations as genetic markers to follow the fate of resistant cells because they are present only in PC-PDX21-B6 or PC-PDX27-C1 cells, which, compared with the rest of cells isolated from PC-PDX21 or PC-PDX-27, are resistant to MEK162 (Figures 17D and E). Indeed, treatment with MEK162 increased the allele frequency of the mutations *LRRC69* E193Q or *FLT3* P934L, showing that the

selective pressure exerted by the Mek1/2 inhibitor led to the selection of Mek1/2 inhibitor-resistant cells within a relatively short period of time (Figure 18A).

It should be noted that although their frequencies (47% and 37% for *LRRC69* E193Q and *FLT3* P934L, respectively) indicated heterozygosity, the enrichment induced by MEK162 shows that the *LRRC69* E193Q is homo- or hemizygous. After 1 month of treatment with the Mek1/2 inhibitor, the frequency of this mutation reached ~ 90% (Figure 18A, PC-PDX21) demonstrating that the resistant cells, homo- or hemizygous for *LRRC69* E193Q, overgrew the sensitive ones. Thus, the initial B6 colony most likely contained more than one cell clone. These results were confirmed by analyzing the dynamics of another mutation (*CCDC151* L11V) (Figure 18A, PC-PDX27).

Treatment with MEK162 resulted in an allele frequency shift from around 25% to ~ 50% for the mutation *FLT3* P934L (Figure 18A, PC-PDX27), indicating that this mutation probably exists in heterozygosity. To confirm *in vivo* the enrichment of resistant cells, we determined the frequencies of markers for resistant cells (mutations in *LRRC69* and *FLT3* P934L) in PC-PDX 21 and PC-PDX 27 treated without or with MEK162 after 1 month. We found that these mutations were present at very low allele frequency (Figure 18B). However, xenografts after 1 month of treatment with MEK162 displayed an increase in the frequency of the mutant alleles (Figure 18B), further supporting the conclusion that tumors likely become refractory to Mek1/2 inhibition through selection of primary resistant cells. Moreover, the fact that these two mutations were also found in the original tumors confirms that they were not random mutations acquired during the *in vitro* expansion of cell cultures.

Collectively, these results show that Mek1/2 inhibition adds efficacy to chemotherapy in pancreatic tumors. However, the selection of pre-existing cells resistant to the treatment may compromise the long-term efficacy of this therapy in a significant proportion of patients.

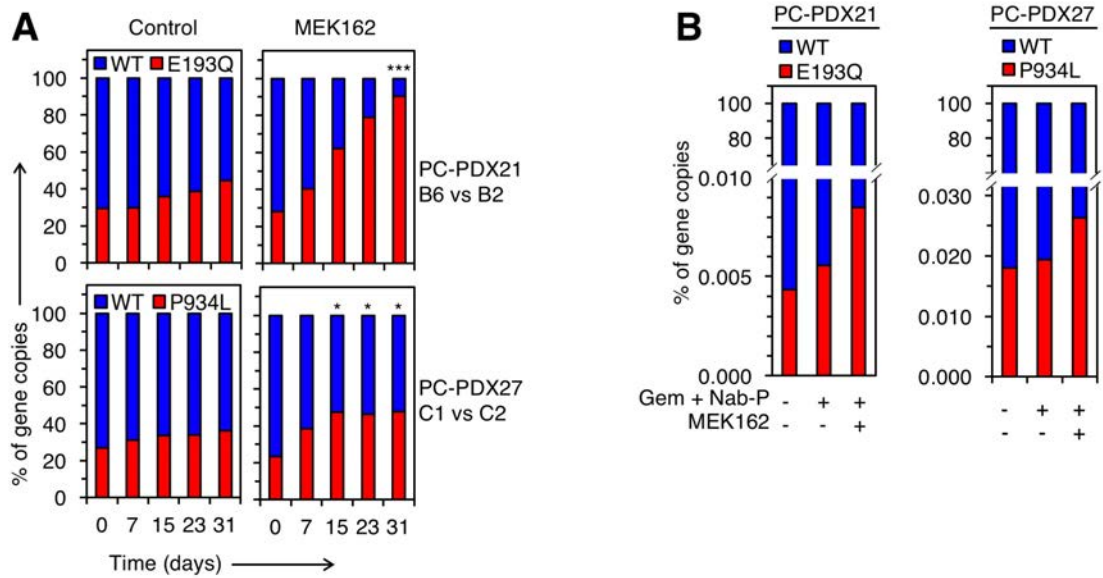


Figure 18. Selection of pre-existing MEK162-resistant cell populations by treatment with MEK162 *in vitro* and *in vivo* (A) Cells from colonies B2 and B6 from PC-PDX21 (upper panels) or colonies C1 and C2 from PC-PDX27 (lower panels) were mixed 1:1 and cultured in the absence or presence of MEK162. At the indicated time-points the percentages of wild type and mutant LRR69 E193Q or FLT3 P934L alleles were determined with ddPCR. The results are expressed as averages of three independent experiments. P values were calculated using the two-sided Student's t test. (B) The allele frequencies of LRR69 E193Q or FLT3 P934L mutant alleles were determined in DNA isolated from tumors resected after the indicated treatments of PC-PDX21 or PC-PDX27 (see Figure 15).

In this first part of the thesis, we show that intratumor heterogeneity plays a role in resistance to Mek1/2 in pancreatic cancer tumors. Little is known about the molecular mechanisms that regulate resistance to this therapy and could also explain the failure of Mek1/2 inhibition in pancreatic cancer patients, recently observed in clinical trials (Jeffrey R Infante et al. 2014; Van Cutsem et al. 2018). Thus, the second part of this thesis will unveil the mechanisms of resistance to Mek1/2 inhibition in pancreatic cancer.

SECTION 2: The transcription factor Slug uncouples cell proliferation from the Raf-Mek-Erk signaling pathway

2.1 Generation of *in vitro* models of acquired resistance to Mek1/2 inhibition.

Given the need to identify the mechanisms of resistance to Mek1/2 inhibition that could explain the recently reported failure of this therapy in pancreatic cancer patients, we sought to develop models of resistance.

To generate *in vitro* resistance to MEK1/2 inhibition, we chronically treated cultures from the pancreatic cancer cell line MIA PaCa-2 with the Mek1/2 inhibitor MEK162. We followed two independent strategies, that consisted in growing the cells in the presence of constant (R1) or increasing concentrations (R2) of the inhibitor (Figure 19A and B).

Thus, after 6 months of treatment, we successfully generated two pools of resistant cells (named as R1 and R2). We observed that the IC₅₀ for MEK162 shifted around 60-fold, from ~120 nM in the parental MIA PaCa-2 cells to ~7000 nM in the resistant cells (Figure 19C and D).

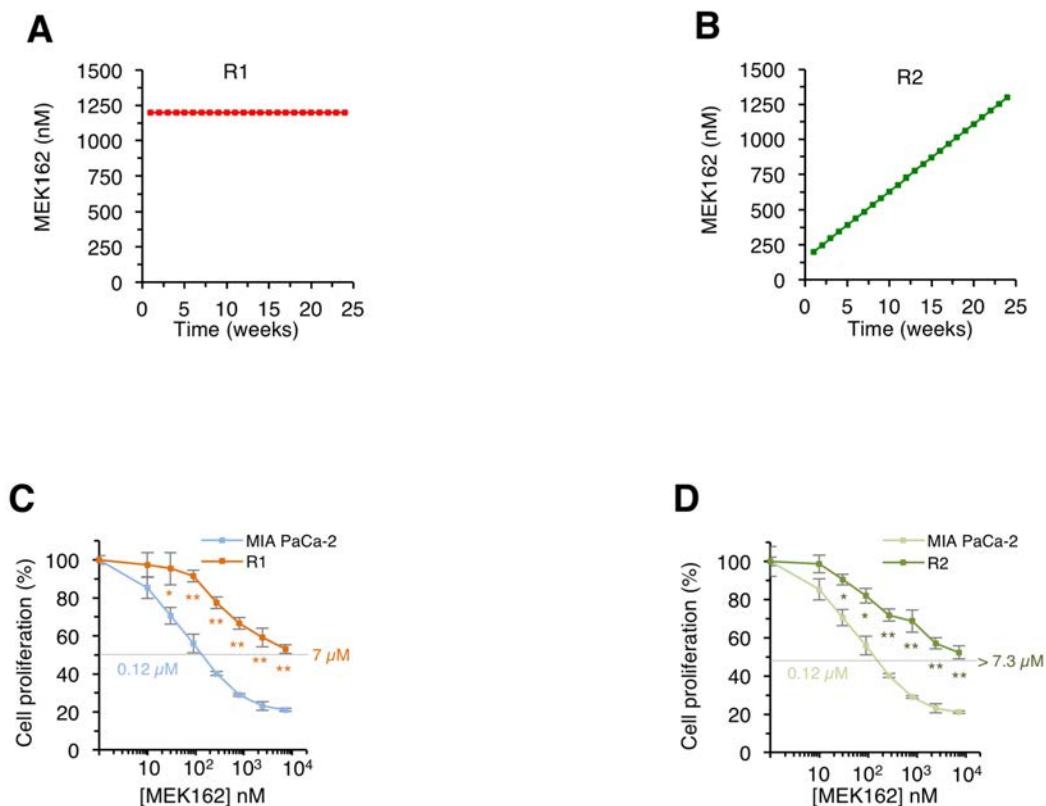


Figure 19. Generation of cell cultures resistant to Mek1/2 inhibition. (A) Strategy R1 for generating resistance, constant selection pressure. (B) Strategy R2 for generating resistance, increasing selection pressure (C) Dose-response assay in MIA PaCa-2 cells and the R1-derived cells, treated with different concentrations of MEK162 for 3 days. Then, cell proliferation was measured with the crystal violet staining assay. The error bars correspond to 95% confidence intervals of three independent experiments. P values were calculated using the two-sided Student's t test. (D) Dose-response assay in MIA PaCa-2 cells and the R2-derived cells, treated with different concentrations of MEK162 for 3 days. The results are expressed as averages and the error bars correspond to 95% confidence intervals of three independent experiments. P values were calculated using the two-sided Student's t test.

After a long time under selective pressure, it might be reasonable that the pool of resistant cells harbored a heterogeneous cell population, and those independent cell populations could have evolved independently, that is, developing different mechanisms of resistance. To identify the multiple mechanisms of resistance that could be existing within the resistant pools of cells, we decided to establish clonal populations starting from one single cell. Throughout the expansion process, the clonal cultures were maintained in the absence of MEK162. Interestingly, we observed that all the clones generated displayed similar degrees of resistance to MEK162 (Figure 20A and B). Therefore, we selected five clones (with different cell growth rates) to characterize the potential mechanisms of resistance to Mek1/2 inhibition. Two of the selected clones came from the strategy R1 (clones R1-1 and R1-16), whereas three came from strategy R2 (R2-1, R2-3 and R2-39). Additionally, MEK162 resistant cells were also resistant to trametinib (also known as Mekinist or GSK1120212), a potent novel Mek1/2 inhibitor that prevents feedback reactivation of Erk1/2, compared to parental cells (Figure 20 C and D).





Figure 20. Generation of MEK162-resistant clones. (A) Dose-response assay in MIA PaCa-2 cells and the clones obtained from R1. Cells were treated with different concentrations of MEK162 for 3 days and cell proliferation was measured by crystal violet staining assay. P values were calculated using the two-sided Student's t test. (B) Dose-response assay in MIA PaCa-2 cells and the clones obtained from R2. (C) Dose-response assay to trametinib in MIA PaCa-2 cells and R1 clones, treated with different concentrations for 3 days. Then, cell proliferation was measured with the crystal violet staining assay. P values were calculated using the two-sided Student's t test. (D) Dose-responses to trametinib in MIA PaCa-2 and R2 clones, treated with different concentrations for 3 days. Then, cell proliferation was measured with the crystal violet staining assay. The results are expressed as averages and the error bars correspond to 95% confidence intervals of three independent experiments. P values were calculated using the two-sided Student's t test.

Recent reports indicate that drug vacation regimes restore sensitivity to B-Raf inhibitors in *BRAF* mutant melanoma (Sun, L. Wang, et al. 2014b; Seghers et al. 2012). For this reason, we assessed whether the resistance to MEK162 could be maintained after a long period of drug absence. Certainly, after 3 months without treatment with MEK162, cells did not recover sensitivity to the Mek1/2 inhibitor (Figure 21A), indicating that the mechanism of resistance does not require continuous selective pressure.

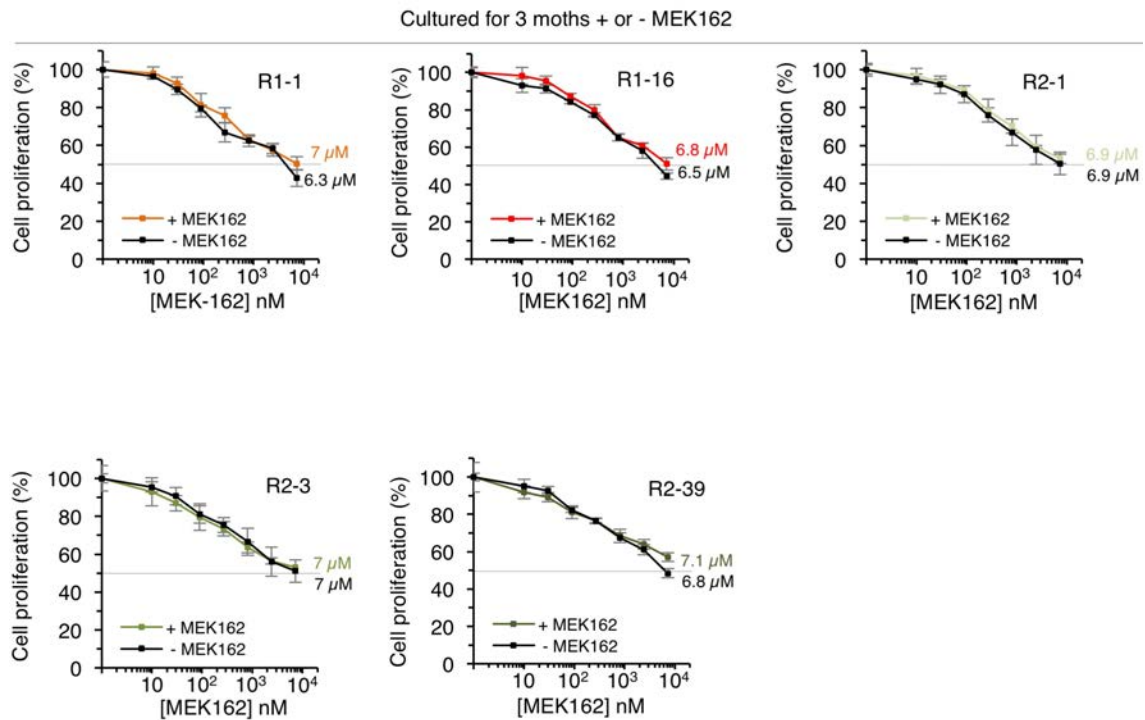
A

Figure 21. Resistance is maintained in the absence of selective pressure. (A) Dose-response assay in the resistant clones cultured 3 months with or without MEK162. For the assay, cells were treated with different concentrations of MEK162 for 3 days and cell proliferation was measured by crystal violet staining assay. The results are expressed as averages and the error bars correspond to 95% confidence intervals of three independent experiments. P values were calculated using the two-sided Student's t test.

2.2 Resistance to MEK162 is recapitulated *in vivo*.

To determine the relevance of the differences in IC₅₀ observed *in vitro*, we analyzed the response of resistant cells to Mek1/2 inhibition *in vivo*. We subcutaneously engrafted parental and resistant cells in immunodeficient mice and, when tumors were palpable, mice were treated with MEK162 (15 mg/kg) or vehicle for one month. While the growth of parental MIA PaCa-2 cells was prevented by treating mice with MEK162, the Mek1/2 inhibitor had little or no effect on the *in vivo* growth of the R2-39 resistant cells (Figure 22A and B).



Figure 22. Recapitulated resistance *in vivo*. (A) Response to MEK162 treatment in MIA PaCa-2-derived tumors (n = 3 in each group). The results are expressed as tumor volume averages and the error bars correspond to 95% confidence intervals. P values were calculated using the two-sided Student's t test. (B) Response to MEK162 treatment in R2-39-derived tumors (n = 3 in each group). The results are expressed as tumor volume averages and the error bars correspond to 95% confidence intervals. P values were calculated using the two-sided Student's t test.

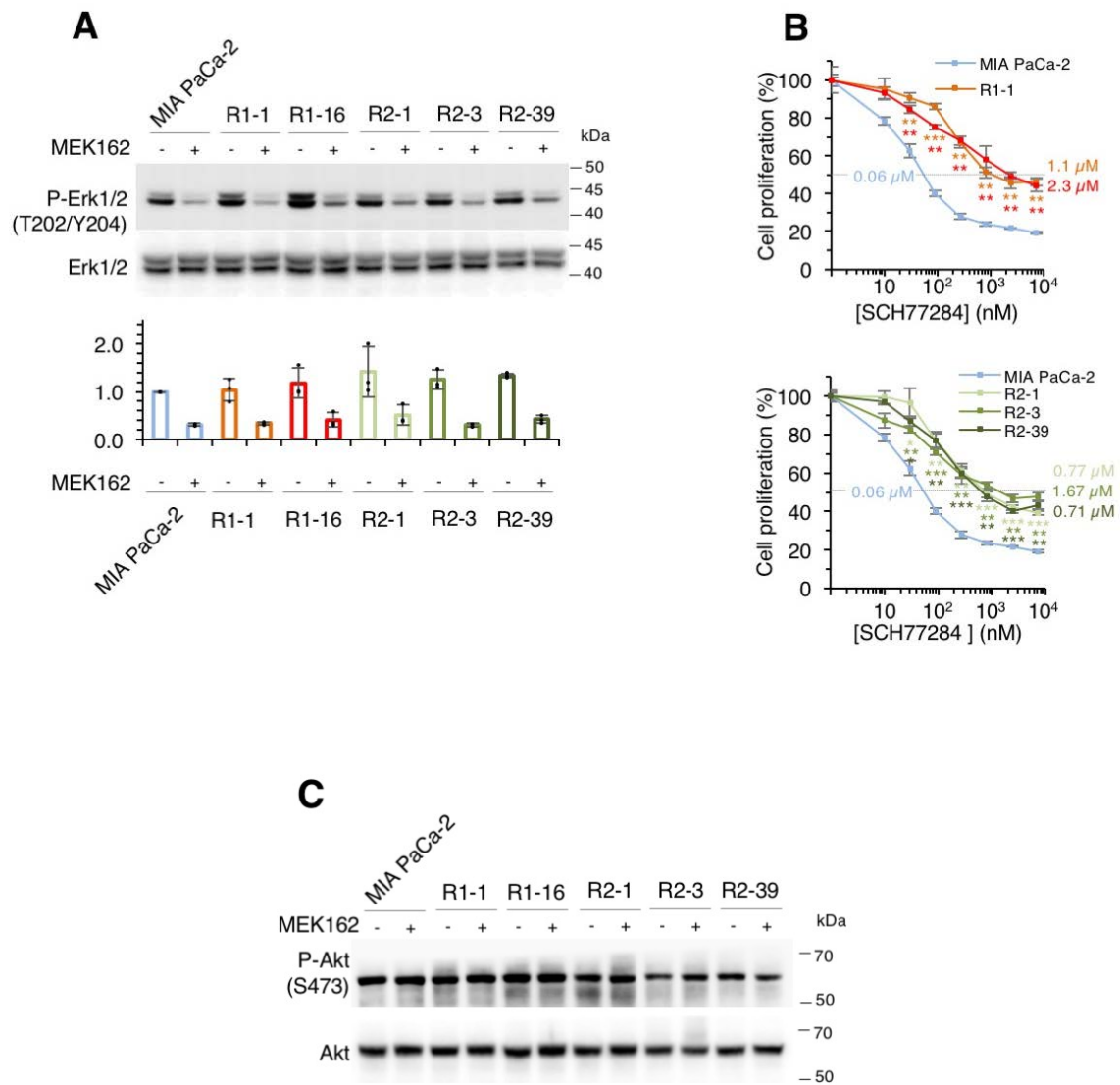
Overall, we have successfully developed a model of resistance to Mek1/2 inhibition that will allow us to identify possible mechanisms of resistance in *KRAS* mutant pancreatic cancer. Thus, we next proceeded to investigate the molecular mechanisms of resistance using different types of analyses.

2.3 Mek1/2 inhibition prevents Erk1/2 phosphorylation in parental and resistant cells.

Because the vast majority of mechanisms of acquired resistance described to date reinstate the activation of Erk1/2 in the presence of the Mek1/2 inhibitor (Caunt et al. 2015), we analyzed the levels of phosphorylated Erk1/2 in resistant cells. We found that phospho-Erk1/2 levels were very similar to those of parental cells and that the Mek1/2 inhibitor reduced the phosphorylation of Erk1/2 in resistant and parental cells to the same extent (Figure 23A). These results suggest that resistant cells are no longer dependent on the Raf-Mek-Erk pathway. Confirming this hypothesis, resistant cells were also insensitive to an Erk1/2 inhibitor (Figure 23B).

Some cells acquire resistance to Raf/Mek inhibitors by activating different RTKs to sustain cell proliferation through compensatory pathways, such as the PI3K-Akt pathway

(Turke et al. 2012; Kitai et al. 2016). Thus, we analyzed the levels of phospho-Akt in parental and resistant cells. Results showed similar, or lower, phospho-Akt levels in resistant cells compared to parental cells (Figure 23C). We then extended the analysis to a panel of phosphokinases (which covers the most important kinases such as p38, AKT, JNK or STAT) in one of the resistant cells. Results did not show evidence of activation of any compensatory pathway (Figure 23D).



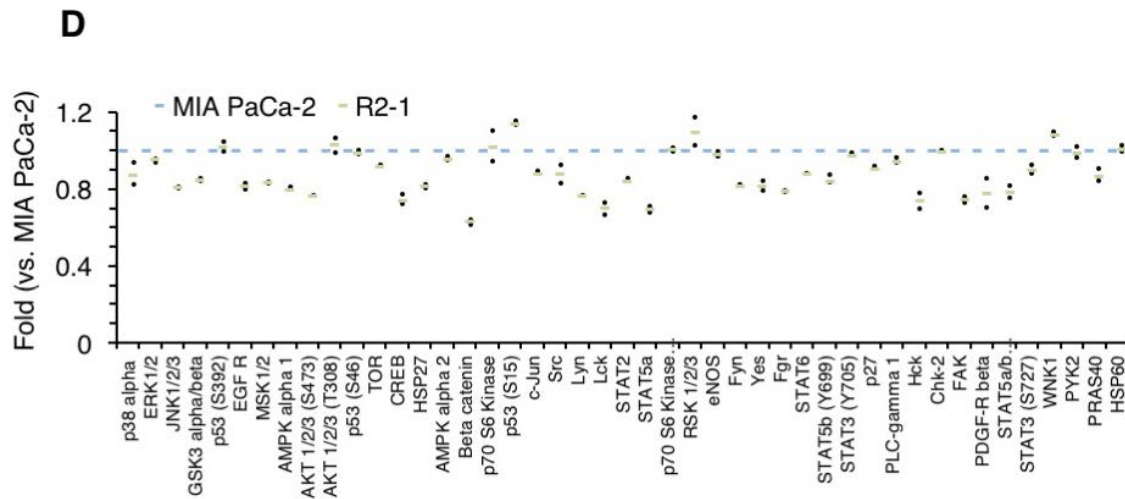


Figure 23. Analysis of the activation of compensatory pathways in resistant cells. (A) Analysis of Erk1/2 phosphorylation upon Mek1/2 inhibition. Cells were treated with MEK162 for 24 h and lysates were analyzed by Western Blot with antibodies against p-Erk1/2 and Erk1/2 (upper panel). Quantification of p-Erk1/2 expression was determined using total Erk1/2 as endogenous control. Each condition was normalized to its untreated control (lower panel). (B) Dose-response assay from parental and resistant cells to the Erk1/2 inhibitor SCH77284. Cells were treated with different concentrations of SCH77284 for 3 days and cell proliferation was measured by crystal violet staining assay. The results are expressed as averages and the error bars correspond to 95% confidence intervals of three independent experiments. P values were calculated using the two-sided Student's t test. (C) Total and phosphorylated Akt levels in parental and resistant cells treated without and with MEK162. (D) Human phospho-kinase array quantification. Lysates from MIA PaCa-2 and R2-1 cells were incubated in membranes containing pre-coated antibodies against a total of 43 phosphorylation sites of 37 proteins and 2 related total proteins. The expression of each protein (in duplicate) was determined by normalizing to reference points.

As we did not find differential activation in any of the kinases assessed, we decided to characterize the mutational landscape of parental and resistant cells in order to study the presence of acquired mutations that could explain the resistant phenotype.

2.4 Exome sequencing analysis.

Resistance to Mek1/2 inhibition can be acquired through gain of function mutations in Mek1 and Mek2 or other components of the pathway (Emery et al. 2009; Anon 2013). To determine whether these, or functionally equivalent mutations, are responsible for the resistance in our models, we analyzed and compared the sequences of the exomes of the different resistant clones with that of MIA Paca-2 cells. While we did not find common

mutations in all resistant clones, we found mutations in 41 and 9 common genes in the resistant R1 and R2 clones, respectively (Figure 24A and B). The algorithm PolyPhen-2 (Adzhubei et al. 2010), that predicts the impact of amino acid substitution in the structure and function of the resulting protein, predicted relevant functional effects (scores ranging from 0, tolerated, to 1, deleterious) of 17 and 1 of the mutations found in R1 and R2 clones, respectively (threshold score >0.8) (Figure 24B). However, the corresponding genes did not have any obvious functional relation to the B-Raf-Mek1/2-Erk1/2 or alternative cell proliferation pathways and, thus, we did not further characterize them.

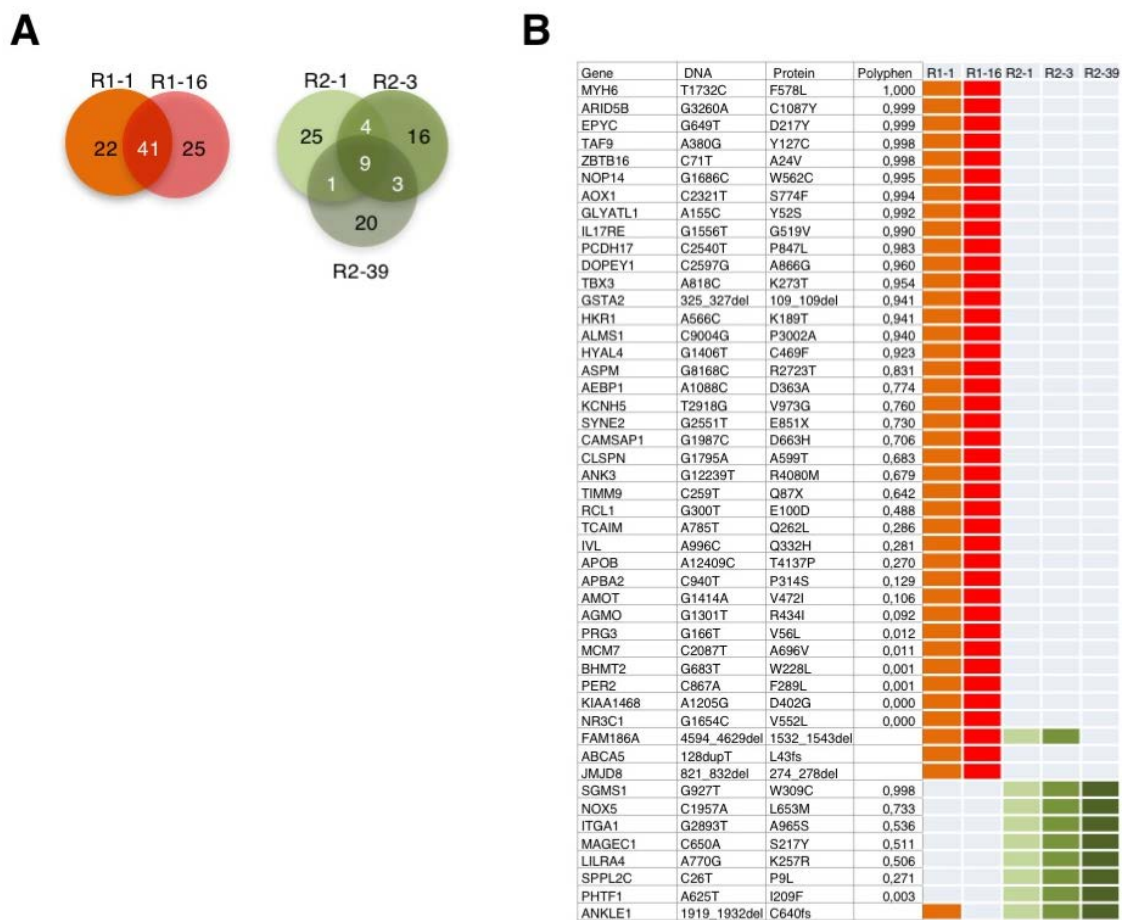


Figure 24. Exome sequencing in parental and resistant cells. (A) Venn diagram showing the mutations exclusive and common shared between the R1 (left) and R2-derived (right) resistant clones (B) Table showing shared mutations with more than 20% allele frequency and their functional relevance assessed by PolyPhen-2 algorithm. Scores >0.8 are considered of functional relevance.

Collectively, these results indicated that the cells obtained could be a model for a previously unidentified mechanism of resistance.

2.5 RNA sequencing analysis reveals commonly altered gene signatures in resistant cells

Since the mutational profile of the resistant cells could not explain the resistance, we decided to analyze gene expression. Transcriptomic analysis by RNA-seq showed that 239 and 218 genes were acutely up- or downregulated in R1 and R2 resistant cells compared to parental MIA PaCa-2 cells (≥ 4 -fold; $q < 0.0001$), respectively. The expression of 68 of these genes was altered both in R1 and R2 (Figure 25A, B), indicating that a common mechanism could explain their resistances. Gene set enrichment analysis (GSEA) identified numerous biological processes that differed between parental and resistant cells (Figure 25C). In agreement with a recent report, inhibition of Mek1/2 led to the expression of a type I interferon signature (Lulli et al. 2017). Consistently with the expected effect of prolonged Mek1/2 inhibition, genes regulated by K-Ras signaling were significantly downregulated, as were Myc targets and E2F transcriptional regulators (Hayes et al. 2016).

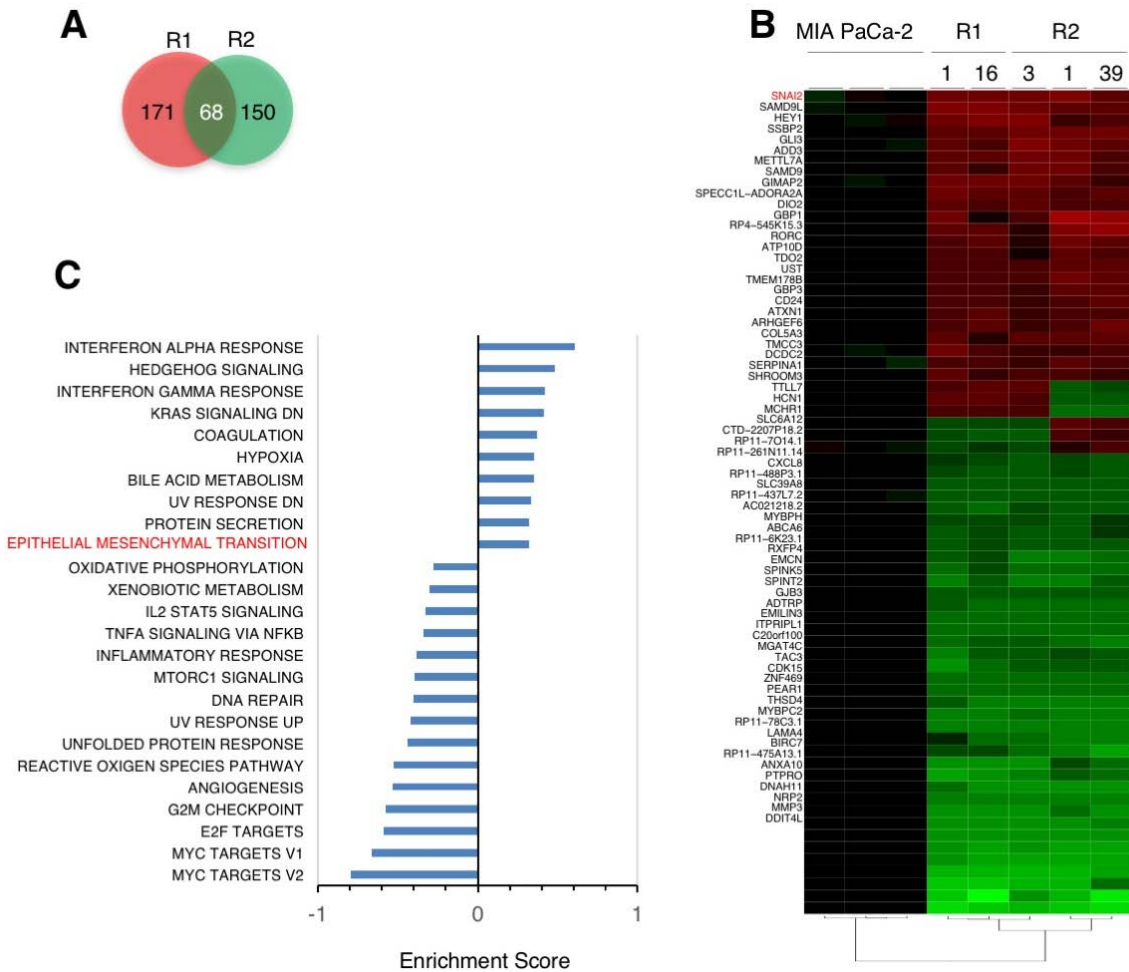


Figure 25. RNA sequencing analysis in parental and resistant cells. (A) Venn diagram showing differentially expressed genes (≥ 4 -fold) with statistical significance ($q < 0.0001$) found in resistant, compared to parental cells. (B) Heatmap of the top up and downregulated genes. Red boxes represent upregulation, whereas green boxes refer to down-regulation in resistant cells. *SNAI2* appears highlighted in red as the most consistently upregulated gene. (C) GSEA report of statistically significant enriched gene sets (hallmarks of cancer database) in the transcriptomic analysis, showing positive or negative enrichment in the resistant cells. Highlighted in red, the enrichment in epithelial to mesenchymal transition signature.

Additionally, we observed a remarkable enrichment of the epithelial to mesenchymal transition (EMT) signature (Figure 25C and 26A), which was consistent with the upregulation of the expression of *SNAI2*, the gene encoding Slug (Figure 25B), one of the prototypical transcription factors that mediates EMT (Nieto et al. 2016). Analysis of the expression of Slug (mRNA and protein) confirmed its increased expression in all resistant cells (Figure 26B and C).

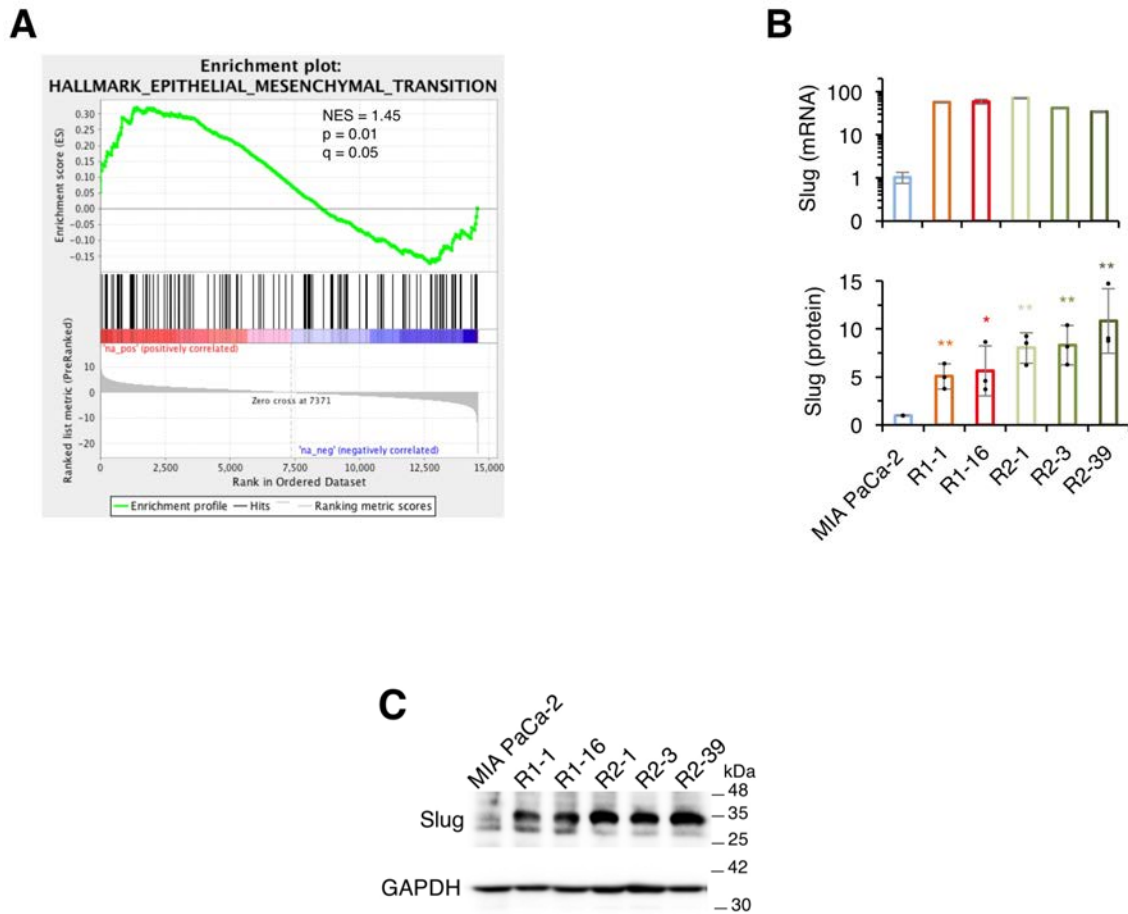


Figure 26. Validation of *SNAI2* (Slug) upregulation in resistant cells. (A) GSEA plot of the enrichment in EMT signature in MEK162-resistant vs parental cells. (B) Upper panel, Slug mRNA levels determined by quantitative real-time PCR and normalized to the levels in MIA PaCa-2. GAPDH was used as endogenous control. Lower panel, Slug protein expression in parental and resistant cells. GAPDH was used as loading control. The values are normalized to MIA PaCa-2 cells. The results are expressed as averages and the error bars correspond to 95% confidence intervals of three independent experiments. P values were calculated using the two-sided Student's t test. (C) Western blot showing Slug protein expression in parental and resistant cells.

Additionally, we observed that the treatment of MIA PaCa-2 cells with MEK162 resulted in a rapid increase in the transcript levels of *SNAI2* (Figure 27A). The upregulation of *SNAI2* expression was reversible, upon removal of the inhibitor, the levels of *SNAI2* transcript decreased. However, repeated treatments with the Mek1/2 inhibitor led to an increase in the expression of Slug, even after removing the inhibitor (Figure 27B). Thus, long-term inhibition of Mek1/2 results in stable, irreversible upregulation of *SNAI2*

expression, as it is observed in the resistant cells maintained for months in the absence of Mek1/2 inhibitor.



Figure 27. Changes in the expression of Slug transcript in MIA PaCa-2 cells upon Mek1/2 inhibition. (A) Levels of Slug mRNA at 6, 12, 24 and 48 hours after treatment with either vehicle or MEK162. GAPDH was used as endogenous control. Data are normalized to vehicle-treated cells at 6 hours. (B) Slug mRNA levels after several rounds of treatment and withdrawal of MEK162. Data are normalized to untreated cells before the start of the treatments.

In conclusion, the obtained resistant cells display a different transcriptome profile, characterized by the enrichment in an EMT gene signature and a remarkable increase in the expression of the EMT transcription factor Slug. Thus, we next proceeded to assess the mesenchymal features of resistant cells in comparison to the parental ones.

2.6 Resistant cells exhibit a mesenchymal phenotype.

MIA Paca-2 are considered epithelial cells with mesenchymal characteristics (Gradiz et al. 2016). We found that they expressed detectable levels of vimentin and fibronectin, two mesenchymal markers, but we were not able to detect the classical epithelial marker E-Cadherin. Consistent with a more mesenchymal phenotype, resistant cells expressed higher levels of these markers (Figure 28A). Thus, prolonged inhibition of the Mek1/2 signaling results in resistance to Mek1/2 inhibitors and, concomitantly, to the apparent acquisition of a more mesenchymal phenotype.

Transcription factors that induce EMT are frequently co-regulated and act in coordination. However, resistant cells express similar transcript levels of five well-known

EMT transcription factors, such as *SNAI1*, *SNAI3*, *TBX2*, *TWIST2* and *ZEB1*, compared to parental cells (Figure 28B), indicating that *SNAI2* is the only EMT transcription factor acting on resistant cells. Consistently, inhibition of Mek1/2 did not cause the overexpression of any of the additional EMT transcription factors analyzed (Figure 28C).

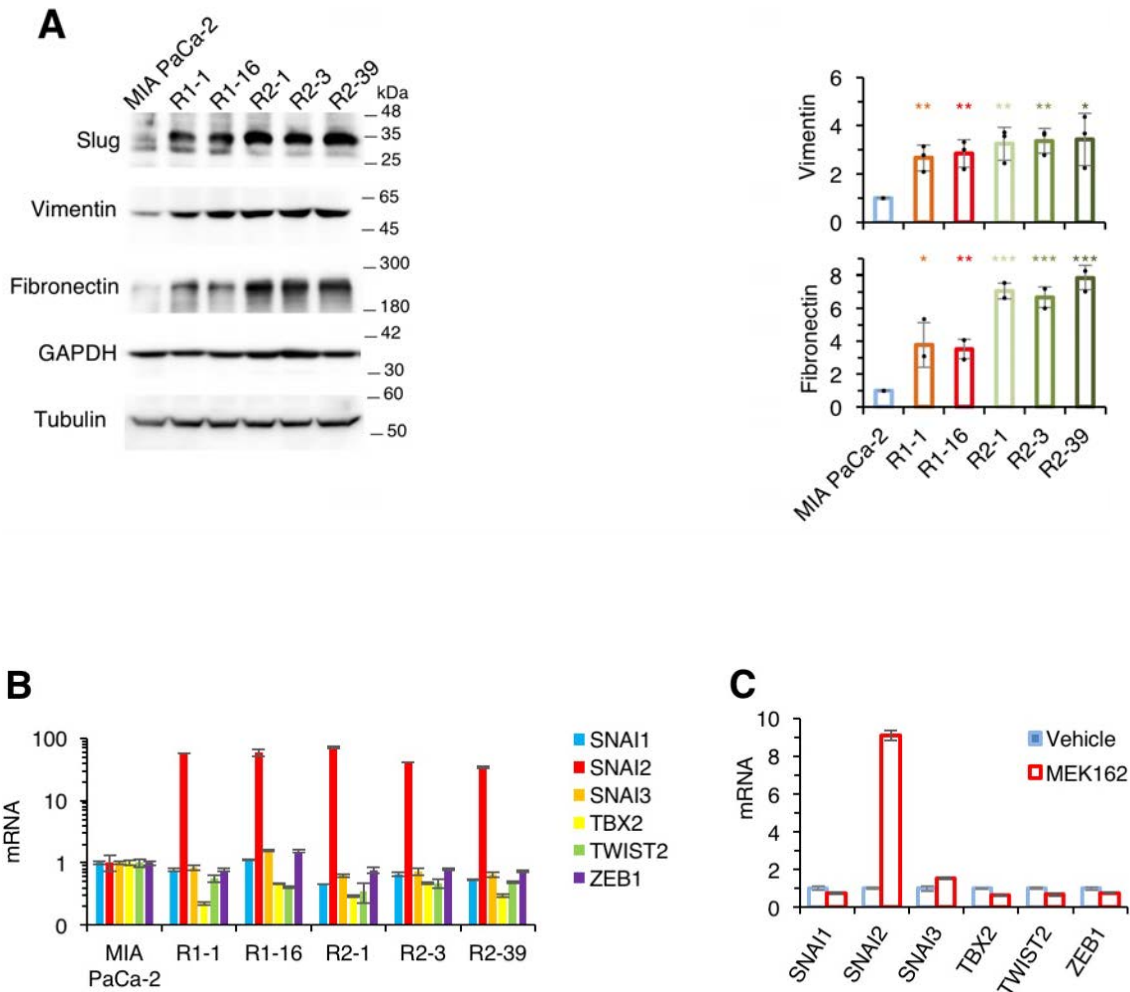


Figure 28. Analysis of mesenchymal markers in parental and resistant cells. (A) Left, Parental and resistant cells were analyzed by Western Blot with antibodies against Slug, vimentin and fibronectin. GAPDH and tubulin were used as loading controls. (A) Right, Western blot quantification of the mesenchymal markers vimentin and fibronectin. Data are normalized to parental MIA PaCa-2 expression. The results are expressed as averages and the error bars correspond to 95% confidence intervals of three independent experiments. P values were calculated using the two-sided Student's t test. (B) mRNA levels of the indicated EMT-TFs in parental and resistant cells determined by quantitative real-time PCR. Each color represents a gene (C) mRNA levels of the indicated EMT-TFs in MIA PaCa-2 cells treated with vehicle or MEK162.

Therefore, resistant cells show increased mesenchymal features, consistent with the enrichment in EMT signature, which may imply an increased metastatic potential.

2.6 MEK162 resistant cells display increased metastatic traits *in vitro* and *in vivo*.

The acquisition of mesenchymal traits can lead to an increased metastatic ability (Nieto et al. 2016). To determine if this was the case of the resistant cells, we compared their behaviors with that of parental cells in several assays. Resistant cells had increased ability to adhere to fibronectin, to migrate and to invade through matrigel (Figure 29A-C). Thus, compared to parental cells, resistant cells displayed increased metastatic capacities *in vitro*.

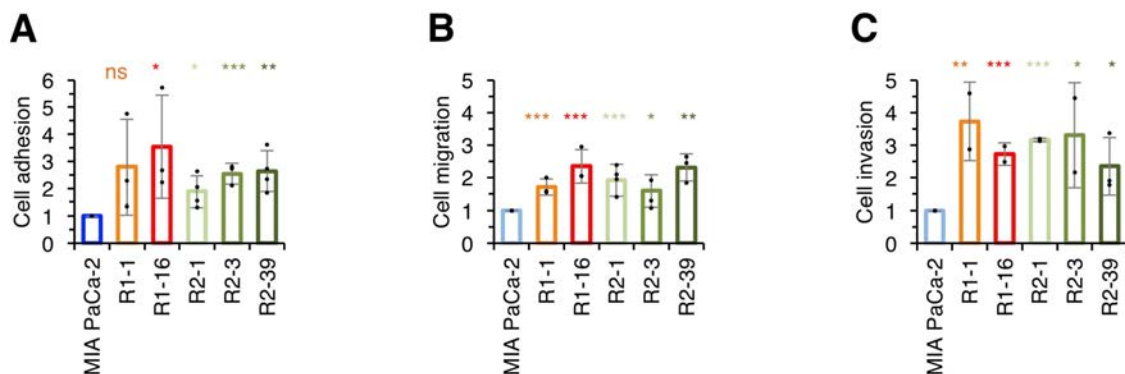


Figure 29. Resistant cells exhibit more aggressive features *in vitro*. Cells were labeled with 5 μ M of Cell Tracker Green reagent and kept overnight in serum-free medium. 24 hours later, the different assays were performed. (A) Adhesion to fibronectin. (B) Transwell migration assay. (C) Cell invasion through matrigel. At the end of each experiment cell number was assessed by means of quantification of Cell Tracker Green-stained cells. Data are normalized to MIA PaCa-2 cells. The results are expressed as averages and the error bars correspond to 95% confidence intervals of three independent experiments. P values were calculated using the two-sided Student's t test.

To confirm these results *in vivo*, we orthotopically implanted parental and resistant cells expressing luciferase into pancreases of immunodeficient mice. After 54 days, we

detected metastatic growths in liver, diaphragm, spleen, lungs and lymph nodes (Figure 30A). Quantitative analyses showed that resistant cells exhibited higher metastatic ability than parental cells (Figure 30B).

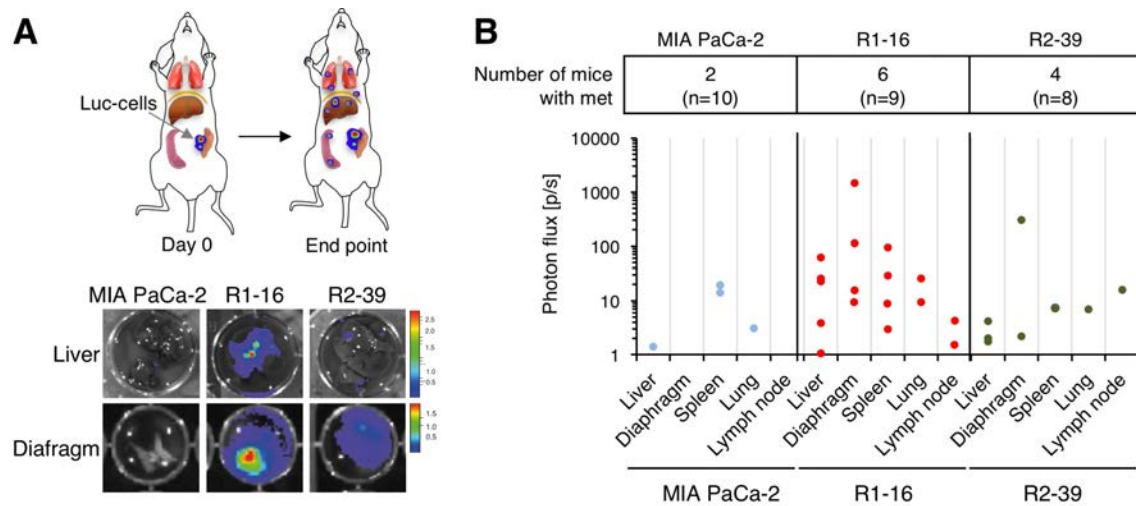


Figure 30. Resistant cells are more metastatic *in vivo*. (A) Upper panel, Parental and resistant cells expressing firefly luciferase were injected into the pancreases of immunodeficient mice. 54 days later, metastatic growths were detected *ex vivo* in liver, diaphragm, spleen, lungs and lymph nodes. Lower panel, Representative luminescence images of the detected metastases in liver and diaphragm (B) *Ex vivo* quantification of metastases by luminescence (photon flux [p/s]). The colored spots represent detected metastatic growths. Blue spots for MIA PaCa-2, red for R1-16 and green for R2-39. The total number of mice with metastases are indicated (n).

Overall, concomitantly with the acquisition of resistance to Mek1/2 inhibition, cells increased expression of the transcription factor Slug, acquired mesenchymal traits, and became more metastatic. Next, we assessed the potential nexus between the increased mesenchymal phenotype and resistance to Mek1/2 inhibition.

2.7 Slug is a central regulator of resistance to Mek1/2 inhibition in pancreatic cancer cells

As Slug has been also described to promote cell proliferation, its expression might be part of a compensatory mechanism intended to evade growth arrest upon Mek1/2 inhibition in Raf/Mek/Erk-dependent cells.

Overexpression of Slug in parental cells resulted in a shift in the IC₅₀ for the Mek1/2 inhibitor comparable to that of resistant cells, that is, almost two orders of magnitude (Figure 31A). Interestingly, Slug expression also increased the expression of fibronectin and vimentin in MIA PaCa-2 cells (Figure 31B). However, some transcription factors may have overlapping functions with Slug (Nieto et al. 2016). To analyze whether similar transcription factors can cause resistance to Mek1/2 inhibition, we overexpressed Snail, another Snail family transcription factor, structurally similar to Slug. Intriguingly, we found that Snail had no effect on the sensitivity to MEK162 (Figure 31C). This correlates with the previous results showing that Snail is not specifically induced in resistant cells or after treatment with MEK162. Therefore, resistance is specifically induced by Slug.

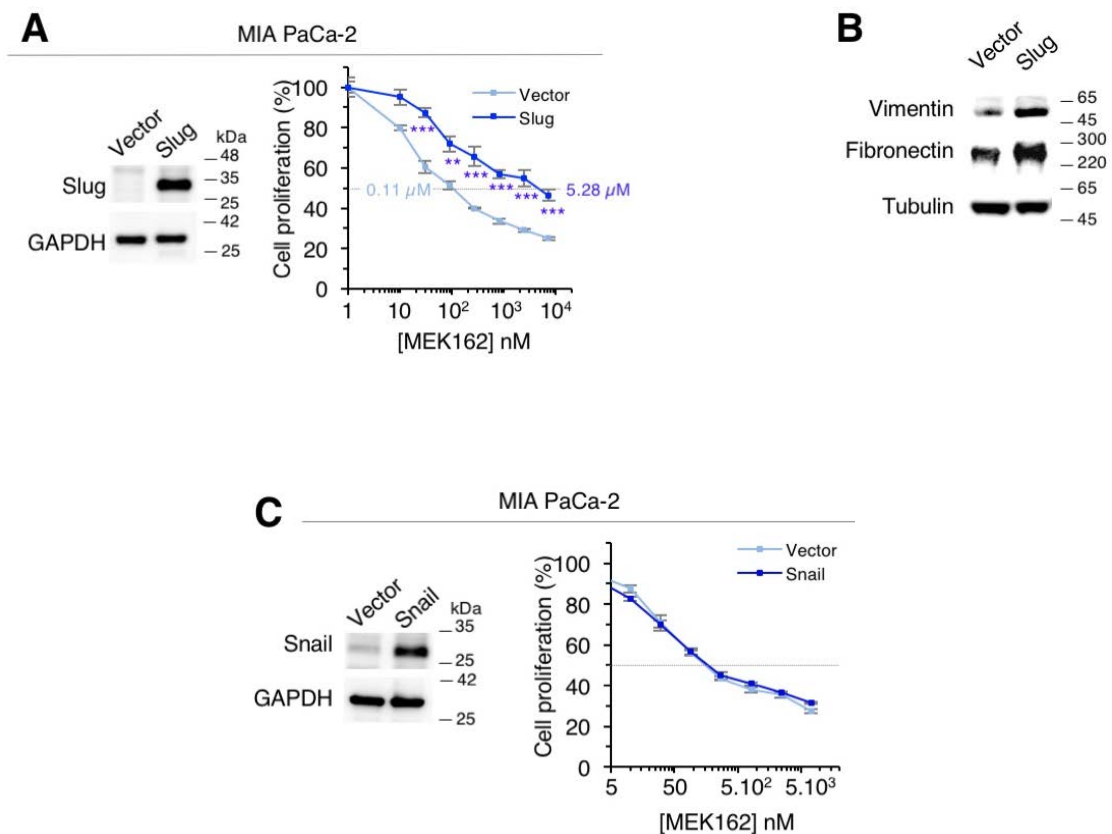
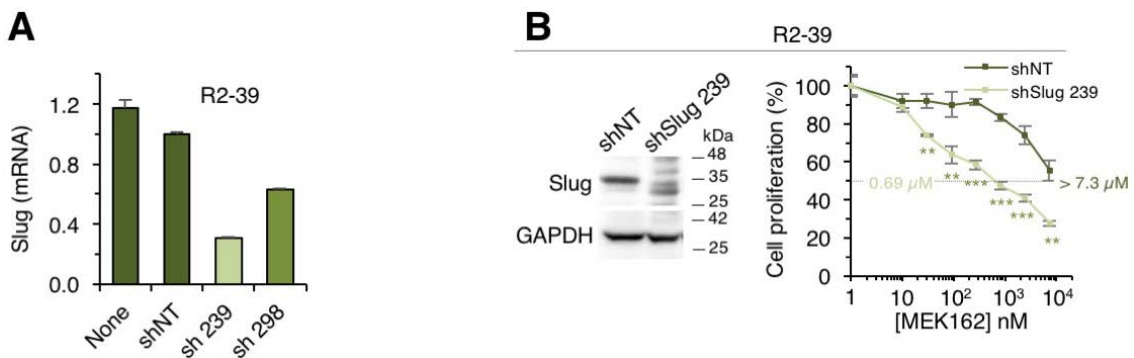


Figure 31. Slug overexpression in parental cells recapitulates the resistant phenotype *in vitro*. (A) Left, Western blot showing the expression of Slug in MIA PaCa-2 cells transduced with either vector or Slug. Right, Dose-response assay in MIA PaCa-2 cells expressing either vector or Slug, treated with different concentrations of MEK162 for 3 days. Then, cell proliferation was measured with the crystal violet staining assay. The results are expressed as averages and the error bars correspond to 95% confidence intervals of three independent experiments. P values were calculated using the two-sided Student's t test. (B) Western blot showing the expression of vimentin and fibronectin in MIA PaCa-2 cells expressing either vector or Slug. Tubulin was used as endogenous control. (C) Left, western blot showing the expression of Snail in MIA PaCa-2 cells expressing either vector or Snail. (C) Right, dose-response assay to MEK162 in MIA PaCa-2 cells expressing either vector or Snail. Cell proliferation was measured with the crystal violet staining assay. The results are expressed as averages and the error bars correspond to 95% confidence intervals of three independent experiments. P values were calculated using the two-sided Student's t test.

Conversely, Slug silencing restored the sensitivity to Mek1/2 inhibition in resistant cells. In order to downregulate the expression of Slug, we tested five independent shRNAs. Two of them effectively reduced the mRNA levels of Slug in resistant cells (Figure 32A). Importantly, the most efficient shRNA (shSlug 239) restored the sensitivity to MEK162 (Figure 32B and D). The less efficient shRNA (shSlug 298) also increased sensitivity to MEK162, albeit to a lesser extent (Figure 32C).



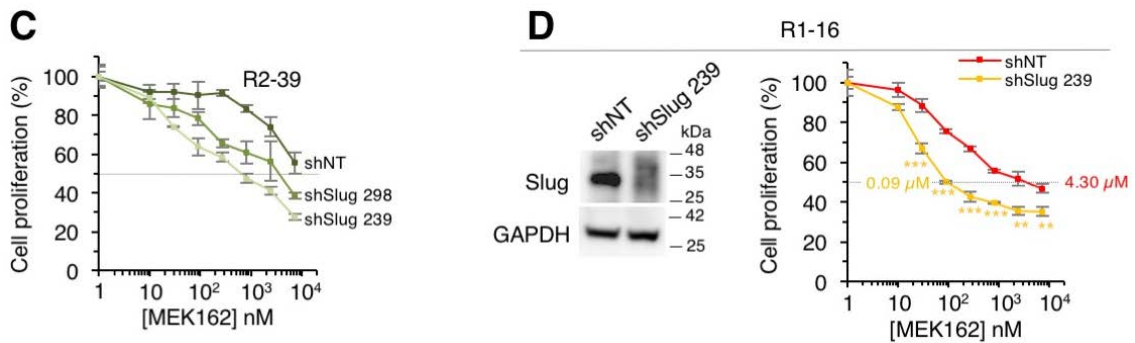


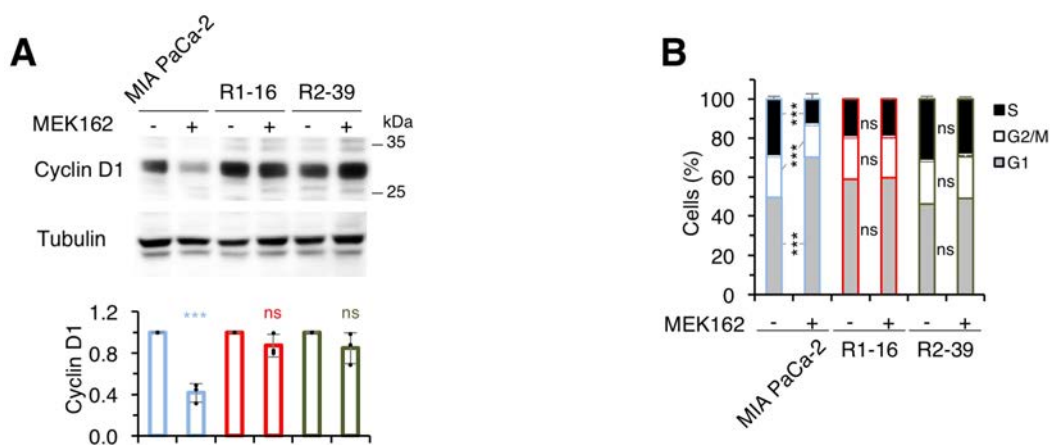
Figure 32. Slug silencing restores sensitivity to Mek1/2 inhibition. (A) Slug mRNA levels determined by quantitative real-time PCR in R2-39 cells and R2-39 cells expressing either a non-targeting shRNA (shNT) or two shRNAs targeting Slug (sh2339 and sh298). Data are normalized to the levels in R2-39 expressing shNT. GAPDH was used as endogenous control. (B) Left, Western blot showing the expression of Slug in R2-39 cells expressing either shNT or the most efficient shRNA targeting Slug (shSlug 239). GAPDH was used as loading control. (B) Right, Dose-response assay in R2-39 cells expressing either shNT or the most efficient shRNA targeting Slug (shSlug 239). Cells were treated with different concentrations of MEK162 for 3 days and cell proliferation was measured by crystal violet staining assay. The results are expressed as averages and the error bars correspond to 95% confidence intervals of three independent experiments. P values were calculated using the two-sided Student's t test. (C) Dose-response assay in R2-39 cells expressing either shNT or an shRNA targeting Slug (sh2339 or sh298). Cells were treated with different concentrations of MEK162 for 3 days and cell proliferation was measured by crystal violet. The results are expressed as averages and the error bars correspond to 95% confidence intervals of three independent experiments. P values were calculated using the two-sided Student's t test. (D) Left, Western blot showing the expression of Slug in R1-16 cells expressing either shNT or the most efficient shRNA targeting Slug (shSlug 239). GAPDH was used as loading control. (D) Right, Dose-response assay in R2-39 cells expressing either shNT or the most efficient shRNA targeting Slug (shSlug 239). Cells were treated with different concentrations of MEK162 for 3 days and cell proliferation was measured by crystal violet staining assay. The results are expressed as averages and the error bars correspond to 95% confidence intervals of three independent experiments. P values were calculated using the two-sided Student's t test.

Thus, gain and loss of function analyses showed the causal role of Slug, which reversibly promoted the transition to a condition in which cell proliferation is independent of activation of the B-Raf-Mek1/2-Erk1/2 pathway. Nevertheless, the mechanism by which Slug promotes cell proliferation in the absence of Mek/Erk signaling needs to be addressed.

2.9 Slug prevents Cyclin D1 decrease by Mek1/2 inhibition

Cellular proliferation requires cell cycle progression through the accumulation of D-type cyclins (Matsushime et al. 1994). The B-Raf-Mek-Erk pathway is a major regulator of the expression of D-cyclins (Albanese et al. 1995). Given that Erk1/2 signaling regulates cyclin D1 and its expression is crucial for cell cycle progression, we hypothesized that resistant cells would maintain the expression of cyclin D1 and cell cycle progression in the presence of MEK162, owing to compensatory mechanisms.

Consistently, treatment of parental cells with the Mek1/2 inhibitor led to a marked decrease in the levels of Cyclin D1 and arrest in the G1 phase of the cell cycle. In contrast, in resistant cells, Mek1/2 inhibition had little or no effect on the levels of cyclin D1 or on the distribution of cells in the different phases of the cell cycle (Figure 33A and B). Thus, acquisition of resistance led to the uncoupling of the regulation of Cyclin D1 from the B-Raf-Mek-Erk pathway. Gain and loss of function analyses showed that Slug is sufficient (Figure 33C) and required (Figure 33D) to promote such uncoupling.



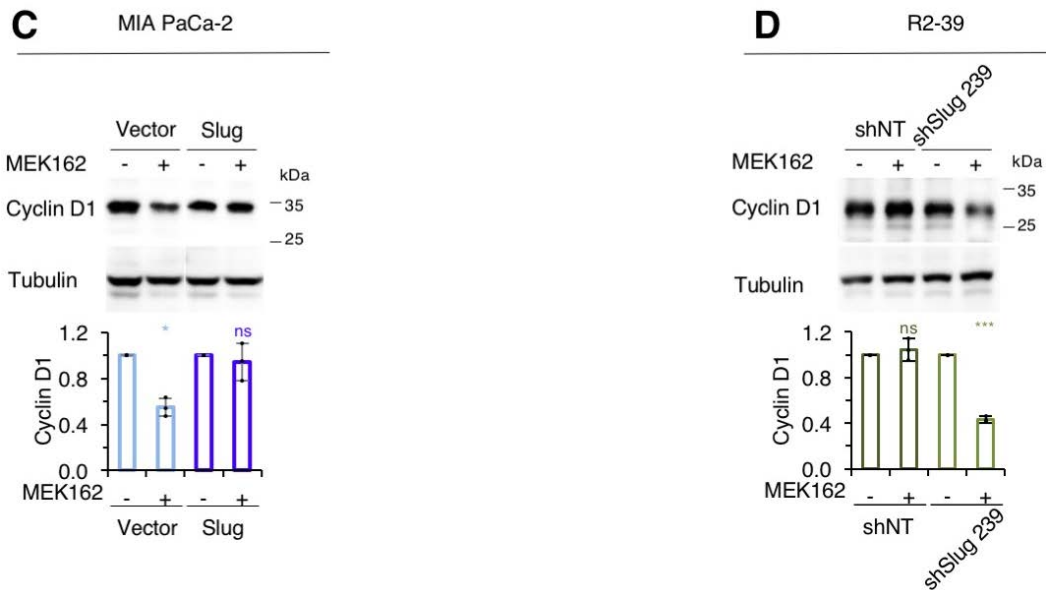


Figure 33. Resistant cells uncouple cyclin D1 regulation from the Raf-Mek-Erk pathway and Slug promotes such uncoupling. (A, upper panel) Western blot showing the protein levels of cyclin D1 in parental and resistant cells treated with vehicle or 90 nM MEK162 for 24 hours. (A, lower panel) Western blot quantification. The results are expressed as averages and the error bars correspond to 95% confidence intervals of three independent experiments. P values were calculated using the two-sided Student's t test. (B) Cell cycle distribution analysis in MIA PaCa-2 and resistant cells treated with vehicle or 90 nM MEK162 for 24 hours. The percentages of cells in each phase of the cell cycle were analyzed by propidium iodide staining and flow cytometry. (C, upper panel) Western blot showing the protein levels of cyclin D1 in MIA PaCa-2 expressing vector or Slug treated with vehicle or 90 nM MEK162 for 24 hours. (C, lower panel) Western blot quantification. The results are expressed as averages and the error bars correspond to 95% confidence intervals of three independent experiments. P values were calculated using the two-sided Student's t test. (D, upper panel) Western blot showing the protein levels of cyclin D1 in MIA PaCa-2 expressing vector or Slug treated with vehicle or 90 nM MEK162 for 24 hours. (D, lower panel) Western blot quantification. The results are expressed as averages and the error bars correspond to 95% confidence intervals of three independent experiments. P values were calculated using the two-sided Student's t test.

Thus, resistant cells with inhibited Erk1/2 signaling are able to resume proliferation owing to Slug expression. Once described the role of Slug in cell proliferation, we next assessed its role in the acquisition of metastatic traits observed in resistant cells.

2.10 Slug regulates the metastatic ability of resistant cells.

To address this aspect, we used the MIA PaCa-2 cells and the resistant clones engineered to over- or under-express Slug, characterized in Figure 31 and 32. Compared with parental cells, MIA PaCa-2 cells overexpressing Slug displayed higher adhesive, migratory and invasive abilities *in vitro* (Figure 34A). Conversely, the knockdown of Slug in resistant cells resulted in decreased aggressiveness (Figure 34B and C).

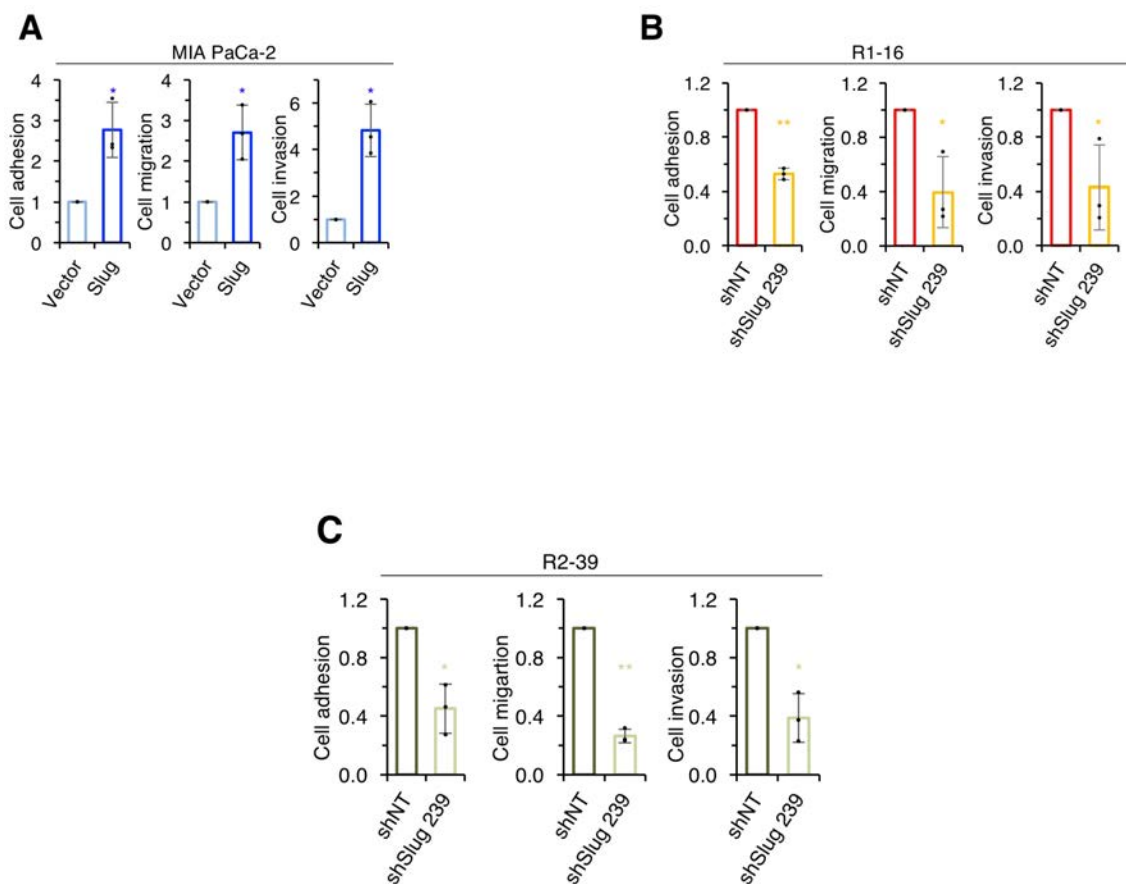
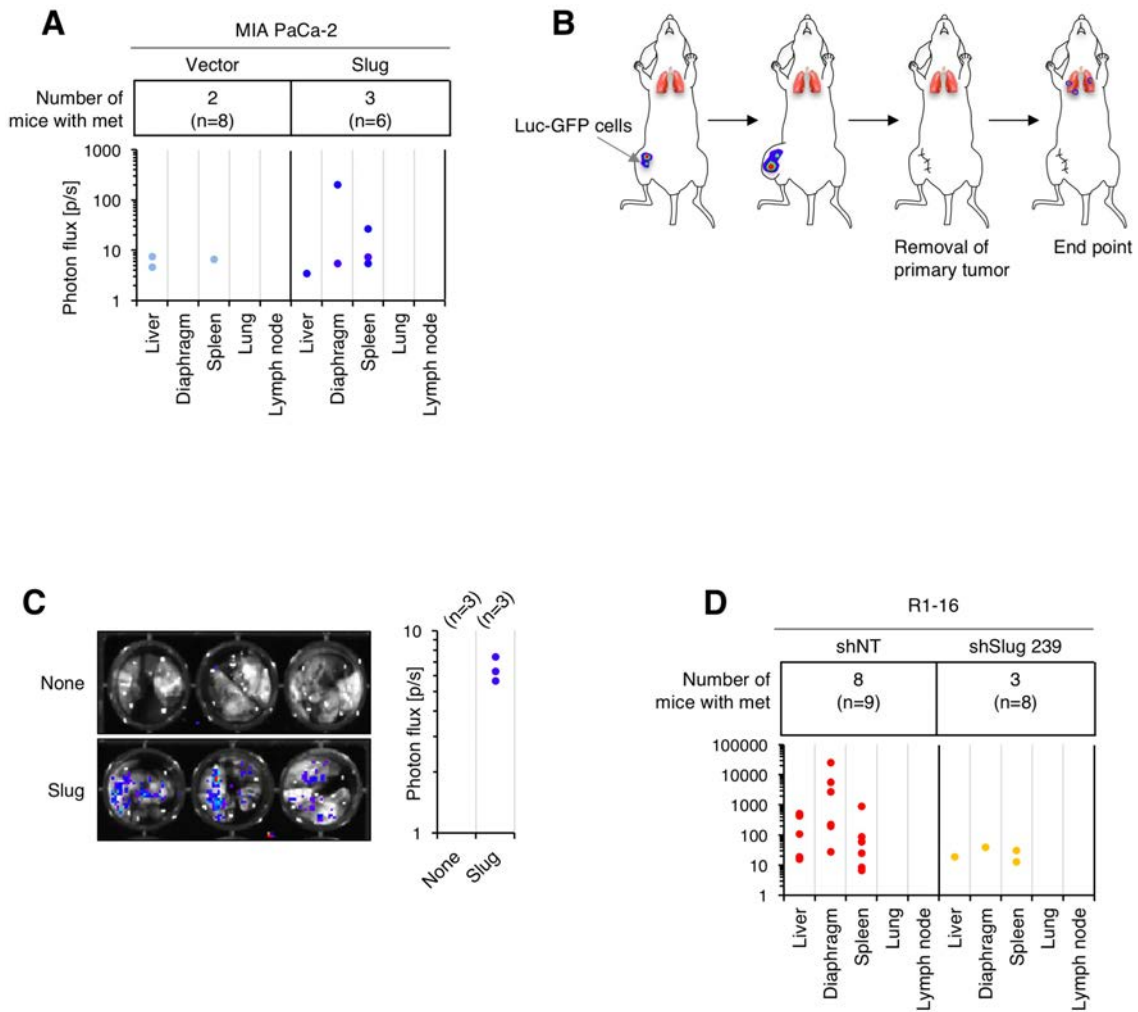


Figure 34. Role of Slug in the acquisition of metastatic traits *in vitro*. Cells were labeled with 5 μ M of Cell Tracker Green reagent and kept overnight in serum-free medium. 24 hours later, the different assays were performed. (A) Adhesion to fibronectin, migration and cell invasion through matrigel assays in MIA PaCa-2 cells expressing vector or Slug. (B) Adhesion, migration and invasion assays in R1-16 cells expressing non-targeting shRNA (sNT) or shRNA targeting Slug (shSlug 239). (C) Adhesion, migration and invasion assays in R2-39 cells expressing non-targeting shRNA or shRNA targeting Slug. In all the experiments, the results are expressed as averages and the error bars correspond to 95% confidence intervals of three independent experiments. P values were calculated using the two-sided Student's t test.

In vivo analyses were consistent with the *in vitro* assays. Overexpression of Slug in MIA PaCa-2 cells led to increased metastases from pancreas to diaphragm and spleen in an orthotopic model (Figure 35A). Moreover, we also engrafted MIA PaCa-2 cells expressing either vector or Slug subcutaneously to analyze their fate for 3 months. Surprisingly, we found that Slug overexpression caused increased metastatic dissemination and growth, exclusively to the lung, with a penetrance of 100% (Figure 35B and C). Conversely, we observed a decrease in the metastatic growths of resistant cells upon Slug silencing in an orthotopic model (Figure 35 D and E). These results clearly show that the acquisition of resistance to Mek1/2 inhibition through Slug overexpression resulted in more aggressive tumors, whose aggressiveness was also dependent on Slug expression.



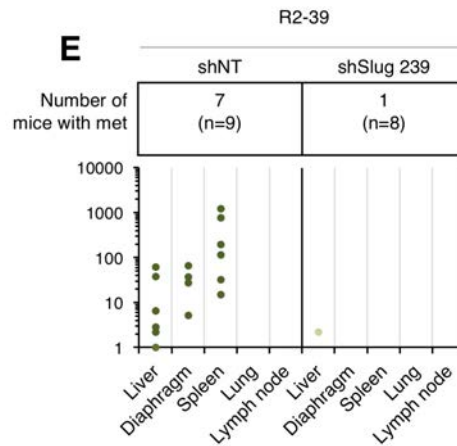


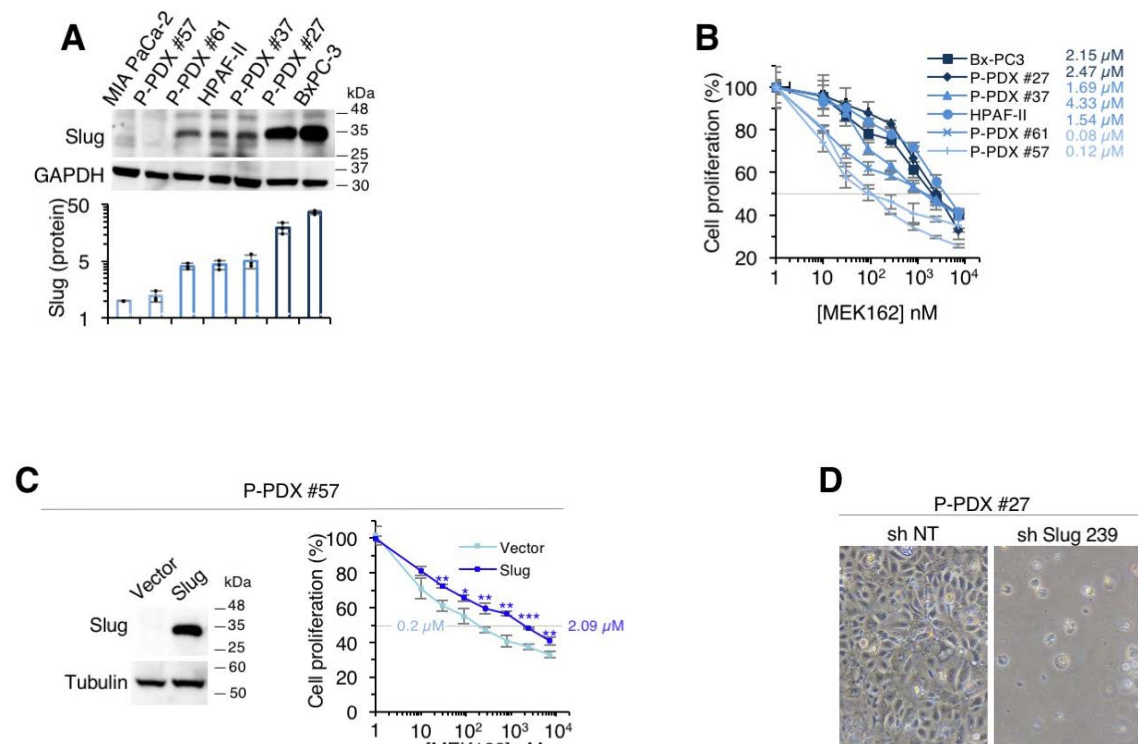
Figure 35. Slug regulates the acquisition of metastatic traits *in vivo*. (A). Quantification of the detected metastases in mice orthotopically injected with either vector or Slug-overexpressing MIA PaCa-2 cells. The colored spots represent detected metastatic growths, measured by luminescence as photon flux density ([p/s]). The total number of mice with metastases are indicated (n). (B) Schematic representation of the subcutaneous metastasis model. Immunodeficient mice were subcutaneously engrafted with either vector or Slug-overexpressing MIA PaCa-2 cells expressing the luciferase reporter gene. When primary tumor volume was around 1000 mm³, tumors were surgically removed and animals were monitored for the appearance of metastasis as luminescent signals (C) Metastatic growths detected in lung. After several rounds of resection of the primary tumor, we measured metastatic growths by ex vivo quantification of luminescence in lungs (D) Quantification of the detected metastases in mice orthotopically injected with R1-16 cells expressing non-targeting shRNA (sNT) or shRNA targeting Slug (shSlug 239). The colored spots represent detected metastatic growths. The total number of mice with metastases are indicated (n). (E) Quantification of the detected metastases in mice orthotopically injected with R2-39 cells expressing non-targeting shRNA (sNT) or shRNA targeting Slug (shSlug 239). The colored spots represent detected metastatic growths. The total number of mice with metastases are indicated (n).

In conclusion, Slug not only regulates resistance to Mek1/2 inhibition, but also controls the enhanced metastatic ability of the MEK162-resistant cells. The next step will be to validate these findings in additional models of pancreatic cancer.

2.11 Slug expression correlates with resistance to Mek1/2 inhibition in a panel of pancreatic cancer cell lines and in patient-derived xenografts.

We have previously shown that sensitivity to Mek1/2 inhibition varies widely among pancreatic cancer cell lines (Figure 12B). To determine if Slug was related to these differences, we assessed Slug expression in a panel of pancreatic cancer cell lines, including commercial cell lines and cultures established from PC-PDXs (herein referred as P-PDXs). Certainly, we observed an inverse correlation between the levels of Slug and the sensitivity to Mek1/2 inhibition (Figure 36A and B).

To functionally characterize the role of Slug in some of these models, we overexpressed Slug in the low expressing P-PDX #57. As a result, we observed an increase in the IC₅₀ for MEK162 of ~10 fold (Figure 36C). When we attempted to downregulate Slug in cells with the highest endogenous levels, we observed a dramatic loss of viability (Figure 36D), showing that Slug is required for the survival of these cells and precluding the analysis of sensitivity to Mek1/2 inhibition in knock-down cells. We did achieve viable cells upon downregulation of Slug from P-PDX #61 and showed that it resulted in the acquisition of sensitivity to MEK162 (~10-fold decrease in IC₅₀) (Figure 36E).



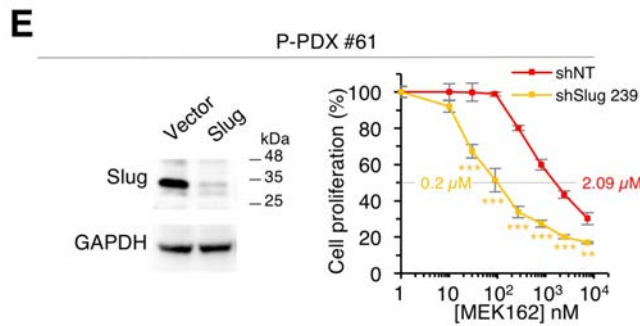


Figure 36. Slug expression and response to MEK162 in pancreatic cancer cell lines and PC-PDXs.

(A) Upper panel, Western blot showing the expression of Slug protein across a panel of pancreatic cancer cell lines and established cultures from PC-PDXs. Lower panel, Quantification of Slug expression. Values are normalized to MIA PaCa-2 cells. GAPDH was used as loading control. The results are expressed as averages and the error bars correspond to 95% confidence intervals of three independent experiments. P values were calculated using the two-sided Student's t test. (B) Dose-response assay to MEK162. Cells were treated with different concentrations of MEK162 for 3 days and cell proliferation was measured by crystal violet staining assay. The results are expressed as averages and the error bars correspond to 95% confidence intervals of three independent experiments. P values were calculated using the two-sided Student's t test. IC50 values are indicated in the graph. (C) Dose-response assay to MEK162 of the sensitive cell line PC-PDX #57 expressing either vector or Slug. The results are expressed as averages and the error bars correspond to 95% confidence intervals of three independent experiments. P values were calculated using the two-sided Student's t test. IC50 values are indicated in the graph (D) Representative pictures of PC-PDX #27 cells expressing non-targeting shRNA (sNT) or shRNA targeting Slug (shSlug 239). (E) Dose-response to MEK162 in PC-PDX #61 cells expressing either non-targeting or Slug-targeting shRNA. The results are expressed as averages and the error bars correspond to 95% confidence intervals of three independent experiments. P values were calculated using the two-sided Student's t test. IC50 values are indicated in the graph

Collectively, correlations and gain and loss of function experiments support that Slug regulates the sensitivity of a variety of pancreatic cancer cells to Mek1/2 inhibition.

Next, we assessed the expression of Slug in patient-derived tumors *in vivo*. We also found that PC-PDXs previously shown to be primarily resistant to Mek1/2 inhibitors *in vivo* (Figure 15A), expressed higher levels of Slug, compared to sensitive PC-PDXs (Figure 37).

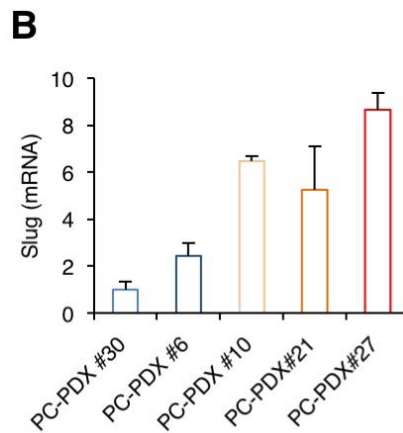
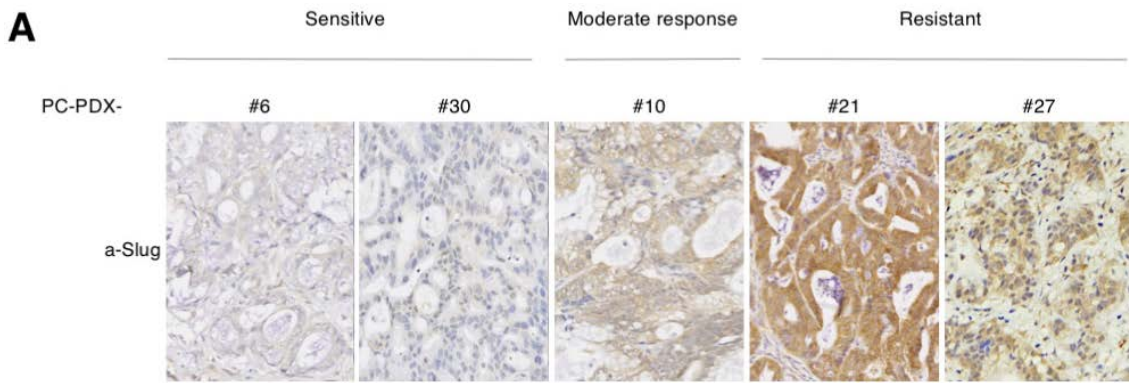


Figure 37. Slug expression correlates with response to MEK162 in PC-PDXs. (A) Representative digital micrographs of Slug-immunostained paraffin-embedded sections from the indicated PC-PDXs. The sections were also stained with hematoxylin. (B) Slug mRNA levels determined by quantitative real-time PCR in PC-PDXs. Data are normalized to PC-PDX #30. GAPDH was used as endogenous control.

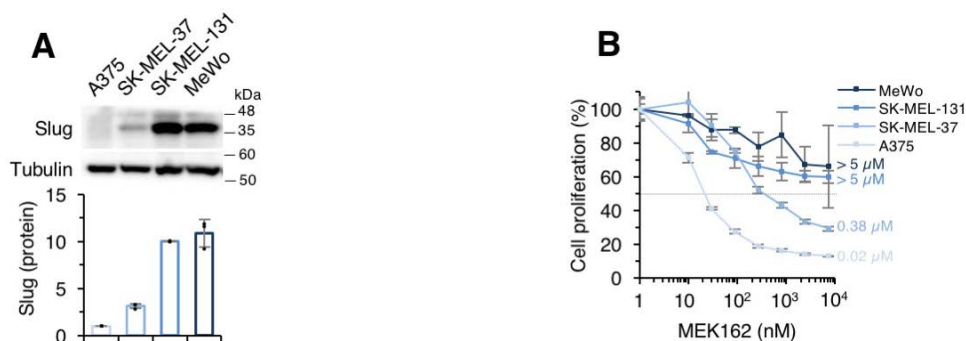
Taken together, these results indicate that Slug expression can predict response to Mek1/2 inhibitors in pancreatic cancer experimental models. Notwithstanding, we hypothesized that these findings may be translated to other cancers with similar genetic backgrounds, such as melanoma.

2.12 Slug expression correlates with resistance to Mek1/2 inhibition in a panel of melanoma cell lines.

As pancreatic cancer, melanoma is frequently characterized by the constitutive activation of the B-Raf-Mek-Erk pathway. Indeed, in more than half of melanomas, activating mutations in *BRAF* drive the malignant progression (Davies et al. 2002). In addition, NF1, a Ras GTPase activating protein, is inactivated in some melanomas, resulting in activation of the B-Raf-Mek-Erk pathway (Nissan et al. 2014). Therefore, we aimed to expand the role of Slug as a mediator of resistance in melanoma models.

First, we also observed a direct correlation between protein levels of Slug and resistance to Mek1/2 inhibition in a panel of melanoma cell lines, harboring either *BRAF* (A375, SK-MEL-37 and SK-MEL-131 cells) or *NF1* (MeWo cells) mutations (Figure 38A and B). The sensitivity of these cells to the B-Raf inhibitor vemurafenib followed a similar trend, as well as the sensitivity to the combination MEK162 + Vemurafenib (Figure 38C).

Second, consistently with our results in pancreatic cancer cells, treatment of the low Slug expressing melanoma A375 cells with the Mek1/2 inhibitor MEK162, upregulated the expression of Slug (Figure 38D). Thus, we aimed to generate a MEK162-resistant model using this cell line. To do so, we treated A375 cells for 3 months with increasing concentrations of MEK162. Strikingly, resistant cells (termed as A375-R2) expressed higher protein levels of Slug compared to the parental cells (Figure 38E).



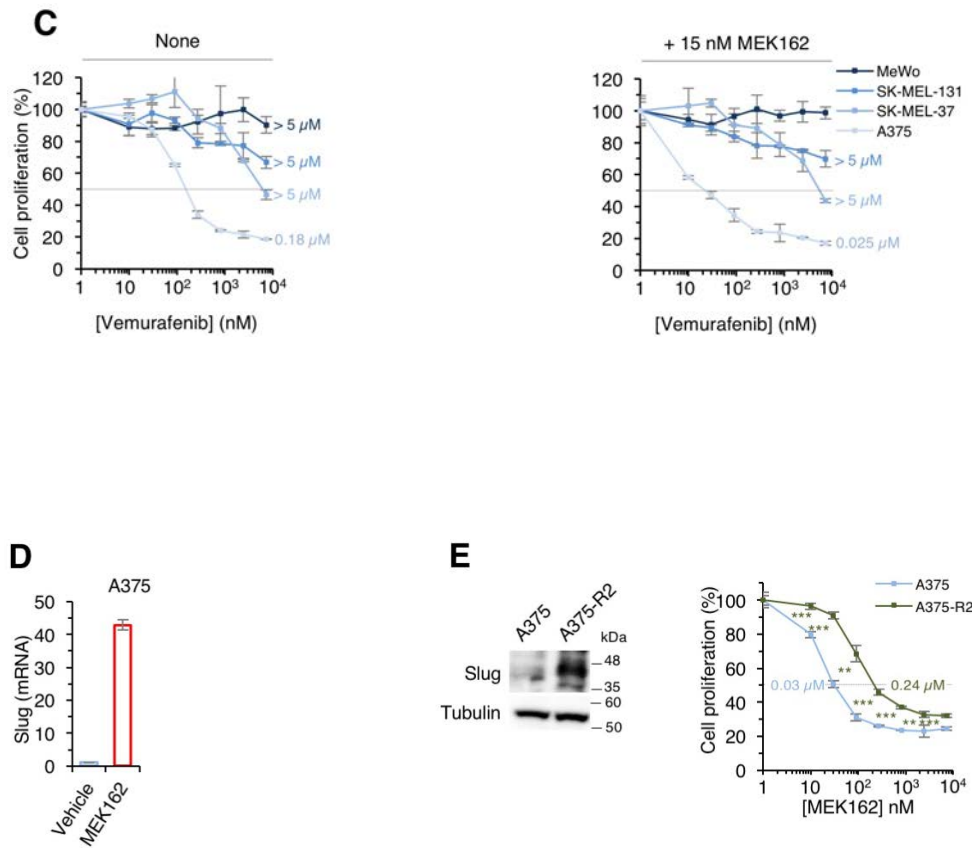
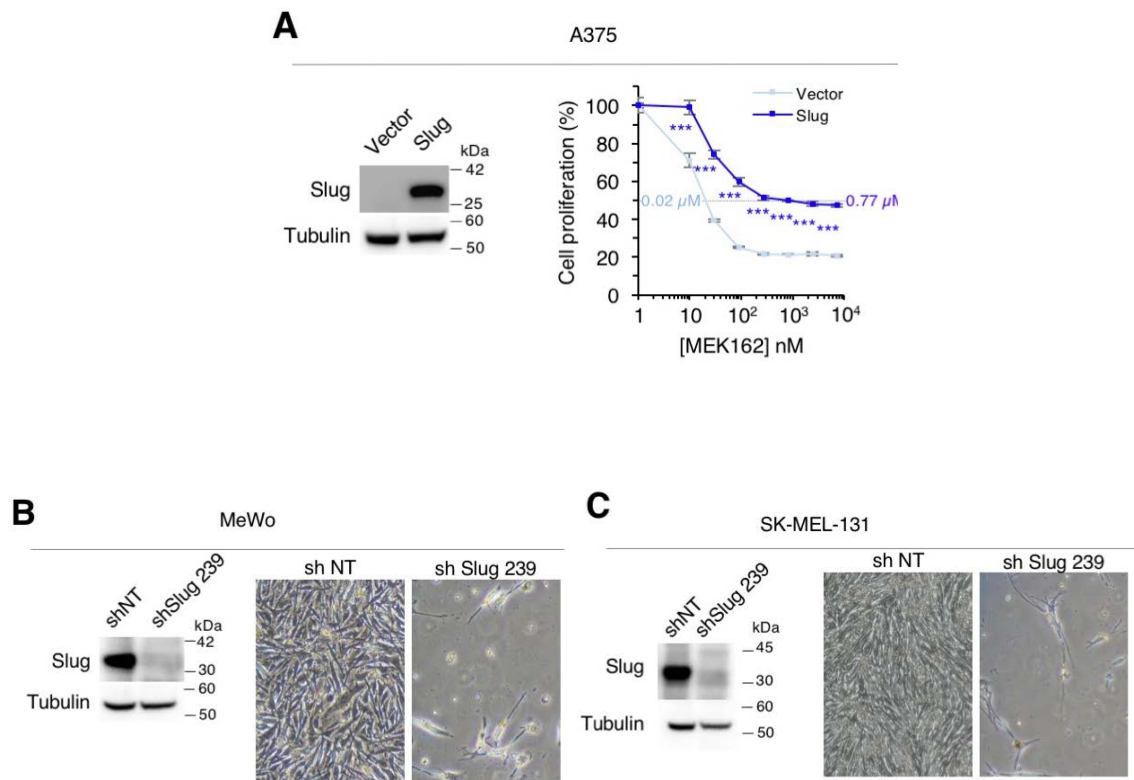


Figure 38. Slug expression and response to MEK162 in melanoma cells. (A) Upper panel, Western blot showing the expression of Slug protein across a panel of melanoma cell lines. Lower panel, Quantification of Slug expression. Values are normalized to A375 cells. Tubulin was used as loading control. The results are expressed as averages and the error bars correspond to 95% confidence intervals of three independent experiments. P values were calculated using the two-sided Student's t test. (B) Dose-response assay to MEK162. Cells were treated with different concentrations of MEK162 for 3 days and cell proliferation was measured by crystal violet staining assay. P values were calculated using the two-sided Student's t test. IC50 values are indicated in the graph. (C) Left, Dose-response assay to vemurafenib. Cells were treated with different concentrations of vemurafenib for 3 days and cell proliferation was measured by crystal violet staining assay. P values were calculated using the two-sided Student's t test. IC50 values are indicated in the graph. Right, Dose-response assay to vemurafenib plus 15 nM MEK162 (approximate IC50 for A375 cells). P values were calculated using the two-sided Student's t test. IC50 values are indicated in the graph (D) Slug mRNA levels in A375 cells treated with either vehicle or MEK162 determined by quantitative real-time PCR. Data are normalized to vehicle-treated cells. GAPDH was used as endogenous control. (E) Left, Western blot showing the expression of Slug in A375 and A375-R2 cells. Tubulin was used as loading control. Right, Dose-response assay to MEK162. Cells were treated with different concentrations of MEK162 for 3 days and cell proliferation was measured by crystal violet staining assay. P values were calculated using the two-sided Student's t test. IC50 values are indicated in the graph.

Third, we also evaluated if Slug expression levels played a casual role in the acquisition of resistance. In fact, we obtained analogous results to the ones observed in pancreatic cancer cells. Overexpression of slug in sensitive A375 cells conferred resistance to Mek1/2 inhibition (Figure 39A). In contrast, knock-down of Slug in the two high-expressing cell lines (SK-MEL-131 and MeWo) resulted in marked loss of cell viability, precluding further analyses (Figure 39B and C). We did succeed in perturbing the expression of Slug in SK-MEL-37 cells, which express intermediate levels of Slug. Again, Slug overexpression and knock-down in this cell line led to acquisition of resistance and sensitization to Mek1/2 inhibition, respectively (Figure 39D and E).



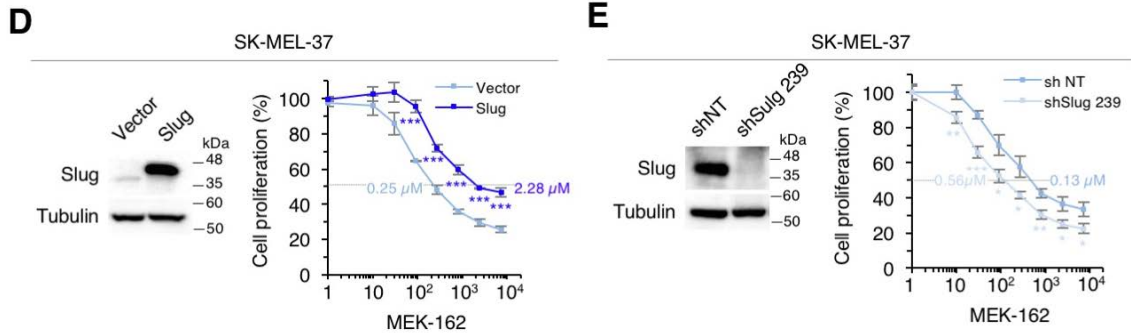


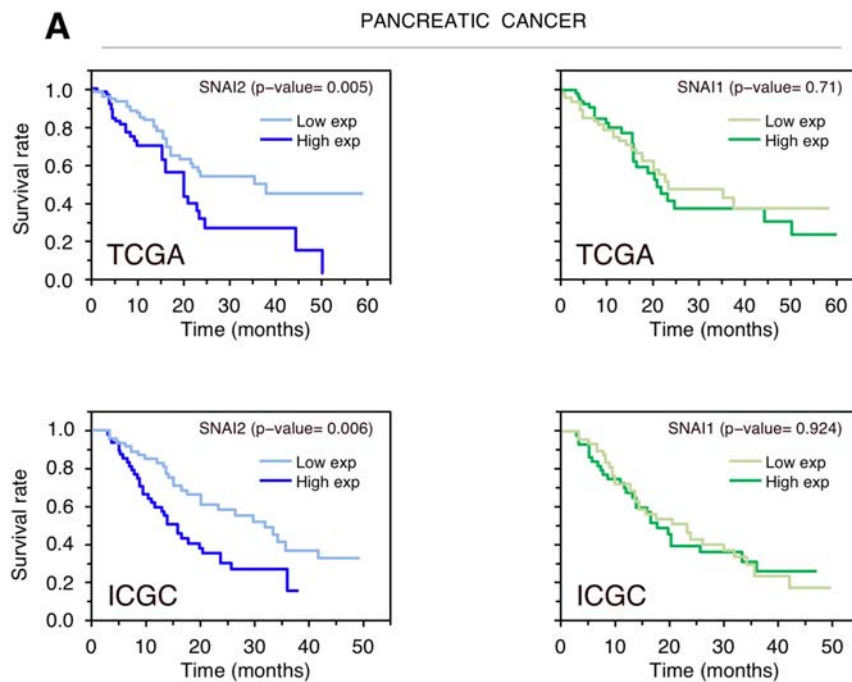
Figure 39. Slug regulates resistance to Mek1/2 inhibition in melanoma cells. (A) Left, Western blot of Slug protein levels in A375 cells expressing either vector or Slug. Tubulin was used as loading control. Right, Dose-response assay to MEK162. Cells were treated with different concentrations of MEK162 for 3 days and cell proliferation was measured by crystal violet staining assay. The results are expressed as averages and the error bars correspond to 95% confidence intervals of three independent experiments. P values were calculated using the two-sided Student's t test. IC₅₀ values are indicated in the graph. (B) Western blot of Slug protein levels in MeWo cells expressing either non-targeting shRNA (sNT) or shRNA targeting Slug (shSlug 239). Tubulin was used as loading control. Representative pictures of MeWo cells expressing either non-targeting shRNA or shRNA targeting Slug. (C) Western blot of Slug protein levels in SK-MEL-131 cells expressing either non-targeting shRNA or shRNA targeting Slug. Tubulin used as loading control. Representative pictures of SK-MEL-131 cells expressing either non-targeting shRNA or shRNA targeting Slug. (D) Left, Western blot of Slug protein levels in SK-MEL-37 cells expressing either vector or Slug. Tubulin used as loading control. Right, Dose-response assay to MEK162. Cells were treated with different concentrations of MEK162 for 3 days and cell proliferation was measured by crystal violet staining assay. The results are expressed as averages and the error bars correspond to 95% confidence intervals of three independent experiments. P values were calculated using the two-sided Student's t test. IC₅₀ values are indicated in the graph (E) Left, Western blot of Slug protein levels in SK-MEL-37 cells either non-targeting shRNA or shRNA targeting Slug. Right, Dose-response assay to MEK162. Cells were treated with different concentrations of MEK162 for 3 days and cell proliferation was measured by crystal violet staining assay. The results are expressed as averages and the error bars correspond to 95% confidence intervals of three independent experiments. P values were calculated using the two-sided Student's t test. IC₅₀ values are indicated in the graph.

Heretofore, we have demonstrated the importance of Slug in modulating resistance to Mek1/2 inhibition as well as conferring metastatic traits by enhancing the aggressive behavior of the cells. As these functions may have an impact in patients, we proceeded to correlate Slug expression with patients' outcome.

2.13 Slug predicts poor outcome in pancreatic cancer and melanoma patients.

To further determine the influence of Slug in the aggressiveness of pancreatic cancer, we queried the Cancer Genome Atlas (TCGA) (<https://www.cancer.gov/tcga>) and the International Cancer Genome Consortium (ICGC) (<https://icgc.org/>) databases. Consistently with the aggressiveness conferred by Slug in our models, high *SNAI2* transcript levels correlate with poor pancreatic cancer patients' outcome, in the two data sets assessed (Figure 40A). By contrast, tumors with high levels of expression of other EMT transcription factors did not have worse outcomes, compared to tumors with low levels (Figure 40A and B), reflecting the particular importance of slug in pancreatic cancer, and confirming our previous results.

The previous *in vitro* results show that Slug also predicts response to Mek1/2 inhibition in melanoma cells (Figure 38A and B). Thus, we also analyzed the levels of Slug in the Human protein atlas database (<http://www.proteinatlas.org/>). We found that high *SNAI2* transcript levels are an unfavorable prognostic factor in melanoma (Figure 40C).



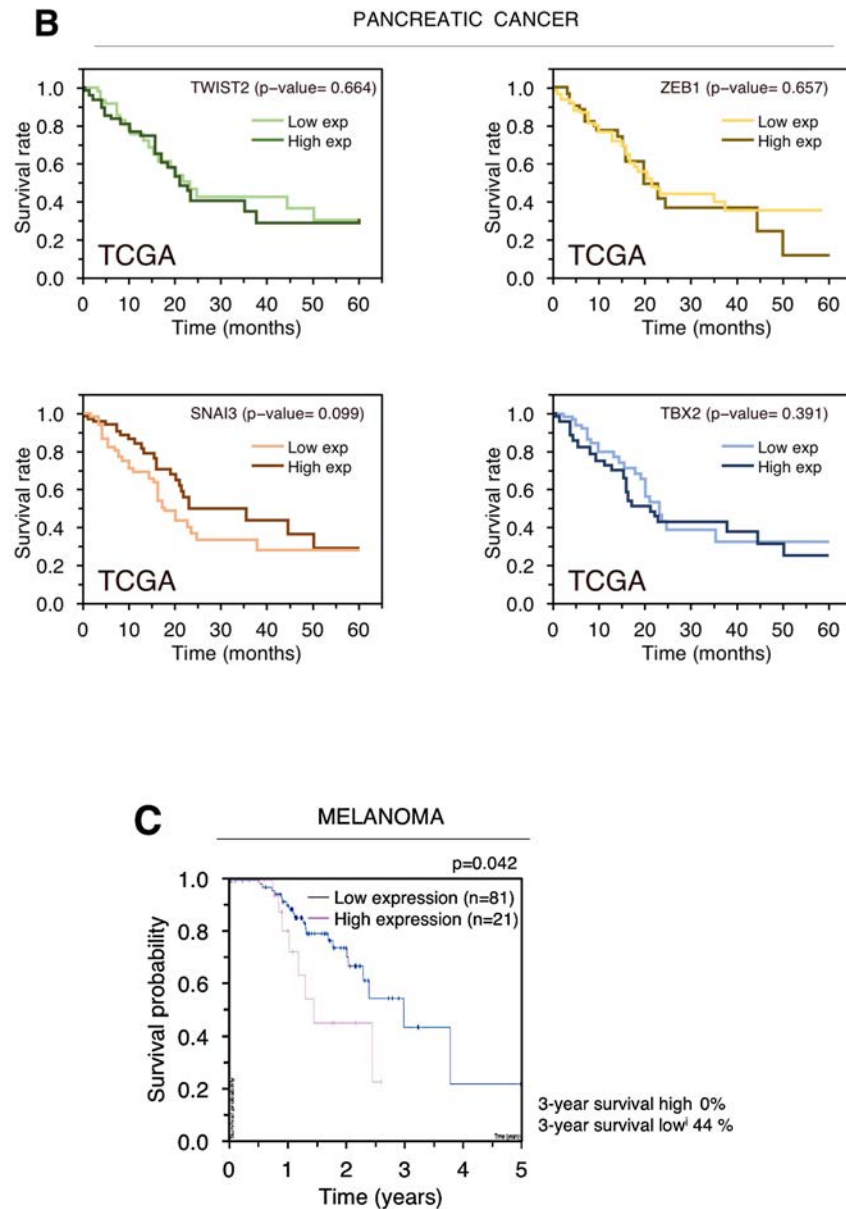


Figure 40. Correlation of *SNAI2* mRNA with patient outcome. (A) Kaplan-Meier survival analysis in patients with high and low *SNAI2* (left panels) and *SNAI1* (right panels) expression in TCGA and ICGC databases. (B) Kaplan-Meier survival analysis in patients with high and low levels of the EMT-TFs *TWIST2*, *ZEB1*, *SNAI3* and *TBX2* expression in TCGA database. (C) Kaplan-Meier survival analysis in melanoma patients stratified by high and low *SNAI2* expression in the human protein atlas database.

In summary, Slug plays a central role in determining sensitivity to inhibition of the B-Raf-Mek-Erk axis as well as in driving the malignant progression in pancreatic cancer and melanoma.

Once identified the impact of Slug expression in patient's survival, we wanted to address the molecular mechanisms involved in Slug regulation in order to find regulators that could be pharmacologically targeted, since there are not currently available inhibitors for Slug.

2.14 ERK5 signaling regulates Slug expression in pancreatic cancer cells with acquired resistance to MEK162.

As described in Figure 23C, analysis of the phosphorylation of intracellular kinases did not identify any activated pathway that could be promoting resistance and, probably, the expression of Slug. The phospho-kinase array included previously described regulators of Slug, such as PI3K, TGF beta or beta catenin signaling effectors. However, none of them were differentially activated. In addition, the array also assessed the activation of 3 members of the MAPK family: Erk1/2, p38 and JNK1/2. Nevertheless, the Erk5 subfamily was not included in the assay. Some reports have indicated that Erk5 can regulate the expression of Slug (Yue et al. 2014; Arnoux et al. 2008). Likewise, it has been recently described that Erk5 is phosphorylated upon Erk1/2 inhibition in pancreatic cancer cells (Vaseva et al. 2018). Therefore, we assessed the levels of Erk5 phosphorylation in the Mek1/2 inhibitor resistant pancreatic cancer cells that we previously generated. Interestingly, we observed a marked expression of phosphorylated Erk5 in the resistant cells (Figure 41A). Consistently with the previous reports, Mek1/2 inhibition led to increased levels of p-ERK5 (Figure 41B). Conversely, ERK5 inhibition also affected Slug mRNA levels, by preventing the concomitant increase in Slug mRNA levels upon treatment with MEK162 in MIA PaCa-2 cells (Figure 41C). In concordance with these observations, Mek5 and Erk5 inhibition led to decreased Slug expression in the resistant cells (Figure 41D).

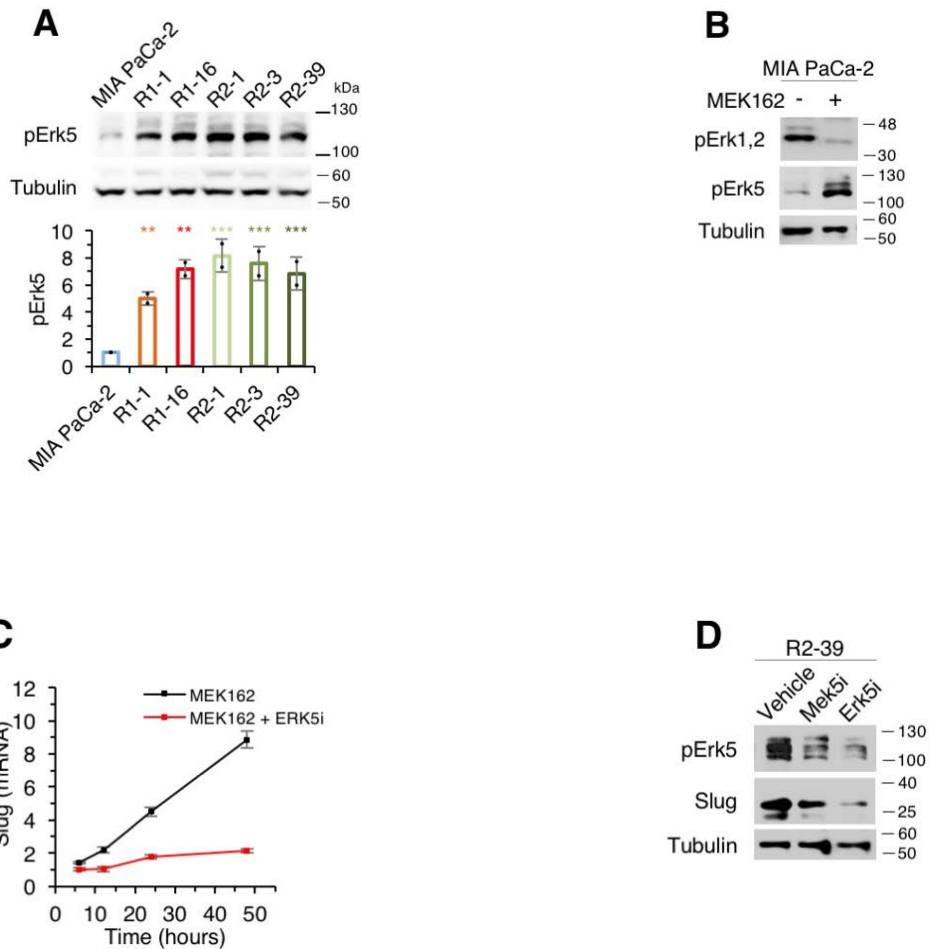


Figure 41. ERK5 activation in Mek1/2 inhibitor resistant cells. (A) Upper panel, Western blot showing the expression of phosphorylated Erk5 in MIA PaCa-2 and resistant cells. Tubulin was used as loading control. Lower panel, Quantification of phospho-Erk5 expression. P values were calculated using the two-sided Student's t test. The results are expressed as averages and the error bars correspond to 95% confidence intervals of three independent experiments. (B) Western blot showing Erk5 phosphorylation in MIA PaCa-2 cells treated with either vehicle or MEK162 for 24 h. (C) Levels of Slug mRNA at 6, 12, 24 and 48 hours in MIA PaCa-2 cells after treatment with either 90 nM MEK162 or MEK162 plus 2.5 μ M of the Erk5 inhibitor XMD8-92 (ERK5i). GAPDH was used as endogenous control. Data are normalized to untreated cells at 6 hours. (D) Western blot showing the effect of the Mek5 inhibitor BIX02189 (Mek5i, 2.5 μ M) and the inhibitor XMD8-92 (Erk5i, 2.5 μ M) on Slug expression in R2-39 cells. Tubulin was used as loading control.

Interestingly, Mek5 and Erk5 inhibition enhanced the sensitivity to MEK162 in the resistant cells, whereas the effect in the parental MIA PaCa-2 cells was minimal (Figure 42A-F). To determine whether the re-sensitizing effect of Erk5 inhibition was only attributed to decreased Slug expression, we overexpressed Slug in a resistant cell line

(R2-39-Slug), obtaining cells expressing high levels of Erk5-independent Slug, apart from the endogenous Erk5-dependent version. As a result, Erk5 inhibition did not sensitize R2-39-Slug cells to MEK162 (Figure 42G), further supporting the causal role of Slug in the resistance to Mek1/2 inhibition.

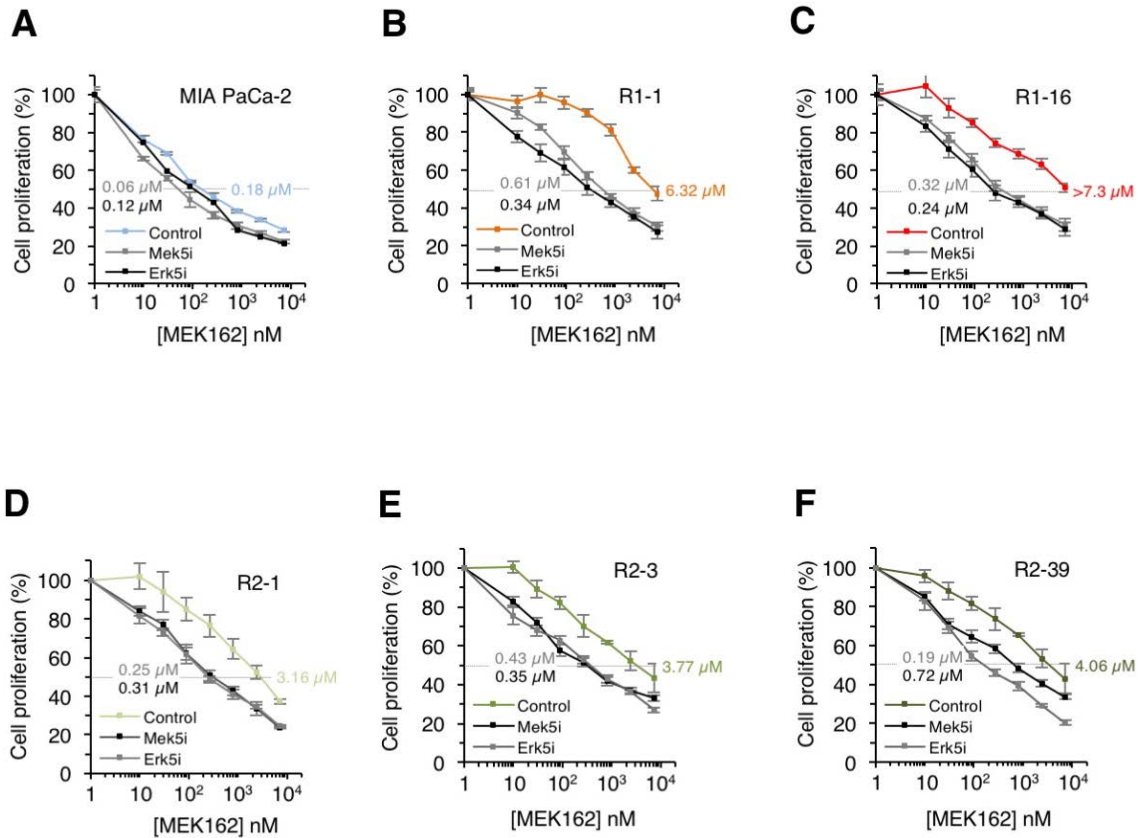


Figure 42. Effect of Mek5 or Erk5 inhibition on the response to MEK162. (A-F) Dose-response assay to MEK162 in MIA PaCa-2, R1-1, R1-16, R2-1, R2-3 and R2-39 cells treated with vehicle, 2.5 μ M of Mek5 inhibitor or 2.5 μ M of Erk5 inhibitor. Cells were treated with different concentrations of MEK162 for 3 days and cell proliferation was measured by crystal violet staining assay. The results are expressed as averages and the error bars correspond to 95% confidence intervals of three independent experiments. For all the experiments, p values were calculated using the two-sided Student's t test. IC50 values are indicated in the graphs. (G) Dose-response assay to MEK162 in R2-39 cells expressing an Erk5-independent Slug. Cells were treated with vehicle or 2.5 μ M of Erk5 inhibitor, and with different concentrations of MEK162 for 3 days and cell proliferation was measured by crystal violet staining assay. The results are expressed as averages and the error bars correspond to 95% confidence intervals of three independent experiments. P values were calculated using the two-sided Student's t test. IC50 values are indicated in the graph.

In summary, we show that Erk5 is consistently activated in the generated resistant cells and that Mek5/Erk5 inhibition leads to decreased Slug expression and re-sensitization to MEK162. Thus, we wanted to correlate these findings in our collection of PC-PDXs.

2.15 p-ERK5 correlates with high Slug expression in PC-PDXs.

We measured the levels of p-ERK5 in the PC-PDXs previously characterized in Figures 15A and 36B. The expression of p-Erk5 is particularly high in the tumors that were primarily resistant to Mek1/2 inhibition and also displayed higher Slug expression (Figure 43), indicating a potential implication of p-Erk5 in the regulation of Slug and the intrinsic resistance to Mek1/2 inhibitors in these PC-PDXs.

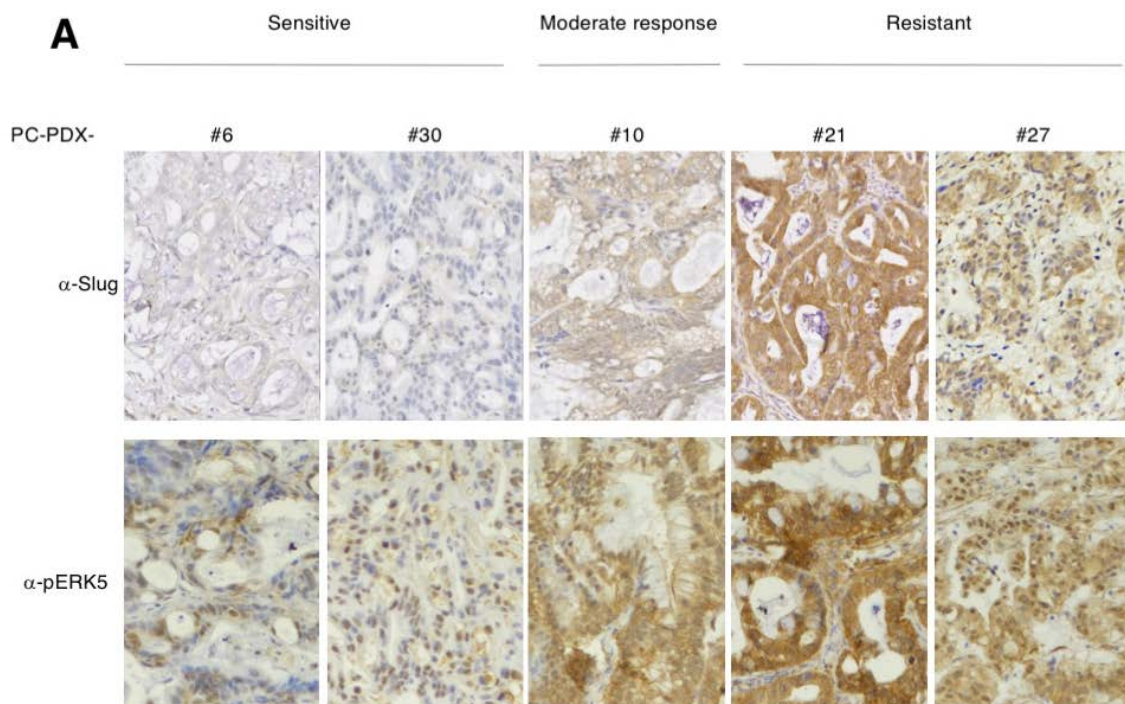


Figure 43. p-ERK5 expression in PC-PDXs. (A) Representative digital micrographs of Slug and p-Erk5-immunostained paraffin-embedded sections from the indicated PC-PDXs. The sections were also stained with hematoxylin.

Collectively, the findings of this part conclude that Slug expression is increased not only as a resistance mechanism to chronic exposure to Mek1/2 inhibitors, but also as an intrinsic resistance mechanism commonly shared by pancreatic cancer and melanoma cells. In addition, its described pro-metastatic effect is consistent with its correlation with poor patient outcome in pancreatic cancer and melanoma. Thus, therapies aimed to prevent the expression of Slug (such as Mek5/Erk5 inhibition) will pave the way for better personalized treatments.

DISCUSSION

The work presented in this thesis provides novel insights regarding the mechanisms of resistance to Mek1/2 inhibition, that contribute to explain the recently reported failure of this therapy in pancreatic cancer patients and to design novel approaches to overcome such resistance and, accordingly, improve patients' outcome.

First, we describe that, although Mek1/2 inhibition may be a relevant therapy in pancreatic cancer, intratumor heterogeneity compromises its effectiveness by the rapid selection of resistant clones in response to the selective pressure imposed by the Mek1/2 inhibitor.

Second, we found that the zinc finger transcription factor Slug promotes resistance to Mek1/2 inhibition in pancreatic cancer and melanoma cells, in addition to correlate with resistance in pancreatic cancer patient-derived tumors. Besides, Slug increases the metastatic ability of pancreatic cancer cells and correlates with poor prognosis in pancreatic cancer and melanoma patients.

Collectively, both represent mechanisms of resistance that must be taken into consideration for designing effective therapies against pancreatic cancer.

Section 1: Pancreatic cancer heterogeneity and response to Mek1/2 inhibition

1.1 PDXs as powerful preclinical tools to study therapies against pancreatic cancer.

Despite the tremendous efforts carried out in the discovery of effective targeted therapies against pancreatic cancer, the vast majority have failed to improve patients' outcome. The intrinsic nature of pancreatic cancer, that entails a high degree intratumor heterogeneity and the complexity of its dense and poorly vascularized microenvironment affects drug accessibility and metabolism in pancreatic cancer, which, in part, may explain the lack of efficacy observed in targeted therapies against PDACs (Neoptolemos et al. 2018).

Thus, in order to design better approaches to treat pancreatic cancer, there is a need of preclinical models that faithfully characterize the processes and molecular mechanisms involved in the progression of this almost incurable disease. In this scenario, patient-

derived xenografts (PDXs) have emerged as a powerful tool to investigate new treatments and biomarkers in cancer research (Byrne et al. 2017). The use of PDX models makes a major contribution in the identification of molecular mechanisms during tumor progression, the role of tumor heterogeneity in the response to targeted therapies and the study of the mechanisms of resistance to current treatments. Besides, these models retain many of the characteristics of the original tumors, including tumor heterogeneity (Byrne et al. 2017). In the first part of this thesis, we have established a collection of pancreatic cancer patient-derived xenografts (PC-PDXs) that preserve the histopathological features and the same driver mutations observed in the original tumors (Figures 13 and 17). These data show the ability of PC-PDXs to faithfully reproduce the original tumors, hence indicating their potential to predict clinical outcomes in patients.

Using *in vitro* and *in vivo* models, we have assessed the efficacy of different therapies intended to inhibit the growth of PDAC in a panel of PC-PDXs and cell lines. To be as close as possible to the clinical setting, we selected therapeutic approaches that resemble those used in patients, in this case Gemcitabine and Nab-Paclitaxel (Hoff et al. 2013) (Figure 12D and 14A). In addition to this chemotherapeutic backbone, we tested the efficacy of Mek1/2 inhibition or DNA de-methylation with the aim of proposing new therapeutic combinations that could benefit PDAC patients in the near future. According to our results, the DNA methylation inhibitor Azacitidine showed promising results both in our *in vitro* and *in vivo* models. Nevertheless, the combination Gem/Nab-P/Aza was toxic *in vivo* and could not be tested (Figure 12E).

Importantly, our data clearly highlight Mek1/2 inhibition as a potentially effective therapy in combination with the standard treatment (Figures 12F and 15). The *in vitro* results indicate that sensitivity to MEK162 according to IC50s vary 40-fold across the different PDAC cell lines tested (Figure 12B). This is particularly intriguing since all these cell lines bear an activating *KRAS* mutation and K-Ras signaling has been shown to be crucial for PDAC development and maintenance (Waters & Der 2018; Bryant et al. 2014; Ying et al. 2012). However, a recent study using murine and human PDAC cell lines showed that genetic ablation of K-Ras by CRISPR/Cas9-mediated knockout resulted in the complete loss of cell viability of nearly 50% of the cells, whereas the other half were K-Ras-independent (Muzumdar et al. 2017), indicating that K-Ras was dispensable in those cells. Likewise, the type of *KRAS* mutation has also been proposed to influence the response to Mek1/2 inhibitors (Brauswetter et al. 2017).

Based on our results, we can expect that only some pancreatic tumors will be sensitive to MEK162. Our data clearly support this possibility since two out of five PC-PDXs (21 and 27) did not respond to the Mek1/2 inhibitor, although they both harbored activating mutations in *KRAS*. PC-PDX 10 exhibits a moderate response to MEK162 presenting a modest tumor shrinkage of only 39% (Figure 15). Therefore, there is a need to find reliable biomarkers to select patients that would potentially benefit of anti-Mek1/2 therapy beyond the mutational status of *KRAS*.

1.2 Role of the desmoplastic compartment in response to Mek1/2 inhibition.

The role of desmoplasia in pancreatic cancer is multifaceted and has opposing roles, making it a longstanding question in the field. The desmoplastic reaction involves the activation of CAFs, responsible of ECM deposition. Pancreatic CAFs have been shown to support pancreatic tumor growth and promote chemoresistance (Apte et al. 2013; Cannon et al. 2018). Furthermore, desmoplasia creates a physical barrier surrounding the tumor that hinders the delivery of therapeutic compounds to the tumor site.

Initial studies characterized the fundamental role of desmoplasia in pancreatic cancer progression through Sonic Hedgehog (SHH) signaling, responsible for the function of pancreatic CAFs (Bailey et al. 2008; Thayer et al. 2003). In the last decade, numerous studies have been assessing the functional consequences of inhibiting SHH signaling. Short-term pharmacological inhibition of SHH led to enhanced delivery of chemotherapy, thus improving survival in a mouse model of pancreatic cancer, by ablating the desmoplastic component (Olive et al. 2009). However, long-term inhibition of SHH enhanced the aggressive behavior of tumor cells leading to increased metastases and decreased survival. The same results were observed in genetic mouse models lacking the expression of *Shh* ligand in the pancreatic cancer epithelium (Rhim et al. 2014). By eliminating the dense desmoplastic component, cancer cells may alleviate the hypoxic and nutrient-deprived nature of the environment, metastasizing to different organs. Collectively, these studies indicate that the stromal compartment restrains PDAC by encapsulating tumor cells and preventing tumor dissemination.

In our PC-PDX models, Mek1/2 inhibition induced, concomitantly, increased levels of desmoplasia (Figure 16), as determined by higher collagen deposition and increased alpha-SMA positive cells in the orthotopic model. Hence, this work buttresses the

inhibitory effect of desmoplasia in tumor progression and provides new insights in the regulation of desmoplasia by Mek1/2 signaling. However, the main limitation of PDX models is the murine origin of the stroma, failing to accurately recapitulate the patient's desmoplastic reaction. Thus, future research is needed to complement these findings. Co-implantation of tumor cells and human CAFs may be a good alternative (Hamada et al. 2012). Likewise, three-dimensional (3D) tumor microenvironment models containing patient-derived tumorspheres (organoids) and matched stromal cells are currently being developed (Tsai et al. 2018). These models may facilitate the study of the interaction between tumor cells and stroma in response to Mek1/2 inhibition.

1.3 Intratumor heterogeneity compromises the effectiveness of anti-Mek1/2 therapies.

As previously mentioned, tumor heterogeneity contributes to the development of resistance to cancer therapies. The existence of diverse tumor cell populations has gained substantial clinical impact in the last years since the appearance of resistant tumor subclones (frequently, with more aggressive potential) has become a major drawback for the efficacy of promising targeted therapies (Bhang et al. 2015; Jamal-Hanjani et al. 2017; Kwak et al. 2015; McGranahan & Swanton 2017). These issues might be circumvented with the establishment of preclinical models that faithfully represent the nature and continuous evolution that takes place in human cancer. The results of this thesis provide novel insights into the biology and treatment of pancreatic cancer, describing that intratumor heterogeneity may represent a major drawback in the response to Mek1/2 inhibition in pancreatic cancer. From the two PC-PDXs that did not respond to MEK162 we isolated *in vitro* different colonies that responded differently to this therapy, with IC50s ranging from ~37.5 to 800 nM (Figure 17D), thereby indicating the presence of diverse tumor cell populations within the tumor.

Further characterization of these cells revealed that they were genetically different and that they likely represent the clonal evolution of the tumor (Figure 17C and E). Besides, we showed *in vitro* and *in vivo* the rapid selection of resistant cell colonies that occurs after the selective pressure imposed by Mek1/2 inhibition (Figure 18). Importantly, the chosen mutations to follow the fate of resistant cells were also found in the original PC-PDXs, confirming that they were not originated during selection in culture. Collectively, these evidences may contribute to explain the lack of efficacy of Mek1/2 inhibition

recently observed in patients with advanced pancreatic cancer (Jeffrey R Infante et al. 2014; Van Cutsem et al. 2018). Considering that the assessment of tumor heterogeneity will be an essential step for the development of effective cancer therapies, there are several emerging technologies aimed to finely dissect the degree of clonal diversity in human tumors, such as single-cell RNA sequencing, multi-region sequencing and analysis of liquid biopsy samples (Dagogo-Jack & Shaw 2018; Liu et al. 2017; Patel et al. 2014; Esposito et al. 2016).

According to the canonical and most accepted theory on PDAC progression, the acquisition of activating mutations in *KRAS* is one of the earliest events during the progression of PDAC (Maitra & Hruban 2008; Waters & Der 2018). However, the fact that in two out of five PC-PDXs we detected different *KRAS* mutations co-existing within the same tumor may reflect the simultaneous appearance of malignant clones or, alternatively, that tumor cells containing two mutations of *KRAS* are selected during tumor evolution. These findings further support recent clinical evidences of case reports indicating the coexistence of different *KRAS* mutations in pancreatic and colorectal tumors (Improta et al. 2013; Visani et al. 2013). Therefore, the clinical implications of harboring distinct *KRAS* mutations within the same tumor as well as the evolution dynamics of these mutations in response to different treatments remain to be elucidated.

In summary, these results point out that Mek1/2 inhibition can be a relevant therapy in pancreatic cancer. Nonetheless, we also anticipate that intratumor heterogeneity and the selection of resistant cells may compromise the efficacy of this therapy. Hence, further research on the potential mechanisms of resistance to Mek1/2 inhibition will be needed in order to refine the long-term efficacy of this therapy.

Section 2: The transcription factor Slug uncouples pancreatic cancer cell proliferation from the Raf-Mek1/2-Erk1/2 pathway

2.1 Generation of models of acquired resistance

The difficulties found to develop efficacious K-Ras inhibitors has prompted the generation of inhibitors of downstream kinases. Although the development of specific Raf-Mek-Erk signaling inhibitors has supposed a major breakthrough in the preclinical and clinical settings, the acquisition of resistance is almost unavoidable. Resistance to different Raf and Mek1/2 inhibitors have been reported in different types of cancer, including melanoma, lung and colorectal cancer (Villanueva et al. 2011; Sun, Hobor, et al. 2014a; Kauko et al. 2018; Ahronian et al. 2015). Pancreatic cancer is far to be an exception as two independent studies indicated the failure of the Mek1/2 inhibitors trametinib and pimasertib in patients with metastatic *KRAS* mutant pancreatic cancer (Jeffrey R Infante et al. 2014; Van Cutsem et al. 2018). In order to better understand the mechanisms of resistance to Mek1/2 inhibition in pancreatic cancer, we generated cell cultures resistant to Mek1/2 inhibitor from the sensitive *KRAS* mutant cell line MIA PaCa-2, previously characterized in the first part of the thesis. To finely dissect the potential mechanisms of resistance, we establish sub-clones from the pools of resistant cells (Figure 20). Interestingly, all of them retained the same degree of resistance after 3 months of drug absence (Figure 21), in contrast to recent reports indicating that drug holiday regimes restore sensitivity to targeted therapies (Sun, L. Wang, et al. 2014b).

Despite this *in vitro* model has led us to identify Slug as a common mechanism of resistance to Mek1/2 inhibition, we open the possibility to establish an *in vivo* resistant model to assess whether the mechanisms *in vitro* can be recapitulated, considering also the contribution of the tumor stroma, that has been recently reported to confer resistance to B-Raf and Mek1/2 inhibitors in *BRAF* mutant melanoma through FAK-dependent signaling (Hirata et al. 2015).

2.2 Contribution of genomic and transcriptomic analyses

Most of the studies about resistance to Raf-Mek-Erk signaling inhibitors reported to date involve the acquisition of mutations and gene amplifications that reinstate Erk1/2 signaling, such as genetic events in *BRAF*, *NRAS*, *NF1*, *EGFR*, *MET*, *MEK1*, *MEK2*,

ERK1 and *ERK2* (Corcoran et al. 2010; Emery et al. 2009; Anon 2013). However, in this thesis we describe a novel mechanism of resistance based on the uncoupling of cell proliferation from the B-Raf-Mek-Erk pathway. Exome sequencing results showed that this particular resistance cannot be explained by the acquisition of mutations within the B-Raf/Mek/Erk pathway or compensatory pathways (Figure 24). Interestingly, we did not detect any common mutations between the two strategies (R1 and R2), suggesting that probably the detected mutations were acquired regardless of the selective pressure imposed by MEK162. Likewise, we also demonstrate that these cells acquire independence of Raf-Mek-Erk signaling through a compensatory mechanism by analyzing the phosphorylation of Erk1/2 after Mek1/2 inhibition, that is equally impaired in parental and resistant cells (Figure 23A).

By contrast, transcriptome analysis by RNA-seq definitely provided more insights in the identification of the mechanisms of resistance as we were able to detect similarities within the gene expression profile in resistant cells. Through GSEA, we detected enrichment in signatures previously described to be affected after Mek1/2 inhibition, like interferon response (Lulli et al. 2017), downregulation of K-Ras signaling, Myc (Marampon et al. 2006) and E2F downstream targets (Korotayev et al. 2008). Interestingly, we did not detect enrichment in signaling pathways that have been previously shown to promote resistance to Raf-Mek-Erk signaling, such as Hippo YAP/TAZ (Lin et al. 2015), STAT3 (H.-J. Lee et al. 2014), PI3K (Wee et al. 2009) or Wnt/beta catenin signaling (G. Chen et al. 2018).

Although we focused more in the enrichment in epithelial to mesenchymal transition, that has been previously described to exert resistance to anti-cancer therapies (Shibue & Weinberg 2017) and it was consistent with the up-regulation of Slug, it would be interesting to explore the contribution of the other significantly enriched gene signatures to the resistant phenotype, as well as their potential nexus to the enrichment in EMT and Slug expression. For instance, inhibition of interferon gene expression has been recently reported to overcome resistance to Mek1/2 inhibition in K-Ras mutant colorectal cell lines (Wagner et al. 2019). Hypoxia has been shown to enhance Slug transcriptional activity by increasing its SUMOylation in non-small-cell lung cancer cells (Hung et al. 2019). Sonic hedgehog signaling elements were also enriched and have been implicated as positive regulators of EMT during renal fibrosis (Ding et al. 2012) and in lung adenocarcinoma cells (H. Li et al. 2016). Moreover, knockdown of the hedgehog transcription factors Gli1 and Gli2 restored sensitivity to B-Raf inhibition in melanoma

cells with acquired resistance (Faião-Flores et al. 2017). Thus, the implication of these gene sets in the regulation of Slug and resistance to Mek1/2 inhibition remain to be addressed.

2.3 Slug uncouples cell proliferation from Raf-Mek-Erk signaling

In this work, we have identified the transcription factor Slug as a critical regulator of resistance to Mek1/2 inhibitors. The expression of Slug makes cell proliferation independent on Raf-Mek-Erk signaling, whereas its genetic silencing restores sensitivity to Mek1/2 inhibition (Figure 31A and 32). However, it has not been previously described how Slug could regulate cell proliferation in the absence of Raf-Mek-Erk signaling, putatively required by *KRAS* mutant cancer cells to proliferate. Some studies indicate that Slug is able control proliferation in prostate and breast cancer cells (Emadi Baygi et al. 2010; Y. Li et al. 2015). Likewise, other studies showed that Slug indirectly prevents the proteasome degradation of cyclin D1 by preventing its ubiquitination (Mittal et al. 2011). In agreement to those results, we have demonstrated that Slug can maintain the expression of cyclin D1 in the presence of MEK162, uncoupling the regulation of cyclin D1 by the Raf-Mek-Erk signaling (figure 33C). In contrast, Slug downregulation by shRNA prevented such uncoupling (Figure 33D). However, the mechanisms by which Slug controls, directly or indirectly, the levels of cyclin D1 in the absence of Mek/Erk signaling remain unclear. As Slug is a transcriptional repressor (Hemavathy et al. 2000), we hypothesize that the transcriptional network activated by Slug culminates in the repression of positive regulators of cyclin D1 ubiquitination. To fully address this open-ended question, the identification of the genes positively and negatively regulated by Slug becomes crucial. Chromatin immunoprecipitation sequencing (ChIP-seq) assays to determine DNA binding sites for Slug and RNA-sequencing comparing resistant cells before and after Slug silencing will definitely contribute to identify the downstream targets of Slug that mediate its functions.

2.4 Slug as a predictor of response to Mek1/2 inhibitors

First, the ability of Slug to predict response to Mek1/2 inhibition in different cellular contexts has been assessed in this thesis. We found a positive correlation between Slug expression and resistance to MEK162 in a panel of pancreatic cancer cells (Figure 36A

and B). When possible, gain and loss of function experiments also showed that Slug is necessary and sufficient to uncouple cell proliferation from the B-Raf-Mek-Erk pathway (Figures 36 C and E). Interestingly, in the cell line P-PDX 27, expressing high endogenous levels of Slug and intrinsically resistant to Mek1/2 inhibition, Slug silencing led to cell death (Figure 36D), highlighting the dependency of these cells on Slug to proliferate and confirming the importance of Slug in the regulation of cell survival. These results are in agreement with the pro-survival effects of Slug previously reported (S. Kim et al. 2014; Merino et al. 2015). Due to technical limitations, we could not silence Slug in all the cell lines (such as P-PDX #37, HPAF-II and BxPC-3) despite of using a total of 7 different shRNAs. It might be reasonable that the deleterious effects of Slug downregulation in these cell lines could activate mechanisms to impair such downregulation. Additionally, experiments intended to generate knock-out cell lines for Slug by CRISPR-Cas9 system are underway.

Second, detectable levels of Slug were identified in 5 out of 7 pancreatic cancer cell lines that, concomitantly, were resistant to MEK162, indicating the intrinsically resistant nature of this disease to Mek1/2 inhibitors and the need of developing new therapeutic approaches that could circumvent this resistance. Our results may meet this clinical need. Indeed, supporting the notion that the expression of the EMT-TF Slug confers independence of Ras-Erk1/2 signaling, Genovese et al. described that the mesenchymal populations identified in pancreatic tumors were more aggressive, pro-metastatic and displayed low engagement to MAPK signaling in genetically engineered mouse models and patient samples (Genovese et al. 2017). These observations also reinforce the results of the above-mentioned study by Muzumdar et al, in which *KRAS* genetic ablation was lethal only to 50% of the PC cell lines tested. In this study, they also described that K-Ras-independent cell lines exhibited enhanced mesenchymal and aggressive features upon *KRAS* ablation, and their genetic signature correlated with poor survival in patients (Muzumdar et al. 2017). However, in these two studies the implication of Slug was not shown, and therefore future research is needed to unveil its role in those K-Ras-independent tumor populations.

Third, we also assessed the expression of Slug in melanoma cell lines harboring activating mutations in Raf-Mek-Erk regulators, such as *BRAF* and *NF1*. Gain and loss of functions of Slug recapitulated the results observed in pancreatic cancer cell lines. As observed in MIA PaCa-2 cells, treatment with MEK162 in the low Slug-expressing A375 cells also increased Slug mRNA levels, indicating that Mek1/2 inhibition leads to the

concomitant increase of Slug expression also in this background. Consistently with what was observed in P-PDX 27 cells, Slug silencing in the highly expressing Sk-Mel-131 and MeWo cells also promoted cell death, supporting the relevance of Slug in cell proliferation also in this background. The cells that tolerated Slug silencing gained dependency of the B-Raf-Mek-Erk pathway, indicating that the number of pathways that sustain cell proliferation is limited and that therapies inhibiting Slug and B-Raf-Mek-Erk will be efficacious in different cellular contexts. The analysis of different cell lines, thus, showed that cells with high levels of Slug are primarily resistant to Mek1/2 inhibition regardless of the mutational status. By contrast, pancreatic cancer and melanoma cells with low levels are sensitive, but they can gain resistance through chronic treatment, which results in increased levels of Slug (Figure 26B and C, Figure 27 and Figure 38E). Importantly, we have shown that this mechanism of acquired resistance is general and that it is not restricted to only pancreatic cancer cells, but also by melanoma cells.

Fourth, the *in vitro* predictive value of Slug was also confirmed *in vivo*. Slug positively correlated with low response to Mek1/2 inhibition in our collection of PC-PDXs. Remarkably, the staining pattern of Slug was almost exclusively restricted to tumor cells, displaying a very weak signal in the stroma (Figure 37). Unexpectedly, in the three tumors that stained positive for Slug, we observed mixed cytoplasmic and nuclear staining of this transcription factor. Due to its transcriptional repressive functions, Slug is expected to be found exclusively in the nuclear compartment. However, cytoplasmic and nuclear staining of Slug has been also reported in thyroid tumors, bladder carcinomas (Q. Yu et al. 2010) colorectal carcinoma (Shiomi et al. 2006) and gastrointestinal sarcoma tumors (Pulkka et al. 2017), among others. Likewise, studies in mouse embryos described that Slug can be localized in nucleus and cytoplasm in specific stages (Bell & Watson 2009). Consistently, the positive staining of Slug correlated with its transcript abundance measured by qRT-PCR (Figure 37B), reinforcing the reliability of the immunostaining. As the cytoplasmic function of Slug has not been described so far, future research will be needed to explain this localization pattern.

Finally, since pancreatic cancer patients are not currently being treated with Mek1/2 or Erk1/2 inhibitors owing to the lack of response in clinical studies, we could not validate the predictive value of Slug in pancreatic cancer patients treated with this therapy. Albeit, in the case of melanoma, samples from responding and non-responding patients to combined B-Raf and Mek1/2 inhibitors are available and the relevance of Slug in the prediction of treatment response will be determined.

2.5 Slug controls the metastatic phenotype of resistant cells

Although EMT has been shown to confer resistance to chemotherapies (Shibue & Weinberg 2017), little is known about its role in resistance to Mek1/2 inhibitors. GSEA showed a consistent and significant enrichment in EMT signature in resistant cells, paralleled by a consistent increase in the expression of the EMT-related transcription factor Slug (Figure 26) and the acquisition of mesenchymal traits (Figure 28A). Despite MIA PaCa-2 cells are considered epithelial cells with mesenchymal features (Gradiz et al. 2016), we observed an increase in the expression of the mesenchymal markers vimentin and fibronectin in resistant cells (Figure 28A).

The acquisition of mesenchymal traits is usually followed by an increase in the metastatic ability of the cells (Nieto et al. 2016). In agreement to this tenet, MEK162 resistant cells displayed enhanced metastatic ability *in vitro* and *in vivo*. Consistently, according to the ability of Slug to induce EMT and aggressive behavior (Emadi Baygi et al. 2010; C. Wang et al. 2012; Alves et al. 2018), we observed that Slug expression regulates the metastatic ability of resistant cells as well as it promotes aggressiveness in MIA PaCa-2 cells (Figure 34 and 35).

Interestingly, our findings contravene a recent report indicating that EMT was dispensable for metastasis in pancreatic cancer (Zheng et al. 2015). In that study, conditional genetic deletion of the EMT-TFs Snail and Twist1 in KPC mice did not abrogate metastasis, despite the gain and loss of expression in epithelial and mesenchymal markers, respectively. In contrast to our work, the specific role of Slug was not assessed in that model. Thus, it might be reasonable that Snail and Twist1 would not be as determinant as Slug for the metastatic ability of pancreatic cancer cells. In fact, these results are consistent with our observation that Snail overexpression did not have any effect in response to Mek1/2 inhibition (Figures 31C). Besides, Snail and Twist1/2 were not differentially expressed in resistant cells in the RNA-seq (Figures 25B and 28B). Although that study was carried out in genetically engineered mouse models and our work has been done with human cell lines and PC-PDXs, it contributes to explain that not all EMT-TFs could be redundant in pancreatic cancer. Furthermore, the effects of the EMT-TFs may be disease-specific and can also differ between organisms (Stemmler et al. 2019). Therefore, future studies will carefully describe the role of the different EMT-TFs in the metastatic ability of pancreatic cancer.

In agreement with these evidences, our results clearly demonstrate that Slug is the only EMT transcription factor that correlates with poor survival in pancreatic cancer patients (Figure 40), indicating a specific role of Slug in this type of tumor and highlighting the importance of designing novel therapies targeting it.

2.6 Targeting Slug expression: Erk5 signaling

The ability of Slug to confer resistance to Mek1/2 inhibition together with the acquisition of a more metastatic phenotype indicates the potential use of Slug as a biomarker to stratify patients that could benefit from anti-Mek1/2 therapies as well as it confirms the value of Slug as a promising target to inhibit in pancreatic cancer.

Unfortunately, Slug inhibitors are not available nowadays. As we could not pharmacologically target Slug directly, we attempted to analyze activated pathways that may regulate its expression in resistant cells. Our results confirmed recent reports showing that Erk5 (which is encoded by the *MAPK7* gene) signaling pathway contributes to the upregulation of Slug (Javaid et al. 2015). Indeed, in resistant cells, Erk5 is constitutively activated and its pharmacological inhibition results in decreased Slug expression (Figure 41). Confirming the role of Erk5 in the positive regulation of Slug and, thus, in the sensitivity of Mek1/2 inhibition, Mek5 and Erk5 inhibition did not have an effect on parental cells but re-sensitized resistant cells to Mek1/2 inhibition (Figure 42A-F). Interestingly, resistant cells expressing an ERK5-independent Slug version could not be re-sensitized to Mek1/2 inhibition upon ERK5 inhibition, emphasizing the critical role of Slug in the resistance to Mek1/2 inhibition (Figure 42G).

Furthermore, we found increased levels of phospho-Erk5 in those PC-PDXs that did not respond to MEK162, which also correlated with increased levels of Slug, thus unveiling a potential therapeutic approach to treat pancreatic cancers. Given the urgent clinical need to identify novel approaches to treat pancreatic cancer, Erk5 appears as an interesting candidate to target and we are starting to elucidate the effect of Erk5 signaling inhibition, alone and in combination to Mek1/2 inhibition, in tumor growth as well as in the expression of Slug in the MEK162-resistant PC-PDXs.

As mentioned above, Slug inhibitor molecules are not currently available. As an interesting aside, these results have provided the bases for the development of a Slug-specific protein targeting approach, based on induced target protein degradation. Using

this technology, based on Proteolysis Targeting Chimeras (PROTACs), we are starting to design a compound that, upon binding, will specifically tag Slug for elimination.

In summary, this work describes the novel role of the transcription factor Slug as a mechanism of resistance to Mek1/2 inhibition in pancreatic cancer, that contributes to explain the failure of this therapy in unselected patients with pancreatic ductal adenocarcinoma and the acquisition of resistance in melanoma patients. Additionally, it also underscores the ability of Slug to predict treatment response, thereby indicating the potential use of Slug as a biomarker for selecting patients that will potentially benefit from Mek1/2 and Erk1/2 inhibitors. Besides, the pro-metastatic effects of Slug together with its correlation with poor survival in patients, definitely makes it an interesting vulnerability to target in order to improve patients' outcome.

CONCLUSIONS

SECTION 1:

1. Mek1/2 inhibition can be a relevant therapy for the treatment of pancreatic cancer.
2. Intratumor heterogeneity may represent a major drawback for this therapeutic approach, compromising its efficacy.
3. Selective pressure imposed by Mek1/2 inhibition results in the rapid selection of resistant cells.
4. The elucidation of the mechanisms of resistance to Mek1/2 inhibitors will be the next step in refining this therapeutic strategy to improve long-term efficacy.

SECTION 2:

1. The transcription factor Slug induces resistance to Mek1/2 inhibition.
2. Slug uncouples cell proliferation from Raf-Mek-Erk signaling, by preventing Mek1/2 inhibitor-induced cyclin D1 downregulation.
3. MEK162-resistant cells exhibit increased metastatic ability and Slug knockdown impairs metastatic spread.
4. Slug predicts poor response to Mek1/2 inhibitors in pancreatic cancer and melanoma cell lines, as well as in PC-PDXs.
5. Slug correlates with poor survival in pancreatic cancer and melanoma patients.
6. Pancreatic cancer cells with acquired resistance to MEK162 express increased levels of phosphorylated Erk5, and it regulates the expression of Slug.
7. p-Erk5 expression correlates with resistance in PC-PDXs, becoming an attractive target to treat pancreatic cancer.

REFERENCES

- Adzhubei, I.A. et al., 2010. A method and server for predicting damaging missense mutations. *Nature methods*, 7(4), pp.248–249.
- Aguirre, A.J. et al., 2003. Activated Kras and Ink4a/Arf deficiency cooperate to produce metastatic pancreatic ductal adenocarcinoma. *Genes & development*, 17(24), pp.3112–3126.
- Ahronian, L.G. et al., 2015. Clinical Acquired Resistance to RAF Inhibitor Combinations in BRAF-Mutant Colorectal Cancer through MAPK Pathway Alterations. *Cancer Discovery*, 5(4), pp.358–367.
- Albanese, C. et al., 1995. Transforming p21ras mutants and c-Ets-2 activate the cyclin D1 promoter through distinguishable regions. *The Journal of biological chemistry*, 270(40), pp.23589–23597.
- Almoguera, C. et al., 1988. Most human carcinomas of the exocrine pancreas contain mutant c-K-ras genes. *Cell*, 53(4), pp.549–554.
- Alves, C.L. et al., 2018. SNAI2 upregulation is associated with an aggressive phenotype in fulvestrant-resistant breast cancer cells and is an indicator of poor response to endocrine therapy in estrogen receptor-positive metastatic breast cancer. *Breast cancer research : BCR*, 20(1), p.60.
- Andea, A., 2003. Clinicopathological Correlates of Pancreatic Intraepithelial Neoplasia: A Comparative Analysis of 82 Cases With and 152 Cases Without Pancreatic Ductal Adenocarcinoma. *Modern Pathology*, 16(10), pp.996–1006.
- Anon, 2013. Concurrent MEK2 Mutation and BRAF Amplification Confer Resistance to BRAF and MEK Inhibitors in Melanoma. 4(6), pp.1090–1099. Available at: <http://dx.doi.org/10.1016/j.celrep.2013.08.023>.
- Ansieau, S. et al., 2008. Induction of EMT by twist proteins as a collateral effect of tumor-promoting inactivation of premature senescence. *Cancer Cell*, 14(1), pp.79–89.
- Antoon, J.W. et al., 2013. MEK5/ERK5 signaling suppresses estrogen receptor expression and promotes hormone-independent tumorigenesis. V. Cheriyath, ed. *PLOS ONE*, 8(8), p.e69291.
- Apte, M.V. et al., 2013. A starring role for stellate cells in the pancreatic cancer microenvironment. *Gastroenterology*, 144(6), pp.1210–1219.
- Arnoux, V. et al., 2008. Erk5 controls Slug expression and keratinocyte activation during wound healing. M. B. Omary, ed. *Molecular biology of the*

- cell*, 19(11), pp.4738–4749.
- Bailey, J.M. et al., 2008. Sonic hedgehog promotes desmoplasia in pancreatic cancer. *Clinical Cancer Research*, 14(19), pp.5995–6004.
- Baines, A.T., Xu, D. & Der, C.J., 2011. Inhibition of Ras for cancer treatment: the search continues. *Future medicinal chemistry*, 3(14), pp.1787–1808.
- Bardeesy, N. & DePinho, R.A., 2002. Pancreatic cancer biology and genetics. *Nature Reviews Cancer*, 2(12), pp.897–909.
- Bardeesy, N. et al., 2006. Smad4 is dispensable for normal pancreas development yet critical in progression and tumor biology of pancreas cancer. *Genes & development*, 20(22), pp.3130–3146.
- Bell, C.E. & Watson, A.J., 2009. SNAI1 and SNAI2 are asymmetrically expressed at the 2-cell stage and become segregated to the TE in the mouse blastocyst. J. M. Baltz, ed. *PLOS ONE*, 4(12), p.e8530.
- Bernard, V. et al., 2019. Single-Cell Transcriptomics of Pancreatic Cancer Precursors Demonstrates Epithelial and Microenvironmental Heterogeneity as an Early Event in Neoplastic Progression. *Clinical Cancer Research*, 25(7), pp.2194–2205.
- Bhang, H.-E.C. et al., 2015. Studying clonal dynamics in response to cancer therapy using high-complexity barcoding. *Nat Med*, 21(5), pp.440–448.
- Bollag, G. et al., 2010. Clinical efficacy of a RAF inhibitor needs broad target blockade in BRAF-mutant melanoma. *Nature*, 467(7315), pp.596–599.
- Brauswetter, D. et al., 2017. Molecular subtype specific efficacy of MEK inhibitors in pancreatic cancers. B. E. Rich, ed. *PLOS ONE*, 12(9), p.e0185687.
- Bryant, K.L. et al., 2014. KRAS: feeding pancreatic cancer proliferation. *Trends in Biochemical Sciences*, pp.1–10.
- Burris, H.A. et al., 1997. Improvements in survival and clinical benefit with gemcitabine as first-line therapy for patients with advanced pancreas cancer: a randomized trial. *J Clin Oncol*, 15(6), pp.2403–2413.
- Buschbeck, M. et al., 2005. Abl-kinase-sensitive levels of ERK5 and its intrinsic basal activity contribute to leukaemia cell survival. *EMBO reports*, 6(1), pp.63–69.
- Byrne, A.T. et al., 2017. Interrogating open issues in cancer precision medicine with patient-derived xenografts. *Nature Publishing Group*, pp.1–15.
- Campbell, P.J. et al., 2010. The patterns and dynamics of genomic instability in metastatic pancreatic cancer. *Nature*, 467(7319), pp.1109–1113.

- Cannon, A. et al., 2018. Desmoplasia in pancreatic ductal adenocarcinoma: insight into pathological function and therapeutic potential. *Genes & cancer*, 9(3-4), pp.78–86.
- Cano, A. et al., 2000. The transcription factor snail controls epithelial-mesenchymal transitions by repressing E-cadherin expression. *Nature Cell Biology*, 2(2), pp.76–83.
- Carl, T.F. et al., 1999. Inhibition of neural crest migration in *Xenopus* using antisense slug RNA. *Developmental Biology*, 213(1), pp.101–115.
- Casas, E. et al., 2011. Snail2 is an essential mediator of Twist1-induced epithelial mesenchymal transition and metastasis. *Cancer Research*, 71(1), pp.245–254.
- Caunt, C.J. et al., 2015. MEK1 and MEK2 inhibitors and cancer therapy: the long and winding road. *Nature Reviews Cancer*, 15(10), pp.577–592.
- Chang, T.-H. et al., 2011. Slug Confers Resistance to the Epidermal Growth Factor Receptor Tyrosine Kinase Inhibitor. *American Journal of Respiratory and Critical Care Medicine*, 183(8), pp.1071–1079.
- Chapman, P.B. et al., 2011. Improved survival with vemurafenib in melanoma with BRAF V600E mutation. *New England Journal of Medicine*, 364(26), pp.2507–2516.
- Chen, G. et al., 2018. Wnt/ β -Catenin Pathway Activation Mediates Adaptive Resistance to BRAF Inhibition in Colorectal Cancer. *Molecular cancer therapeutics*, 17(4), pp.806–813.
- Chen, X. & Song, E., 2018. Turning foes to friends: targeting cancer-associated fibroblasts. *Nature Reviews Drug Discovery*, pp.1–17.
- Chung, J.-H. et al., 2011. Clinical and molecular evidences of epithelial to mesenchymal transition in acquired resistance to EGFR-TKIs. *Lung cancer (Amsterdam, Netherlands)*, 73(2), pp.176–182.
- Cobaleda, C. et al., 2007. Function of the Zinc-Finger Transcription Factor SNAI2 in Cancer and Development. *Annual Review of Genetics*, 41(1), pp.41–61.
- Conroy, T. et al., 2011. FOLFIRINOX versus gemcitabine for metastatic pancreatic cancer. *New England Journal of Medicine*, 364(19), pp.1817–1825.
- Corcoran, R.B. et al., 2010. BRAF gene amplification can promote acquired resistance to MEK inhibitors in cancer cells harboring the BRAF V600E mutation. *Science signaling*, 3(149), pp.ra84–ra84.
- Cros, J. et al., 2018. Tumor Heterogeneity in Pancreatic Adenocarcinoma.

Pathobiology, 85(1-2), pp.64–71.

Dagogo-Jack, I. & Shaw, A.T., 2018. Tumour heterogeneity and resistance to cancer therapies. *Nature Reviews Clinical Oncology*, 15(2), pp.81–94.

Davies, H. et al., 2002. Mutations of the BRAF gene in human cancer. *Nature*, 417(6892), pp.949–954.

de Bruin, E.C. et al., 2014. Reduced NF1 expression confers resistance to EGFR inhibition in lung cancer. *Cancer Discovery*, 4(5), pp.606–619.

DeLuca, D.S. et al., 2012. RNA-SeQC: RNA-seq metrics for quality control and process optimization. *Bioinformatics (Oxford, England)*, 28(11), pp.1530–1532.

DeRose, Y.S. et al., 2011. Tumor grafts derived from women with breast cancer authentically reflect tumor pathology, growth, metastasis and disease outcomes. *Nat Med*, 17(11), pp.1514–1520.

Ding, H. et al., 2012. Sonic hedgehog signaling mediates epithelial-mesenchymal communication and promotes renal fibrosis. *Journal of the American Society of Nephrology : JASN*, 23(5), pp.801–813.

Drew, B.A., Burow, M.E. & Beckman, B.S., 2012. MEK5/ERK5 pathway: The first fifteen years. *BBA - Reviews on Cancer*, 1825(1), pp.37–48.

Elloul, S. et al., 2005. Snail, Slug, and Smad-interacting protein 1 as novel parameters of disease aggressiveness in metastatic ovarian and breast carcinoma. *Cancer*, 103(8), pp.1631–1643.

Emadi Baygi, M. et al., 2010. Slug/SNAI2 regulates cell proliferation and invasiveness of metastatic prostate cancer cell lines. *Tumour biology : the journal of the International Society for Oncodevelopmental Biology and Medicine*, 31(4), pp.297–307.

Emery, C.M. et al., 2009. MEK1 mutations confer resistance to MEK and B-RAF inhibition. *Proceedings of the National Academy of Sciences of the United States of America*, 106(48), pp.20411–20416.

Esposito, A. et al., 2016. Liquid biopsies for solid tumors: Understanding tumor heterogeneity and real time monitoring of early resistance to targeted therapies. *Pharmacology & therapeutics*, 157, pp.120–124.

Faião-Flores, F. et al., 2017. Targeting the hedgehog transcription factors GLI1 and GLI2 restores sensitivity to vemurafenib-resistant human melanoma cells. *Oncogene*, 36(13), pp.1849–1861.

Ferrone, C.R. et al., 2015. Radiological and surgical implications of neoadjuvant treatment with FOLFIRINOX for locally advanced and borderline resectable pancreatic cancer. *Ann Surg*, 261(1), pp.12–17.

- Figura, von, G. et al., 2014. The chromatin regulator Brg1 suppresses formation of intraductal papillary mucinous neoplasm and pancreatic ductal adenocarcinoma. *Nature Cell Biology*, 16(3), pp.255–267.
- Fisher, R., Pusztai, L. & Swanton, C., 2013. Cancer heterogeneity: implications for targeted therapeutics. *British Journal of Cancer*, 108(3), pp.479–485.
- Flaherty, K.T., Infante, Jeffery R, et al., 2012a. Combined BRAF and MEK inhibition in melanoma with BRAF V600 mutations. *New England Journal of Medicine*, 367(18), pp.1694–1703.
- Flaherty, K.T., Robert, C., et al., 2012b. Improved survival with MEK inhibition in BRAF-mutated melanoma. *New England Journal of Medicine*, 367(2), pp.107–114.
- Genovese, G. et al., 2017. Synthetic vulnerabilities of mesenchymal subpopulations in pancreatic cancer. *Nature*, 542(7641), pp.362–366.
- Gore, J. & Korc, M., 2014. Pancreatic Cancer Stroma: Friend or Foe? *Cancer Cell*, 25(6), pp.711–712.
- Gradiz, R. et al., 2016. MIA PaCa-2 and PANC-1 - pancreas ductal adenocarcinoma cell lines with neuroendocrine differentiation and somatostatin receptors. *Nature Publishing Group*, 6(1), p.21648.
- Grau, Y., Carteret, C. & Simpson, P., 1984. Mutations and Chromosomal Rearrangements Affecting the Expression of Snail, a Gene Involved in Embryonic Patterning in DROSOPHILA MELANOGASTER. *Genetics*, 108(2), pp.347–360.
- Hackeng, W.M., Hruban, R.H., Offerhaus, G.J.A. & Brosens, L.A.A., 2016a. Surgical and molecular pathology of pancreatic neoplasms. *Diagnostic Pathology*, 11(1), p.47.
- Hackeng, W.M., Hruban, R.H., Offerhaus, G.J.A. & Brosens, L.A.A., 2016b. Surgical and molecular pathology of pancreatic neoplasms. *Diagnostic Pathology*, 11(1), p.47.
- Hahn, S.A. et al., 1996. DPC4, a candidate tumor suppressor gene at human chromosome 18q21.1. *Science*, 271(5247), pp.350–353.
- Hajra, K.M., Chen, D.Y.-S. & Fearon, E.R., 2002. The SLUG zinc-finger protein represses E-cadherin in breast cancer. *Cancer Research*, 62(6), pp.1613–1618.
- Halilovic, E. et al., 2010. PIK3CA mutation uncouples tumor growth and cyclin D1 regulation from MEK/ERK and mutant KRAS signaling. *Cancer Research*, 70(17), pp.6804–6814.
- Hamada, S. et al., 2012. Pancreatic stellate cells enhance stem cell-like

- phenotypes in pancreatic cancer cells. *Biochemical and Biophysical Research Communications*, 421(2), pp.349–354.
- Hanahan, D. & Weinberg, R.A., 2011. Hallmarks of Cancer: The Next Generation. *Cell*, 144(5), pp.646–674.
- Harada, T. et al., 2002. Interglandular cytogenetic heterogeneity detected by comparative genomic hybridization in pancreatic cancer. *Cancer Research*, 62(3), pp.835–839.
- Haupt, S., Alsheich-Bartok, O. & Haupt, Y., 2006. Clues from worms: a Slug at Puma promotes the survival of blood progenitors. *Cell death and differentiation*, 13(6), pp.913–915.
- Hayes, T.K. et al., 2016. Long-Term ERK Inhibition in KRAS-Mutant Pancreatic Cancer Is Associated with MYC Degradation and Senescence-like Growth Suppression. *Cancer Cell*, 29(1), pp.75–89.
- Hemavathy, K. et al., 2000. Human Slug is a repressor that localizes to sites of active transcription. *Molecular and Cellular Biology*, 20(14), pp.5087–5095.
- Herreros-Villanueva, M. et al., 2012. Mouse models of pancreatic cancer. *World J Gastroenterol*, 18(12), pp.1286–1294.
- Hidalgo, M., 2010. Pancreatic Cancer. *New England Journal of Medicine*, 362(17), pp.1605–1617.
- Hidalgo, M. et al., 2014. Patient-Derived Xenograft Models: An Emerging Platform for Translational Cancer Research. *Cancer Discovery*, 4(9), pp.998–1013.
- Hingorani, S.R. et al., 2003. Preinvasive and invasive ductal pancreatic cancer and its early detection in the mouse. *Cancer Cell*, 4(6), pp.437–450.
- Hingorani, S.R. et al., 2005. Trp53R172H and KrasG12D cooperate to promote chromosomal instability and widely metastatic pancreatic ductal adenocarcinoma in mice. *Cancer Cell*, 7(5), pp.469–483.
- Hirata, E. et al., 2015. Intravital imaging reveals how BRAF inhibition generates drug-tolerant microenvironments with high integrin β 1/FAK signaling. *Cancer Cell*, 27(4), pp.574–588.
- Hoff, Von, D.D. et al., 2013. Increased Survival in Pancreatic Cancer with nab-Paclitaxel plus Gemcitabine. *New England Journal of Medicine*, 369(18), pp.1691–1703.
- Hruban, R.H. et al., 1993. K-ras oncogene activation in adenocarcinoma of the human pancreas. A study of 82 carcinomas using a combination of mutant-enriched polymerase chain reaction analysis and allele-specific oligonucleotide hybridization. *The American Journal of Pathology*, 143(2),

pp.545–554.

- Hu, B. et al., 2012. Expression of the phosphorylated MEK5 protein is associated with TNM staging of colorectal cancer. *BMC Cancer*, 12(1), p.127.
- Hung, P.-F. et al., 2019. Hypoxia-induced Slug SUMOylation enhances lung cancer metastasis. *J Exp Clin Cancer Res*, 38(1), p.5.
- Ijichi, H. et al., 2006. Aggressive pancreatic ductal adenocarcinoma in mice caused by pancreas-specific blockade of transforming growth factor-beta signaling in cooperation with active Kras expression. *Genes & development*, 20(22), pp.3147–3160.
- Improta, G. et al., 2013. Coexistence of two different mutations in codon 12 of the Kras gene in colorectal cancer: Report of a case supporting the concept of tumoral heterogeneity. *Oncology letters*, 5(5), pp.1741–1743.
- Infante, Jeffrey R et al., 2014. A randomised, double-blind, placebo-controlled trial of trametinib, an oral MEK inhibitor, in combination with gemcitabine for patients with untreated metastatic adenocarcinoma of the pancreas. *Eur J Cancer*, 50(12), pp.2072–2081.
- Inoue, A. et al., 2002. Slug, a highly conserved zinc finger transcriptional repressor, protects hematopoietic progenitor cells from radiation-induced apoptosis in vivo. *Cancer Cell*, 2(4), pp.279–288.
- Inukai, T. et al., 1999. SLUG, a ces-1-related zinc finger transcription factor gene with antiapoptotic activity, is a downstream target of the E2A-HLF oncoprotein. *Molecular cell*, 4(3), pp.343–352.
- Jamal-Hanjani, M. et al., 2017. Tracking the Evolution of Non-Small-Cell Lung Cancer. *New England Journal of Medicine*, 376(22), pp.2109–2121.
- James, G., Goldstein, J.L. & Brown, M.S., 1996. Resistance of K-RasBV12 proteins to farnesyltransferase inhibitors in Rat1 cells. *Proceedings of the National Academy of Sciences of the United States of America*, 93(9), pp.4454–4458.
- Javaid, S. et al., 2015. MAPK7 Regulates EMT Features and Modulates the Generation of CTCs. *Molecular cancer research : MCR*, 13(5), pp.934–943.
- Johannessen, C.M. et al., 2013. A melanocyte lineage program confers resistance to MAP kinase pathway inhibition. *Nature*, 504(7478), pp.138–142.
- Jones, S. et al., 2008. Core Signaling Pathways in Human Pancreatic Cancers Revealed by Global Genomic Analyses. *Science*, 321(5897), pp.1801–1806.

- Kalluri, R. & Weinberg, R.A., 2009. The basics of epithelial-mesenchymal transition. *The Journal of clinical investigation*, 119(6), pp.1420–1428.
- Kalser, M.H. & Ellenberg, S.S., 1985. Pancreatic cancer. Adjuvant combined radiation and chemotherapy following curative resection. *Archives of surgery (Chicago, Ill. : 1960)*, 120(8), pp.899–903.
- Kamisawa, T. et al., 2016. Pancreatic cancer. *Lancet*, 388(10039), pp.73–85.
- Kanda, M. et al., 2012. Presence of somatic mutations in most early-stage pancreatic intraepithelial neoplasia. *Gastroenterology*, 142(4), pp.730–733.e9.
- Kauko, O. et al., 2018. PP2A inhibition is a druggable MEK inhibitor resistance mechanism in KRAS-mutant lung cancer cells. *Sci Transl Med*, 10(450), p.eaaq1093.
- Khorana, A.A. et al., 2017. Potentially Curable Pancreatic Cancer: American Society of Clinical Oncology Clinical Practice Guideline Update. *J Clin Oncol*, 35(20), pp.2324–2328.
- Kim, M.P. et al., 2009. Generation of orthotopic and heterotopic human pancreatic cancer xenografts in immunodeficient mice. *Nature protocols*, 4(11), pp.1670–1680.
- Kim, S. et al., 2014. Slug promotes survival during metastasis through suppression of Puma-mediated apoptosis. *Cancer Research*, 74(14), pp.3695–3706.
- Kindler, H.L. et al., 2010. Gemcitabine plus bevacizumab compared with gemcitabine plus placebo in patients with advanced pancreatic cancer: phase III trial of the Cancer and Leukemia Group B (CALGB 80303). *J Clin Oncol*, 28(22), pp.3617–3622.
- Kitai, H. et al., 2016. Epithelial-to-Mesenchymal Transition Defines Feedback Activation of Receptor Tyrosine Kinase Signaling Induced by MEK Inhibition in KRAS-Mutant Lung Cancer. *Cancer Discovery*, 6(7), pp.754–769.
- Kleeff, J. et al., 2016. Pancreatic cancer. *Nature Publishing Group*, 2, pp.1–23.
- Klein, W.M. et al., 2002. Direct correlation between proliferative activity and dysplasia in pancreatic intraepithelial neoplasia (PanIN): additional evidence for a recently proposed model of progression. *Modern Pathology*, 15(4), pp.441–447.
- Kopetz, S., Lemos, R. & Powis, G., 2012. The promise of patient-derived xenografts: the best laid plans of mice and men. *Clinical Cancer Research*, 18(19), pp.5160–5162.
- Korotayev, K., Chaussepied, M. & Ginsberg, D., 2008. ERK activation is

- regulated by E2F1 and is essential for E2F1-induced S phase entry. *Cellular signalling*, 20(6), pp.1221–1226.
- Krebs, A.M. et al., 2017. The EMT-activator Zeb1 is a key factor for cell plasticity and promotes metastasis in pancreatic cancer. *Nature Cell Biology*, 19(5), pp.518–529.
- Kumar, B. et al., 2015. Auto-regulation of Slug mediates its activity during epithelial to mesenchymal transition. *Biochimica et biophysica acta*, 1849(9), pp.1209–1218.
- Kwak, E.L. et al., 2015. Molecular Heterogeneity and Receptor Coamplification Drive Resistance to Targeted Therapy in MET-Amplified Esophagogastric Cancer. *Cancer Discovery*, 5(12), pp.1271–1281.
- La O, De, J.-P. et al., 2008. Notch and Kras reprogram pancreatic acinar cells to ductal intraepithelial neoplasia. *Proceedings of the National Academy of Sciences of the United States of America*, 105(48), pp.18907–18912.
- Lamouille, S., Xu, J. & Derynck, R., 2014. Molecular mechanisms of epithelial–mesenchymal transition. *Nature Reviews Molecular Cell Biology*, 15(3), pp.178–196.
- Lavoie, J.N. et al., 1996. Cyclin D1 expression is regulated positively by the p42/p44MAPK and negatively by the p38/HOGMAPK pathway. *The Journal of biological chemistry*, 271(34), pp.20608–20616.
- Lee, H.-J. et al., 2014. Drug Resistance via Feedback Activation of Stat3 in Oncogene-Addicted Cancer Cells. *Cancer Cell*, 26(2), pp.207–221.
- Lee, S.-H. et al., 2009. Blocking of p53-Snail binding, promoted by oncogenic K-Ras, recovers p53 expression and function. *Neoplasia (New York, N.Y.)*, 11(1), pp.22–31– 6p following 31.
- Li, H. et al., 2016. Gli promotes epithelial-mesenchymal transition in human lung adenocarcinomas. *Oncotarget*, 7(49), pp.80415–80425.
- Li, Y. et al., 2015. Slug contributes to cancer progression by direct regulation of ER α signaling pathway. *International journal of oncology*, 46(4), pp.1461–1472.
- Lin, L. et al., 2015. The Hippo effector YAP promotes resistance to RAF- and MEK-targeted cancer therapies. *Nature Genetics*, pp.1–9.
- Liu, M. et al., 2017. Multi-region and single-cell sequencing reveal variable genomic heterogeneity in rectal cancer. *BMC Cancer*, 17(1), p.787.
- Lu, H. et al., 2017. PAK signalling drives acquired drug resistance to MAPK inhibitors in BRAF-mutant melanomas. *Nature*, pp.1–19.

- Lulli, D., Carbone, M.L. & Pastore, S., 2017. The MEK Inhibitors Trametinib and Cobimetinib Induce a Type I Interferon Response in Human Keratinocytes. *International journal of molecular sciences*, 18(10), p.2227.
- Lund, K. et al., 2015. Slug-dependent upregulation of L1CAM is responsible for the increased invasion potential of pancreatic cancer cells following long-term 5-FU treatment. R. Samant, ed. *PLOS ONE*, 10(4), p.e0123684.
- Maestro, R. et al., 1999. Twist is a potential oncogene that inhibits apoptosis. *Genes & development*, 13(17), pp.2207–2217.
- Maitra, A. & Hruban, R.H., 2008. Pancreatic Cancer. *Annual Review of Pathology: Mechanisms of Disease*, 3(1), pp.157–188.
- Makohon-Moore, A. & Iacobuzio-Donahue, C.A., 2016. Pancreatic cancer biology and genetics from an evolutionary perspective. *Nature Publishing Group*, 16(9), pp.553–565.
- Mancini, M. et al., 2010. Zinc-finger transcription factor slug contributes to the survival advantage of chronic myeloid leukemia cells. *Cellular signalling*, 22(8), pp.1247–1253.
- Marampon, F., Ciccarelli, C. & Zani, B.M., 2006. Down-regulation of c-Myc following MEK/ERK inhibition halts the expression of malignant phenotype in rhabdomyosarcoma and in non muscle-derived human tumors. *Mol Cancer*, 5(1), p.31.
- Matsushime, H. et al., 1994. D-type cyclin-dependent kinase activity in mammalian cells. *Molecular and Cellular Biology*, 14(3), pp.2066–2076.
- McCracken, S.R.C. et al., 2008. Aberrant expression of extracellular signal-regulated kinase 5 in human prostate cancer. *Oncogene*, 27(21), pp.2978–2988.
- McGranahan, N. & Swanton, C., 2017. Clonal Heterogeneity and Tumor Evolution: Past, Present, and the Future. *Cell*, 168(4), pp.613–628.
- Mehta, P.B. et al., 2003. MEK5 overexpression is associated with metastatic prostate cancer, and stimulates proliferation, MMP-9 expression and invasion. *Oncogene*, 22(9), pp.1381–1389.
- Merino, D. et al., 2015. Pro-apoptotic Bim suppresses breast tumor cell metastasis and is a target gene of SNAI2. *Oncogene*, 34(30), pp.3926–3934.
- Michl, P. & Gress, T.M., 2013. Current concepts and novel targets in advanced pancreatic cancer. *Gut*, 62(2), pp.317–326.
- Miranda, M. et al., 2015. MEK5-ERK5 pathway associates with poor survival of breast cancer patients after systemic treatments. *Oncoscience*, 2(2), pp.99–

101.

- Mittal, M.K. et al., 2011. SLUG-induced elevation of D1 cyclin in breast cancer cells through the inhibition of its ubiquitination. *The Journal of biological chemistry*, 286(1), pp.469–479.
- Montero, J.C. et al., 2009. Expression of Erk5 in early stage breast cancer and association with disease free survival identifies this kinase as a potential therapeutic target. M. V. Blagosklonny, ed. *PLOS ONE*, 4(5), p.e5565.
- Morris, J.P., Wang, S.C. & Hebrok, M., 2010. KRAS, Hedgehog, Wnt and the twisted developmental biology of pancreatic ductal adenocarcinoma. *Nature Publishing Group*, 10(10), pp.683–695.
- Muzumdar, M.D. et al., 2017. Survival of pancreatic cancer cells lacking KRAS function. *Nat Commun*, 8(1), p.1090.
- Nakamura, T. et al., 2007. Zonal heterogeneity for gene expression in human pancreatic carcinoma. *Cancer Research*, 67(16), pp.7597–7604.
- Neoptolemos, J.P. et al., 2017. Comparison of adjuvant gemcitabine and capecitabine with gemcitabine monotherapy in patients with resected pancreatic cancer (ESPAC-4): a multicentre, open-label, randomised, phase 3 trial. *Lancet*, 389(10073), pp.1011–1024.
- Neoptolemos, J.P. et al., 2018. Therapeutic developments in pancreatic cancer: current and future perspectives. *Nature Reviews Gastroenterology & Hepatology*, pp.1–16.
- Nieto, M.A., 2002. The snail superfamily of zinc-finger transcription factors. *Nature Reviews Molecular Cell Biology*, 3(3), pp.155–166.
- Nieto, M.A. et al., 1994. Control of cell behavior during vertebrate development by Slug, a zinc finger gene. *Science*, 264(5160), pp.835–839.
- Nieto, M.A. et al., 2016. EMT: 2016. *Cell*, 166(1), pp.21–45.
- Nissan, M.H. et al., 2014. Loss of NF1 in cutaneous melanoma is associated with RAS activation and MEK dependence. *Cancer Research*, 74(8), pp.2340–2350.
- Nithianandarajah-Jones, G.N. et al., 2012. ERK5: structure, regulation and function. *Cellular signalling*, 24(11), pp.2187–2196.
- Nitsche, U. et al., 2015. Resectability After First-Line FOLFIRINOX in Initially Unresectable Locally Advanced Pancreatic Cancer: A Single-Center Experience. *Annals of Surgical Oncology*, 22 Suppl 3(S3), pp.S1212–20.
- Nüsslein-Volhard, C., Wieschaus, E. & Kluding, H., 1984. Mutations affecting the pattern of the larval cuticle in *Drosophila melanogaster* : I. Zygotic loci on

- the second chromosome. *Wilhelm Roux's archives of developmental biology*, 193(5), pp.267–282.
- Olive, K.P. et al., 2009. Inhibition of Hedgehog signaling enhances delivery of chemotherapy in a mouse model of pancreatic cancer. *Science*, 324(5933), pp.1457–1461.
- Olmeda, D. et al., 2008. Snai1 and Snai2 collaborate on tumor growth and metastasis properties of mouse skin carcinoma cell lines. *Oncogene*, 27(34), pp.4690–4701.
- Ortiz-Ruiz, M.J. et al., 2014. Therapeutic potential of ERK5 targeting in triple negative breast cancer. *Oncotarget*, 5(22), pp.11308–11318.
- Ottaiano, A. et al., 2017. Gemcitabine mono-therapy versus gemcitabine plus targeted therapy in advanced pancreatic cancer: a meta-analysis of randomized phase III trials. *Acta oncologica (Stockholm, Sweden)*, 56(3), pp.377–383.
- Patel, A.P. et al., 2014. Single-cell RNA-seq highlights intratumoral heterogeneity in primary glioblastoma. *Science*, 344(6190), pp.1396–1401.
- Pavan, S. et al., 2018. A kinome-wide high-content siRNA screen identifies MEK5-ERK5 signaling as critical for breast cancer cell EMT and metastasis. *Oncogene*, 37(31), pp.4197–4213.
- Petrelli, F. et al., 2015. FOLFIRINOX-based neoadjuvant therapy in borderline resectable or unresectable pancreatic cancer: a meta-analytical review of published studies. *Pancreas*, 44(4), pp.515–521.
- Pérez-Losada, J. et al., 2003. The radioresistance biological function of the SCF/kit signaling pathway is mediated by the zinc-finger transcription factor Slug. *Oncogene*, 22(27), pp.4205–4211.
- Pérez-Losada, J. et al., 2002. Zinc-finger transcription factor Slug contributes to the function of the stem cell factor c-kit signaling pathway. *Blood*, 100(4), pp.1274–1286.
- Pérez-Mancera, P.A. et al., 2005. SLUG in cancer development. *Oncogene*, 24(19), pp.3073–3082.
- Portal, A. et al., 2015. Nab-paclitaxel plus gemcitabine for metastatic pancreatic adenocarcinoma after Folfirinox failure: an AGEO prospective multicentre cohort. *British Journal of Cancer*, 113(7), pp.989–995.
- Prat, A. et al., 2010. Phenotypic and molecular characterization of the claudin-low intrinsic subtype of breast cancer. *Breast cancer research : BCR*, 12(5), p.R68.
- Prior, I.A., Lewis, P.D. & Mattos, C., 2012. A comprehensive survey of Ras

- mutations in cancer. *Cancer Research*, 72(10), pp.2457–2467.
- Pulkka, O.-P. et al., 2017. SLUG transcription factor: a pro-survival and prognostic factor in gastrointestinal stromal tumour. *British Journal of Cancer*, 116(9), pp.1195–1202.
- Pylayeva-Gupta, Y., Grabocka, E. & Bar-Sagi, D., 2011. RAS oncogenes: weaving a tumorigenic web. *Nature Reviews Cancer*, 11(11), pp.761–774.
- Rahib, L. et al., 2014. Projecting Cancer Incidence and Deaths to 2030: The Unexpected Burden of Thyroid, Liver, and Pancreas Cancers in the United States. *Cancer Res*, 74(11), p.2913.
- Rhim, A.D. et al., 2014. Stromal elements act to restrain, rather than support, pancreatic ductal adenocarcinoma. *Cancer Cell*, 25(6), pp.735–747.
- Rougier, P. et al., 2013. Randomised, placebo-controlled, double-blind, parallel-group phase III study evaluating aflibercept in patients receiving first-line treatment with gemcitabine for metastatic pancreatic cancer. *Eur J Cancer*, 49(12), pp.2633–2642.
- Roy, N. et al., 2015. Brg1 promotes both tumor-suppressive and oncogenic activities at distinct stages of pancreatic cancer formation. *Genes & development*, 29(6), pp.658–671.
- Ryan, D.P., Hong, T.S. & Bardeesy, N., 2014. Pancreatic Adenocarcinoma. *New England Journal of Medicine*, 371(11), pp.1039–1049.
- Samatar, A.A. & Poulikakos, P.I., 2014. Targeting RAS–ERK signalling in cancer: promises and challenges. *Nature Reviews Drug Discovery*, 13(12), pp.928–942.
- Sánchez-Martín, M. et al., 2003. Deletion of the SLUG (SNAI2) gene results in human piebaldism. *American journal of medical genetics. Part A*, 122A(2), pp.125–132.
- Sánchez-Martín, M. et al., 2002. SLUG (SNAI2) deletions in patients with Waardenburg disease. *Human molecular genetics*, 11(25), pp.3231–3236.
- Scheffzek, K. et al., 1997. The Ras-RasGAP complex: structural basis for GTPase activation and its loss in oncogenic Ras mutants. *Science*, 277(5324), pp.333–338.
- Scheidig, A.J., Burmester, C. & Goody, R.S., 1999. The pre-hydrolysis state of p21(ras) in complex with GTP: new insights into the role of water molecules in the GTP hydrolysis reaction of ras-like proteins. *Structure (London, England : 1993)*, 7(11), pp.1311–1324.
- Schindelin, J. et al., 2012. Fiji: an open-source platform for biological-image analysis. *Nature methods*, 9(7), pp.676–682.

- Schutte, M. et al., 1997. Abrogation of the Rb/p16 tumor-suppressive pathway in virtually all pancreatic carcinomas. *Cancer Research*, 57(15), pp.3126–3130.
- Sebolt-Leopold, J.S. et al., 1999. Blockade of the MAP kinase pathway suppresses growth of colon tumors in vivo. *Nat Med*, 5(7), pp.810–816.
- Seghers, A.C. et al., 2012. Successful rechallenge in two patients with BRAF-V600-mutant melanoma who experienced previous progression during treatment with a selective BRAF inhibitor. *Melanoma research*, 22(6), pp.466–472.
- Sherr, C.J., 2001. The INK4a/ARF network in tumour suppression. *Nature Reviews Molecular Cell Biology*, 2(10), pp.731–737.
- Shi, Y. & Massagué, J., 2003. Mechanisms of TGF-beta signaling from cell membrane to the nucleus. *Cell*, 113(6), pp.685–700.
- Shibue, T. & Weinberg, R.A., 2017. EMT, CSCs, and drug resistance: the mechanistic link and clinical implications. *Nature Reviews Clinical Oncology*, 14(10), pp.611–629.
- Shioiri, M. et al., 2006. Slug expression is an independent prognostic parameter for poor survival in colorectal carcinoma patients. *British Journal of Cancer*, 94(12), pp.1816–1822.
- Simanshu, D.K., Nissley, D.V. & McCormick, F., 2017. RAS Proteins and Their Regulators in Human Disease. *Cell*, 170(1), pp.17–33.
- Simões, A.E.S., Rodrigues, C.M.P. & Borralho, P.M., 2016. The MEK5/ERK5 signalling pathway in cancer: a promising novel therapeutic target. *Drug discovery today*, 21(10), pp.1654–1663.
- Simpson, P., 1983. Maternal-Zygotic Gene Interactions during Formation of the Dorsoventral Pattern in Drosophila Embryos. *Genetics*, 105(3), pp.615–632.
- Smalley, K.S.M. et al., 2008. Increased cyclin D1 expression can mediate BRAF inhibitor resistance in BRAF V600E-mutated melanomas. *Molecular cancer therapeutics*, 7(9), pp.2876–2883.
- Smit, V.T. et al., 1988. KRAS codon 12 mutations occur very frequently in pancreatic adenocarcinomas. *Nucleic acids research*, 16(16), pp.7773–7782.
- Stemmler, M.P. et al., 2019. Non-redundant functions of EMT transcription factors. *Nature Cell Biology*, 21(1), pp.102–112.
- Sticht, C. et al., 2008. Activation of MAP kinase signaling through ERK5 but not ERK1 expression is associated with lymph node metastases in oral squamous cell carcinoma (OSCC). *Neoplasia (New York, N.Y.)*, 10(5),

pp.462–470.

Sun, C., Hobor, S., et al., 2014a. Intrinsic Resistance to MEK Inhibition in KRAS Mutant Lung and Colon Cancer through Transcriptional Induction of ERBB3. *Nature*, 508(7494), pp.86–93.

Sun, C., Wang, L., et al., 2014b. Reversible and adaptive resistance to BRAF(V600E) inhibition in melanoma. *Nature*, 508(7494), pp.118–122.

Tesser-Gamba, F. et al., 2012. MAPK7 and MAP2K4 as prognostic markers in osteosarcoma. *Hum Pathol*, 43(7), pp.994–1002.

Thayer, S.P. et al., 2003. Hedgehog is an early and late mediator of pancreatic cancer tumorigenesis. *Nature*, 425(6960), pp.851–856.

Tran, H.D. et al., 2014. Transient SNAIL1 expression is necessary for metastatic competence in breast cancer. *Cancer Research*, 74(21), pp.6330–6340.

Trapnell, C. et al., 2012. Differential gene and transcript expression analysis of RNA-seq experiments with TopHat and Cufflinks. *Nature protocols*, 7(3), pp.562–578.

Tsai, S. et al., 2018. Development of primary human pancreatic cancer organoids, matched stromal and immune cells and 3D tumor microenvironment models. *BMC Cancer*, 18(1), p.335.

Turke, A.B. et al., 2012. MEK inhibition leads to PI3K/AKT activation by relieving a negative feedback on ERBB receptors. *Cancer Research*, 72(13), pp.3228–3237.

Uchikado, Y. et al., 2005. Slug Expression in the E-cadherin preserved tumors is related to prognosis in patients with esophageal squamous cell carcinoma. *Clinical Cancer Research*, 11(3), pp.1174–1180.

Van Cutsem, E. et al., 2018. Phase I/II trial of pimasertib plus gemcitabine in patients with metastatic pancreatic cancer. *International Journal of Cancer*, 143(8), pp.2053–2064.

Vaseva, A.V. et al., 2018. KRAS Suppression-Induced Degradation of MYC Is Antagonized by a MEK5-ERK5 Compensatory Mechanism. *Cancer Cell*, 34(5), pp.807–822.e7.

Villanueva, J., Vultur, A. & Herlyn, M., 2011. Resistance to BRAF inhibitors: unraveling mechanisms and future treatment options. *Cancer Research*, 71(23), pp.7137–7140.

Visani, M. et al., 2013. Multiple KRAS mutations in pancreatic adenocarcinoma: molecular features of neoplastic clones indicate the selection of divergent populations of tumor cells. *International journal of surgical pathology*, 21(6),

pp.546–552.

- Wagner, S. et al., 2019. Suppression of interferon gene expression overcomes resistance to MEK inhibition in KRAS-mutant colorectal cancer. *Oncogene*, 38(10), pp.1717–1733.
- Wang, C. et al., 2012. Deregulation of Snai2 is associated with metastasis and poor prognosis in tongue squamous cell carcinoma. *International Journal of Cancer*, 130(10), pp.2249–2258.
- Wang-Gillam, A. et al., 2016. Nanoliposomal irinotecan with fluorouracil and folinic acid in metastatic pancreatic cancer after previous gemcitabine-based therapy (NAPOLI-1): a global, randomised, open-label, phase 3 trial. *Lancet*, 387(10018), pp.545–557.
- Waters, A.M. & Der, C.J., 2018. KRAS: The Critical Driver and Therapeutic Target for Pancreatic Cancer. *Cold Spring Harbor perspectives in medicine*, 8(9), p.a031435.
- Wee, S. et al., 2009. PI3K pathway activation mediates resistance to MEK inhibitors in KRAS mutant cancers. *Cancer Research*, 69(10), pp.4286–4293.
- Weldon, C.B. et al., 2002. Identification of mitogen-activated protein kinase kinase as a chemoresistant pathway in MCF-7 cells by using gene expression microarray. *Surgery*, 132(2), pp.293–301.
- Whyte, D.B. et al., 1997. K- and N-Ras are geranylgeranylated in cells treated with farnesyl protein transferase inhibitors. *The Journal of biological chemistry*, 272(22), pp.14459–14464.
- Wilentz, R.E. et al., 2000. Loss of expression of Dpc4 in pancreatic intraepithelial neoplasia: evidence that DPC4 inactivation occurs late in neoplastic progression. *Cancer Research*, 60(7), pp.2002–2006.
- Winter, J.M. et al., 2012. Survival after Resection of Pancreatic Adenocarcinoma: Results from a Single Institution over Three Decades. *Annals of Surgical Oncology*, 19(1), pp.169–175.
- Witkiewicz, A.K. et al., 2015. Whole-exome sequencing of pancreatic cancer defines genetic diversity and therapeutic targets. *Nat Commun*, 6(1), p.6744.
- Wu, W.-S. et al., 2005. Slug antagonizes p53-mediated apoptosis of hematopoietic progenitors by repressing puma. *Cell*, 123(4), pp.641–653.
- Xu, Z. et al., 2010. Role of Pancreatic Stellate Cells in Pancreatic Cancer Metastasis. *The American Journal of Pathology*, 177(5), pp.2585–2596.

- Yachida, S. & Iacobuzio-Donahue, C.A., 2009. The Pathology and Genetics of Metastatic Pancreatic Cancer. *Archives of Pathology & Laboratory Medicine*, 133(3), pp.413–422.
- Yachida, S. et al., 2012. Clinical significance of the genetic landscape of pancreatic cancer and implications for identification of potential long-term survivors. *Clinical Cancer Research*, 18(22), pp.6339–6347.
- Yeh, T.C. et al., 2007. Biological characterization of ARRY-142886 (AZD6244), a potent, highly selective mitogen-activated protein kinase kinase 1/2 inhibitor. *Clinical Cancer Research*, 13(5), pp.1576–1583.
- Ying, H. et al., 2012. Oncogenic Kras maintains pancreatic tumors through regulation of anabolic glucose metabolism. *Cell*, 149(3), pp.656–670.
- Yu, J. et al., 2015. Time to progression of pancreatic ductal adenocarcinoma from low-to-high tumour stages. *Gut*, 64.
- Yu, Q. et al., 2010. Expression of transcription factors snail, slug, and twist in human bladder carcinoma. *J Exp Clin Cancer Res*, 29(1), p.119.
- Yue, B. et al., 2014. ERK5 silencing inhibits invasion of human osteosarcoma cell via modulating the Slug/MMP-9 pathway. *European review for medical and pharmacological sciences*, 18(18), pp.2640–2647.
- Yun, G. et al., 2018. Tumor heterogeneity of pancreas head cancer assessed by CT texture analysis: association with survival outcomes after curative resection. *Nature Publishing Group*, 8(1), p.7226.
- Zheng, X. et al., 2015. Epithelial-to-mesenchymal transition is dispensable for metastasis but induces chemoresistance in pancreatic cancer. *Nature*, 527(7579), pp.525–530.

